
Electronic Thesis and Dissertation Repository

8-21-2018 10:00 AM

Development of an EMG-based Muscle Health Model for Elbow Trauma Patients

Emma Farago, *The University of Western Ontario*

Supervisor: Trejos, Ana Luisa, *The University of Western Ontario*

A thesis submitted in partial fulfillment of the requirements for the Master of Engineering Science degree in Electrical and Computer Engineering

© Emma Farago 2018

Follow this and additional works at: <https://ir.lib.uwo.ca/etd>



Part of the [Biomedical Commons](#)

Recommended Citation

Farago, Emma, "Development of an EMG-based Muscle Health Model for Elbow Trauma Patients" (2018).
Electronic Thesis and Dissertation Repository. 5559.
<https://ir.lib.uwo.ca/etd/5559>

This Dissertation/Thesis is brought to you for free and open access by Scholarship@Western. It has been accepted for inclusion in Electronic Thesis and Dissertation Repository by an authorized administrator of Scholarship@Western. For more information, please contact wlsadmin@uwo.ca.

Development of an EMG-based Muscle Health Model for Elbow Trauma Patients

Emma Farago

M.E.Sc. Thesis, 2018

Department of Electrical and Computer Engineering
The University of Western Ontario

Abstract

Musculoskeletal (MSK) conditions are a leading cause of pain and disability worldwide. Rehabilitation is critical for recovery from these conditions and for the prevention of long-term disability. Robot-assisted therapy has been demonstrated to provide improvements to stroke rehabilitation in terms of efficiency and patient adherence. However, there are no wearable robot-assisted solutions for patients with MSK injuries. One of the limiting factors is the lack of appropriate models that allow the use of biosignals as an interface input. Furthermore, there are no models to discern the health of MSK patients as they progress through their therapy.

This thesis describes the design, data collection, analysis, and validation of a novel muscle health model for elbow trauma patients. Surface electromyography (sEMG) data sets were collected from the injured arms of elbow trauma patients performing 10 upper-limb motions. The data were assessed and compared to sEMG data collected from the patients' contralateral healthy limbs. A statistical analysis was conducted to identify trends relating the sEMG signals to muscle health.

sEMG-based classification models for muscle health were developed. Relevant sEMG features were identified and combined into feature sets for the classification models. The classifiers were used to distinguish between two levels of health: healthy and injured (50% baseline accuracy rate). Classification models based on individual motions achieved cross-validation accuracies of 48.2–79.6%. Following feature selection and optimization of the models, cross-validation accuracies of up to 82.1% were achieved.

This work suggests that there is a potential for implementing an EMG-based model of muscle health in a rehabilitative elbow brace to assess patients recovering from MSK elbow trauma.

However, more research is necessary to improve the accuracy and the specificity of the classification models.

Keywords: Electromyography, rehabilitation, musculoskeletal injury

Acknowledgements

First and foremost, I would like to express my appreciation for the guidance provided by my supervisor, Dr. Ana Luisa Trejos. Her support and encouragement throughout the past two years has motivated me to acquire the skills and knowledge to complete this thesis. She has been a constant source of inspiration to me.

I am deeply indebted to Shrikant Chinchalkar, who provided me with insight and expertise towards my project, and assisted me with recruiting patients. I was very fortunate to have his support, and the support of the hand therapy team at St. Joseph's Hospital over the course of this project.

I would like to express my gratitude to Dr. Dan Lizotte for his help with data analysis and interpretation, and for his insights as a thesis examiner. The input provided by my other thesis examiners, Dr. James Lacefield and Dr. Ilia Polushin, is also greatly appreciated.

I am extremely fortunate to have been a part of the Wearable Biomechatronics Laboratory. I would like to thank all of the colleagues I have worked with over the past two years for their assistance, encouragement, expertise, and friendship. I would also like to extend special thanks to Julian Saldarriaga for his assistance with EMG feature extraction, and to my co-op student Emelyn Kupinski for her assistance with data analysis.

The research in this thesis was funded by the Natural Sciences and Engineering Research Council (NSERC) Canada Graduate Scholarship, the Transdisciplinary Bone & Joint Training Award from the Collaborative Training Program in Musculoskeletal Health Research (CMHR) at Western University, NSERC under grant RGPIN-2014-03815, and by the Ontario Ministry of Economic Development, Trade and Employment and the Ontario Ministry of Research and

Innovation through the Early Researcher Award (A.L. Trejos).

Contents

Abstract	i
Acknowledgements	iii
Table of Contents	v
List of Figures	xi
List of Tables	xiii
Nomenclature and Acronyms	xv
1 Introduction	1
1.1 Motivation	2
1.2 General Problem Statement	3
1.3 Research Objectives and Scope	3
1.4 Overview of the Thesis	4
2 Literature Review	6
2.1 Introduction	6
2.2 Elbow Anatomy	6
2.2.1 Osteology and Articulations	7
2.2.2 Elbow Ligaments	8
2.2.3 Elbow Muscles	8

2.3	Elbow Trauma Rehabilitation	10
2.3.1	Elbow Trauma and Surgical Rehabilitation	10
2.3.1.1	Healing Stage: 0–6 weeks	11
2.3.1.2	Functional Rehabilitation Stage: 6–12 weeks	11
2.3.1.3	Rehabilitative Braces	12
2.3.2	Specific Rehabilitation Practices	12
2.3.2.1	Radial Head Fractures	13
2.3.2.2	Elbow Dislocations	13
2.3.2.3	Arthroscopic Debridement	13
2.3.2.4	Stiff Elbow	13
2.3.2.5	Bicep Tendon Tears	14
2.3.3	Elbow Rehabilitation Challenges	14
2.3.4	Adherence to Therapy	14
2.3.5	Assessment and Outcome Measures	14
2.4	Robotic Rehabilitation	15
2.4.1	Prior Art	15
2.4.1.1	Stationary Robotic Systems	15
2.4.1.2	Wearable Devices	17
2.4.1.3	Health Monitoring Devices for Rehabilitation	17
2.4.2	Efficacy of Robotic Rehabilitation Therapy	18
2.4.3	Towards Robotic Systems for Musculoskeletal Rehabilitation	19
2.5	Muscle Physiology	19
2.5.0.1	Skeletal Muscle Fibres	19
2.5.0.2	The Motor System	19
2.5.0.3	Action Potentials of Muscle Cells	21
2.5.0.4	Motor Unit Action Potentials (MUAPs)	21
2.6	Electromyography (EMG)	22
2.6.1	sEMG and Muscle Force	23
2.6.2	Muscle Activity Profiles	23

2.6.3	Diagnosis of Neuromuscular Disorders	24
2.6.4	Limitations and Challenges of sEMG	24
2.7	sEMG Acquisition	25
2.7.1	Electrodes	26
2.7.1.1	Electrode Configuration	26
2.7.1.2	Inter-electrode Distance	27
2.7.1.3	Electrode Size and Shape	27
2.7.1.4	Electrode Type	27
2.7.1.5	Skin Preparation	28
2.7.1.6	Electrode Placement	28
2.7.2	Amplification	28
2.7.3	Filtering	28
2.7.4	A/D Conversion	29
2.7.5	Normalization of sEMG Signals	29
2.7.5.1	Maximum Voluntary Contraction (MVC)	29
2.7.5.2	Submaximal Contraction	30
2.7.5.3	Mean and Peak sEMG Amplitude	30
2.7.6	Detection of Muscle Activation Onset	30
2.7.6.1	Single-threshold Method	30
2.7.6.2	Double-threshold Method	31
2.7.6.3	Other Methods	31
2.7.6.4	Teager–Kaiser Energy Operator	31
2.8	Pattern Recognition of EMG Signals	32
2.8.1	Data Windowing	33
2.8.2	EMG Feature Extraction	33
2.8.2.1	Time Domain Features	34
2.8.2.2	Time Domain: Energy	34
2.8.2.3	Time domain: Information Complexity	35
2.8.2.4	Time domain: Frequency	35

2.8.2.5	Time domain: Multiple features	35
2.8.2.6	Frequency Domain Features	37
2.8.2.7	Prediction Model Coefficients	39
2.8.2.8	Entropy Features	41
2.8.2.9	Fractal Dimension (FD) Features	43
2.8.2.10	Higher Order Statistics Features	44
2.8.2.11	Time-Scale Features	45
2.8.2.12	Spike Shape Analysis Features	46
2.8.3	Feature Selection and Feature Reduction	47
2.8.3.1	Feature Selection	48
2.8.3.2	Davies–Bouldin Index	48
2.8.3.3	RELIEFF Algorithm	49
2.8.3.4	Individual Feature Evaluation	50
2.8.3.5	Robustness	51
2.8.3.6	Feature Set Evaluation	51
2.8.3.7	Feature Reduction	52
2.8.3.8	Principal Component Analysis (PCA)	52
2.8.4	Classification Models	52
2.8.4.1	Linear Discriminant Analysis (LDA)	52
2.8.4.2	Quadratic Discriminant Analysis (QDA)	53
2.8.4.3	Support Vector Machines (SVM)	53
2.8.4.4	K-Nearest Neighbours Classification (k -NN)	54
2.8.4.5	Decision Trees	54
2.8.4.6	Artificial Neural Networks (ANNs)	55
2.8.4.7	Classification Model Evaluation	55
2.9	Conclusion	56
3	Data Collection and Processing	57
3.1	Equipment	57

3.1.1	Acquisition System	57
3.1.2	Data Recording and Analysis Software	58
3.1.3	Load Cell	60
3.2	Patient Recruitment	61
3.3	Electrode Placement	61
3.4	Motions	62
3.5	Data Collection Protocol	69
3.6	Data Processing	70
3.6.1	Data Segmentation	71
3.6.2	Filtering	71
3.6.3	Feature Extraction	71
3.6.4	Classification	72
3.6.5	Evaluation	73
3.6.6	Optimization of Feature Sets and Models	73
3.6.7	Identification of Patient Characteristics Influencing the Perception of Patient Health	73
4	Results and Discussion	75
4.1	Healthy–Injured Models	75
4.1.1	Preliminary Feature Sets	76
4.1.2	Majority Vote Models	79
4.2	Data Windows	82
4.3	Feature Selection	86
4.3.1	Individual Feature Performances	86
4.3.2	FS4 and FS5 Feature Set Performances	89
4.4	Patient Characteristics	92
4.5	Three-Class Models	93
4.6	Statistical Analysis of Features	98
4.6.1	Paired Difference Tests	99

4.6.2	Returning Patients	110
4.7	Conclusion	114
5	Concluding Remarks	116
5.1	Contributions	117
5.2	Future Work	118
Appendices		137
A	Permissions and Approvals	137
B	MATLAB Code	167
B.1	Segmentation Codes	167
B.2	Feature Function Codes	173
B.3	Feature Generation Codes	195
B.4	Classification	199
B.5	Majority Vote	203
Vita		206

List of Figures

2.1	Anterior and lateral views of the right elbow	7
2.2	Overlapping structure of thick and thin filaments.	20
2.3	Structure of motor unit and muscle fibres.	20
2.4	Triphasic extracellular action potential waveform.	22
2.5	Method for pattern recognition.	33
2.6	EMG signal with overlapping windows.	34
2.7	Illustration of sEMG spikes and peaks.	46
3.1	Trigno base station for charging and RF communication with sEMG sensors.	58
3.2	Trigno sensor.	59
3.3	Data acquisition software.	59
3.4	Data analysis software.	60
3.5	Load cell.	60
3.6	sEMG sensor placement (anterior view).	62
3.7	sEMG sensor placement (posterior view).	63
3.8	Elbow flexion.	64
3.9	Elbow extension.	64
3.10	Forearm pronation.	65
3.11	Forearm supination.	65
3.12	Wrist flexion.	66
3.13	Wrist extension.	66
3.14	Ulnar deviation.	67

3.15 Radial deviation.	67
3.16 Hand close.	68
3.17 Hand open.	68
3.18 Extension MVC.	69
3.19 Segmentation for EMG signal filtered with TKEO.	72
4.1 Classification accuracies for each motion when using the LDA, SVM, and RF classifiers with FS1.	78
4.2 FS1 classification accuracies for 150 ms windows, 250 ms windows, and windows consisting of the full motion.	85
4.3 FS5 classification accuracies for all features and after feature reduction with RELI-EFF.	91
4.4 FS4 classification accuracies with and without patient information.	95
4.5 Average number of times features were used for decision tree splitting rules in RF classifier.	96
4.6 LOG feature values for returning subjects.	115

List of Tables

2.1	Summary of muscles crossing the elbow joint.	9
2.2	Summary of rehabilitative upper-limb exoskeleton systems.	16
2.3	Summary of wearable rehabilitative robotic systems.	17
2.4	Definitions of time domain features that describe EMG signal energy.	36
2.5	Definitions of time domain features that describe EMG information complexity.	37
2.6	Definitions of time domain features that describe EMG signal frequency.	38
2.7	Definitions of time domain features that involve multiple features per window.	38
2.8	Definitions of frequency domain features.	40
2.9	Definitions of higher order statistics features.	45
2.10	Definitions of spike shape features.	47
3.1	Elbow trauma patient information.	61
4.1	Classification accuracies for each feature set.	77
4.2	Range of classification accuracies for each motion.	79
4.3	Majority vote classification accuracies.	80
4.4	Weighted majority vote classification accuracies.	81
4.5	Majority vote classification accuracies of majority vote decisions developed from the top motions.	81
4.6	Classification accuracies for each feature set extracted from window segments of 250 ms with 50% overlap.	83

4.7	Classification accuracies for each feature set extracted from window segments of 150 ms with 50% overlap.	84
4.8	Majority vote classification accuracies for individual features.	87
4.9	Individual feature performances organized by feature category.	88
4.10	Classification accuracies for each new feature set.	90
4.11	Majority vote classification accuracies for feature sets FS4 and FS5.	91
4.12	Classification accuracies for feature sets including patient characteristic features. .	94
4.13	Classification accuracies for three categories of health.	97
4.14	Confusion matrix for elbow flexion with LDA classifier.	98
4.15	Confusion matrix for elbow extension with LDA classifier.	98
4.16	Significant differences for paired difference tests for the LOG feature.	100
4.17	Significant differences for paired difference tests for the MFL feature.	101
4.18	Significant differences for paired difference tests for the MYOP feature.	102
4.19	Significant differences for paired difference tests for the DASDV feature.	103
4.20	Significant differences for paired difference tests for the PSR feature.	104
4.21	Significant differences for paired difference tests for the ApEn feature.	105
4.22	Significant differences for paired difference tests for the MSA feature.	106
4.23	Significant differences for paired difference tests for the MSS feature.	107
4.24	Significant differences for paired difference tests for the MSF feature.	108
4.25	Significant differences for paired difference tests for the MSD feature.	109
4.26	Significant differences for paired difference tests for the MNPPS feature.	110
4.27	Repeated measures comparison for wrist flexion and extension for returning subjects.	112
4.28	Repeated measures comparison for radial and ulnar deviation for returning subjects.	113

Nomenclature and Acronyms

Variables

$A^m(r)$	Probability that two vector sequences match for $m + 1$ points
A_x	x coordinate of spike point A
A_y	y coordinate of spike point A
a_p	p^{th} AR model coefficient
$B^m(r)$	Probability that two vector sequences match for $m + 1$ points
B_x	x coordinate of spike point B
B_y	y coordinate of spike point B
b	Baseline value of the EMG signal
$C_i^m(r)$	Probability that a vector \mathbf{u}_i is within a distance r of another vector \mathbf{u}_j
C_x	x coordinate of spike point C
C_y	y coordinate of spike point C
c_p	p^{th} cepstral analysis model coefficient
$d(\cdot)$	Distance function used for ApEn and SampleEn features
$F(v)$	RMS fluctuation profile for box size v
f_H	Nearest hit
f_j	i^{th} feature vector
f_j	Frequency of the EMG power spectrum at bin j

f_M	Nearest miss
K	Number of windows
$L_m(k)$	Length of curve at time m for time interval k
N	Signal length
N_i	Number of elements in the i^{th} cluster
M	Length of the EMG frequency bin
M_{ij}	Euclidean distance between mean vectors i and j
m	Sequence length for ApEn and SampleEn features
\mathbf{m}_i	Mean vector of cluster i
P	Prediction model order
P_j	j^{th} bin of the EMG power spectrum
R	DB index
R_{ij}	Similarity between clusters i and j
r	Self-similarity tolerance for ApEn and SampleEn features
S_i	Dispersion of cluster i
s	Spectral moment order
T_a	Window length
T_d	Processing delay
T_{inc}	Window increment
\mathbf{u}_i	Vector sequence of EMG signal beginning at sample x_i
W_i	i^{th} sample of the windowing function
w_i	i^{th} sample of white noise
\mathbf{X}_m^k	Time series of the EMG signal beginning at time m with a time interval of k between points
x_i	i^{th} sample of the EMG signal
\bar{x}	Mean of the EMG signal
$y_v(k)$	y coordinate of quadratic least-squares fitted function for box size v

\bar{x} Mean of the EMG signal

Greek Letters

α	Self-similarity parameter
$\Delta(\cdot)$	Distance function
ϵ	Threshold value
ζ_i	feature weight of the i th feature at iteration j
κ	Number of Clusters
ν	Box size
σ	Standard deviation
$\Phi^m(r)$	Probability that two vector sequences match for $m + r$ points
$\Psi(\cdot)$	Teager–Kaiser energy operator

Acronyms

AAC	Average Amplitude Change
AAROM	Assisted Active Range of Motion
A/D	Analog/Digital
ANN	Artificial Neural Network
ApEn	Approximate Entropy
AR	Autoregressive
AROM	Active Range of Motion
ASES-e	American Shoulder and Elbow Surgeons Elbow Scale
BB	Biceps Brachii
BMI	Body Mass Index

BRD	Brachioradialis
CC	Coefficients of Cepstral Analysis
CPM	Continuous Passive Motion
DASDV	Difference Absolute Standard Deviation Value
DASH	Disabilities of the Arm, Shoulder, and Hand
DB	Davies–Bouldin
DFA	Detrended Fluctuation Analysis
DOF	Degree of Freedom
DWT	Discrete Wavelet Transform
ECM	Extracellular Matrix
ECU	Extensor Carpi Ulnaris
EE	Elbow Extension
EF	Elbow Flexion
EMG	Electromyography
FCU	Flexor Carpi Ulnaris
FD	Fractal Dimension
FR	Frequency Ratio
FS	Feature Set
HC	Hand Close
HD-sEMG	High Density Surface Electromyography
HFD	Higuchi's Fractal Dimension
HIST	Histogram of EMG
HO	Hand Open
IED	Inter-electrode Distance
IEMG	Integrated EMG
<i>k</i> -NN	<i>k</i> -Nearest Neighbours

KURT	Kurtosis
LDA	Linear Discriminant Analysis
LHC	Lower Cut-off Frequency of High Frequency Band
LLC	Lower Cut-off Frequency of Low Frequency Band
LOG	Log Detector
MAV	Mean Absolute Value
MAVS	Mean Absolute Value Slope
MDF	Median Frequency
MFL	Maximum Fractal Length
MMAV1	Modified Mean Absolute Value 1
MMAV2	Modified Mean Absolute Value 2
MMT	Manual Muscle Testing
MNF	Mean Frequency
MNP	Mean Power
MNPPS	Mean Number of Peaks Per Spike
MSA	Mean Spike Amplitude
MSD	Mean Spike Duration
MSF	Mean Spike Frequency
MSK	Musculoskeletal
MSS	Mean Spike Slope
MU	Motor Unit
MUAP	Motor Unit Action Potential
MVC	Maximum Voluntary Contraction
MW	Multiple Window
MYOP	Myopulse Percentage Rate
NP	Number of Peaks

NS	Number of Spikes
P	Forearm Pronation
PCA	Principal Component Analysis
PKF	Peak Frequency
PREE	Patient Rated Elbow Evaluation
PROM	Passive Range of Motion
PSR	Power Spectrum Ratio
PT	Pronator Teres
QDA	Quadratic Discriminant Analysis
RF	Random Forest
RICE	Rest, Ice, Compression, Elevation
RCT	Randomized Control Trial
RD	Radial Deviation
RMS	Root Mean Square
ROM	Range of Motion
S	Forearm Supination
SA	Spike Amplitude
SampleEn	Sample Entropy
SDOH	Social Determinants of Health
sEMG	Surface Electromyography
SENIAM	Surface EMG for the Non-Invasive Assessment of Muscles
SKEW	Skewness
SM1	Spectral Moment 1
SM2	Spectral Moment 2
SM3	Spectral Moment 3
SSA	Spike Shape Analysis

SS	Spike Slope
SSC	Slope Sign Change
SSI	Simple Square Integral
SVM	Support Vector Machines
TB1	Triceps Brachii Lateral Head
TB2	Triceps Brachii Long Head
TD	Total Duration
TKEO	Teager–Kaiser Energy Operator
TPP	Total Power
UD	Ulnar Deviation
UHC	Upper Cut-off Frequency of High Frequency Band
ULC	Upper Cut-off Frequency of Low Frequency Band
VAR	Variance of EMG
VCF	Variance of Central Frequency
WAMP	Willison Amplitude
WE	Wrist Extension
WF	Wrist Flexion
WL	Waveform Length
ZC	Zero Crossing

Chapter 1

Introduction

Musculoskeletal (MSK) conditions are disorders or injuries that affect the bones, joints, skeletal muscles and/or connective tissues. MSK conditions are a dominant cause of long-term pain and disability, affecting over 1.2 billion people worldwide [1] and 11 million Canadians annually [2]. MSK injuries are often chronic, and are responsible for 21% of the total years lived with disability in the world [3]. Patients without adequate rehabilitation may suffer pain and disability for years. This results in significant time lost from work, and psychological suffering for both the patient and their family. Prolonged periods of disability also increase the risk of inactivity-associated conditions including cardiovascular disease, diabetes, cancer, osteoporosis, and depression [2].

MSK conditions impose a significant burden on the Canadian economy. In 2010, MSK disorders were estimated to cost the Canadian economy over \$22 billion per year, and MSK injuries were estimated to cost \$15 billion per year [2]. Direct costs including hospitalization, doctor visits, drugs, and private expenditures represented 20% of the total annual cost. Over 80% of the cost was due to time lost from work [2].

Obesity and old age are both major risk factors for MSK conditions. With obesity anticipated to rise over the coming decade, and with a demographically aging global population, the incidence of MSK conditions is expected to increase concomitantly worldwide [3]. By 2031, an estimated 15 million Canadians will be affected annually by MSK conditions [2]. Innovative strategies and treatments must be developed to reduce the imminent burden of these conditions on the economy and on health care and social care systems. A potential area of innovation is in the development

of technologies to assist with rehabilitation and mobility.

1.1 Motivation

Robotic devices have the potential to improve rehabilitation outcomes. Robot-assisted therapy is currently employed for upper-extremity rehabilitation for patients suffering from neurological disorders, primarily stroke. These devices assist patients with performing the repetitive exercises required for stroke rehabilitation and decrease the amount of time therapists spend manually assisting patients [4]. However, these devices are typically expensive, stationary, and confined to the clinic. Mechatronic braces for patients with neurological disorders have been developed to assist with mobility and to provide resistance during therapy [5]. These wearable devices allow patients to perform exercises at home and at their own convenience.

There are currently no smart robotic devices that can assist patients recovering from MSK injuries, despite the numerous potential improvements to the convenience and economy of therapy that such devices could provide. Low adherence to rehabilitation exercises is an ongoing barrier to patient recovery. Patients may fail to adhere to rehabilitation programs as a consequence of a lack of sufficient education and training, or an unwillingness to adhere to regimens that require major lifestyle changes [6]. Supervised exercise programs are more successful than home exercise programs in terms of patient adherence and recovery [4, 7, 8], however these programs require the time and attention of a therapist. Supervised exercise programs are also less accessible for Canadians who live in rural areas and are unable to regularly travel to visit a qualified professional. Wearable robotic rehabilitation devices could allow patients to perform therapy exercises independently, thus mitigating accessibility issues. As well, comparable outcomes to supervised exercise programs could be provided at a reduced cost.

An ideal rehabilitative smart device for MSK injuries would be capable of objectively determining a patient's muscle health as they heal. This would allow for more accurate and objective measurements of health, and would allow therapists to develop treatment recommendations and rehabilitation exercises for individual patient requirements. Furthermore, the amount of mechanical assistance provided by a smart brace to the patient could be modified based on the patient's

health.

Electromyography (EMG), the study of the electrical currents generated during muscle contraction, offers the potential to provide a wearable rehabilitation device with muscle health assessment capabilities. Quantitative EMG analysis is an established diagnostic tool for patients with nerve damage and skeletal muscle damage [9], and there is some evidence that EMG data from patients with MSK injuries conforms to patterns that distinguish the level of injury [10–12]. Little work has been done, however, to quantify EMG data collected from patients with MSK injuries for use in rehabilitation robots. Further research is necessary in order to develop an EMG-based model for health that can be implemented in a wearable device to assess patient muscle health and to inform individualized therapies.

1.2 General Problem Statement

Wearable robotic devices have the potential to improve MSK patient rehabilitation outcomes, and to reduce the cost of rehabilitation. However, there is a lack of research towards identifying EMG patterns associated with MSK patient health. Autonomous assessment of patient muscle health is necessary to 1) improve diagnostics, 2) allow for the development of individualized therapies specific to a patient’s level of health, and 3) create objective outcome measures to inform evidence-based rehabilitation practices.

The purpose of this work is to identify patterns in EMG data that represent the injury levels of patients with MSK elbow injuries. This work proposes that classification models based on EMG data be implemented into the control system of a robotic device to identify the level of muscle health in patients with MSK elbow injuries and to respond accordingly.

1.3 Research Objectives and Scope

This thesis specifically focuses on identifying and classifying patterns of muscle health based on EMG data for patients recovering from MSK elbow trauma. A database of EMG signals was collected from patients with MSK elbow injuries at several stages of healing. A control group of data from healthy limbs was developed.

The primary objectives of this thesis are as follows:

1. To acquire and analyze EMG data from patients with MSK elbow injuries while they perform rehabilitation exercises.
2. To acquire and analyze EMG data from a control group of healthy subjects.
3. To evaluate and generalize the differences in EMG data between the healthy and injured groups.
4. To identify EMG features that are best for evaluating muscle health.
5. To develop a decision system to predict patient muscle health.
6. To evaluate the decision system using new patient data.

1.4 Overview of the Thesis

The structure of this thesis is as follows:

- | | |
|------------------|--|
| Chapter 1 | Introduction: The introductory chapter. |
| Chapter 2 | Literature Review: A review of elbow anatomy, elbow trauma rehabilitation, robotic rehabilitation, muscle physiology, and EMG signal acquisition, processing, and analysis. |
| Chapter 3 | Data Collection and Processing: Outlines the methods of EMG data collection and processing including equipment specifications, data collection protocol, and methods of data processing and data analysis. |
| Chapter 4 | Results and Discussion: Presents the results of the data analysis and explains their significance. |
| Chapter 5 | Concluding Remarks: Highlights the contributions of this work, and provides recommendations for future work. |

Appendix A Permissions and Approvals: Includes ethics permission and approval, consent form, trial form, and permissions for images.

Appendix B MATLAB Code: Describes the MATLAB codes used for EMG analysis.

Chapter 2

Literature Review

2.1 Introduction

This chapter presents a review of the literature in the areas of elbow anatomy (Section 2.2), elbow rehabilitation (Section 2.3), robotic rehabilitative devices (Section 2.4), muscle physiology (Section 2.5), EMG (Section 2.6), surface EMG signal acquisition and processing (Section 2.7), and EMG signal analysis, including EMG feature extraction and classification (Section 2.8). The literature review provided a background into elbow rehabilitation processes and the procedure for collecting, processing, and analyzing surface EMG signals. A literature search was conducted using Google Scholar from September 2016 to August 2018. The keywords used in the search included combinations of the following: elbow rehabilitation, EMG features, EMG control, elbow rehabilitation. A total of 120 papers and books were incorporated into the literature review.

2.2 Elbow Anatomy

The elbow is a critical component of the upper body. The elbow functions as the point of rotation for the forearm, as a link in the lever system that positions the hand in space, and as a load-carrying joint [13]. The elbow also allows for powerful grasping and fine motions of the hand and wrist. The loss of elbow function severely impacts the activities of daily living [14]. This section describes the anatomy of the elbow.

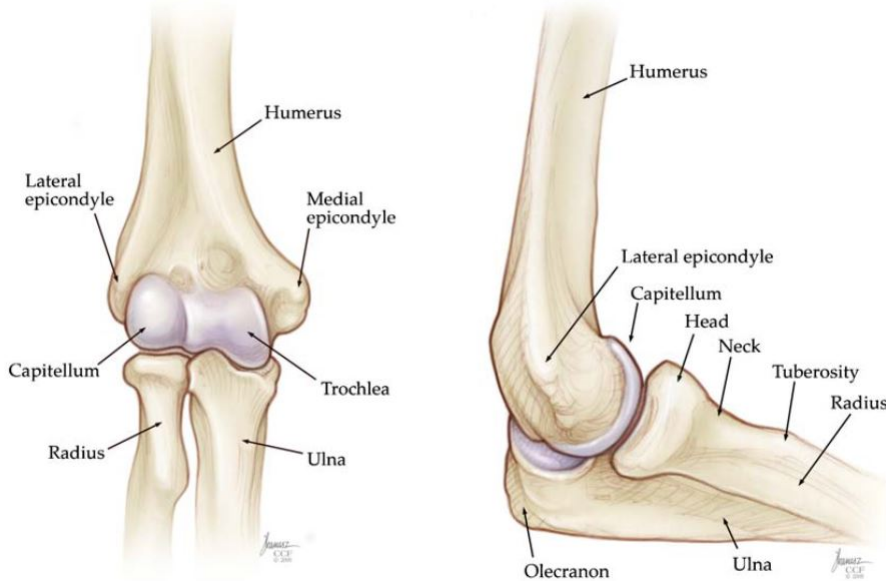


Figure 2.1: Anterior (left) and lateral (right) views of the right elbow. Reprinted, with permission, from [15].

The elbow is generally considered a trochoginglymoid joint with two degrees of freedom: flexion–extension and pronation–supination. The range of motion (ROM) for elbow flexion–extension is $0\text{--}140 \pm 10$ degrees. The ranges of pronation and supination are 75 degrees and 85 degrees respectively. The elbow also exhibits varus–valgus motion during flexion and extension. The axis of elbow flexion follows a helical motion of 3 to 4 degrees during a flexion–extension arc.

2.2.1 Osteology and Articulations

Three bones articulate at the elbow: the humerus, the ulna, and the radius. The humerus is the single long bone from the shoulder to the elbow. In standard anatomical position, the ulna is found in the medial forearm and the radius is found in the lateral forearm (Figure 2.1). These bones provide the following three articulations: 1) ulnohumeral (ulnotrochlear), 2) radiohumeral (radiocapitellar), and 3) proximal radioulnar. The ulnohumeral articulation resembles a hinge (ginglymus) and allows for flexion and extension. The radiohumeral and proximal radioulnar articulations allow for pivoting (trochoid) motion [13]. The three articulations are covered with a single joint capsule [16].

The distal humerus contains two condyles that form the articular surfaces of the trochlea and the capitellum, which interact with the ulna and radius respectively. The trochlea articulates with the sigmoid notch of the proximal ulna. The capitellum articulates with the radial head of the radius [14].

The proximal radioulnar articulation is the major articulation of the elbow and provides stability [13]. The articulation between the radial head and the capitellum is also an important elbow stabilizer [17].

2.2.2 Elbow Ligaments

The two major ligaments of the elbow are the medial and lateral collateral ligaments. The medial collateral ligament provides valgus stability to the elbow and is a stabilizer of the ulnohumeral joint during flexion [16]. The lateral collateral ligament is the primary ligament for providing elbow stability, particularly to the radial head and lateral side of the elbow [17].

The lateral epicondyle, located at the capitellum, is the source of attachment for the lateral collateral ligament and the supinator-extensor muscle groups. The medial epicondyle, located at the trochlea, is the source of attachment for the medial collateral ligament and the flexor-pronator muscle groups [13].

2.2.3 Elbow Muscles

The muscles that cross the elbow joint are summarized in Table 2.1. The primary elbow flexors are the brachialis, biceps brachii, and brachioradialis. The secondary elbow flexors are the pronator teres, extensor carpi radialis longus, and flexor carpi radialis. The primary elbow extensors are the triceps brachii and the anconeus at the posterior of the elbow [18].

Pronation of the forearm is performed by the pronator teres and pronator quadratus. Forearm supination is performed by the biceps and the supinator. The flexor-pronator muscles are located at the medial elbow, and the extensor-supinator muscles are located in the lateral elbow [18].

The majority of the muscles crossing the elbow also provide forearm rotation and flexion-extension of the wrist and fingers [18].

Table 2.1: Summary of muscles crossing the elbow joint [14, 19].

Muscle	Origin	Insertion	Level	Action
Posterior Elbow				
<i>Triceps brachii</i>	Scapula (Long Head) Humerus (Lateral and Medial heads)	Olecranon	Superficial	Elbow extension
<i>Anconeus</i>	Lateral epicondyle	Proximal ulna	Intermediate	Elbow extension, abduction, and stabilization
<i>Extensor carpi ulnaris</i>	Lateral epicondyle	Fifth metacarpal	Superficial	Wrist extension, ulnar deviation
<i>Extensor digitorum communis</i>	Anterolateral epicondyle	Extensor mechanism of each finger	Intermediate	Metacarpal phalangeal joint extension
Lateral Elbow				
<i>Extensor carpi radialis</i>	Lateral epicondyle (brevis) Lateral supra- condylar ridge (longus)	Third metacarpal (brevis) Second metacarpal (longus)	Superficial	Wrist extension, radial deviation
<i>Brachioradialis</i>	Lateral supra- condylar ridge	Distal radius	Superficial	Elbow flexion with forearm in neutral rotation
<i>Supinator</i>	Lateral epicondyle	Proximal radius	Deep	Forearm supination
Medial Elbow				
<i>Flexor digitorum superficialis</i>	Medial epicondyle, Proximal radius	Middle phlanges of the fingers	Superficial/ Intermediate	Flexion of proximal interphalangeal joints
<i>Flexor digitorum profundus</i>	Medial olecranon, Proximal ulna	Distal phlanges of the fingers	Deep	Flexion of distal interphalangeal joints
Anterior Elbow				
<i>Biceps brachii</i>	Scapula	Radius (bicipital tuberosity)	Superficial	Elbow flexion, forearm supination

<i>Prontator teres</i>	Medial epicondyle	Pronator tuberosity of radius	Superficial	Forearm pronation, weak elbow flexion
<i>Flexor carpi radialis</i>	Medial epicondyle	Second and third metacarpals	Superficial	Wrist flexion, weak forearm pronation, radial deviation
<i>Palmaris longus</i>	Medial epicondyle	Palmar aponeurosis	Superficial	Wrist flexion
<i>Flexor carpi ulnaris</i>	Medial epicondyle	Pisiform and fifth metacarpal	Superficial	Wrist flexion, ulnar deviation
<i>Brachialis</i>	Deltoid tuberosity	Ulna	Superficial/ Deep	Elbow flexion

2.3 Elbow Trauma Rehabilitation

Due to the elbow's complex anatomy, rehabilitation from elbow trauma is a challenging process. The elbow capsule is prone to thickening, contracture formation, and stiffening following trauma [16]. Furthermore, there is no standard guideline or protocol for elbow rehabilitation [20]. Most of the scientific evidence to support rehabilitation approaches is based on retrospective and case series studies with small sample sizes, not on randomized control trials (RCTs) [20, 21]. Rehabilitative procedures tested are often poorly described and unreplicable [20]. However, there is expert consensus and some weak clinical evidence to support certain rehabilitative approaches [22]. This section reviews the existing methods of rehabilitation for elbow trauma, and the ongoing challenges of rehabilitation.

2.3.1 Elbow Trauma and Surgical Rehabilitation

The rehabilitation methods used for recovery from elbow trauma and surgical procedures depend on the stages of healing. These can be divided into the healing stage, and the functional rehabilitation stage [20].

2.3.1.1 Healing Stage: 0–6 weeks

In early stages of recovery from elbow injury or surgery, the elbow tissues undergo an inflammatory phase. Elbow trauma typically impacts the lymphatic system of the elbow, resulting in edema. The primary focus during this stage is on pain and edema management [20,22]. Rest, ice, compression, and elevation (RICE) are used to manage pain and edema. Lymphatic drainage is an important step for early rehabilitation [16].

Early mobilization is recommended to improve articular homeostasis, reduce edema and hematoma, and to progressively improve the ROM [20,23]. Active ROM (AROM) and active assisted ROM (AAROM) exercises are introduced at this stage [22]. ROM exercises influence collagen remodeling to ensure full motion of the joints, and to improve venous return and lymphatic drainage, which reduces pain and edema.

Active elbow motion with the forearm in pronation is recommended following damage or repair to the lateral collateral ligament. If both collateral ligaments are damaged, early active motion with the forearm in midprone or neutral rotation is preferable [16].

2.3.1.2 Functional Rehabilitation Stage: 6–12 weeks

The primary focus of the later stage of rehabilitation is to restore elbow function [20,22]. This stage can be further divided into the “intermediate stage of recovery” and the “advanced strengthening” stages [20].

The intermediate stage of recovery involves a focus on restoring elbow extension and forearm pronation [20]. Heat modalities such as hot packs or whirlpool treatments are used to increase the plasticity of the tissues and make them amenable to stretching. Strengthening exercises are performed to enhance the collagen orientation and the elongation of musculotendinous and capsular tissues [16]. Exercises during the intermediate stage of recovery include stretches, functional exercises, AROM, AAROM, and passive ROM (PROM) [20,22]. Forearm pronation-supination exercises are performed actively with the elbow at 90 degrees. AROM exercises of the shoulder, wrist, and fingers are also performed throughout the rehabilitation program. Static progressive splinting may be used to improve the ROM [16]. The required ROM for performing the activities

of daily living is 30–130 degrees. Ranges of 50 degrees for pronation and supination are required for performing the activities of daily living [13].

The advanced strengthening stage introduces strengthening exercises to reduce muscle weakness [20, 22]. Muscle weakness due to pain, soft tissue injury, and/or immobilization, is a common problem following an elbow fracture. Muscle weakness can persist up to 6 months following injury, long after bone healing has occurred, and impacts everyday tasks such as grasping and lifting [22].

Strengthening exercises should not be introduced prematurely, particularly in older patients, as this could place excessive stresses on the healing bone. It is recommended to begin strengthening when the ROM is complete and painless and the power is at least 70% of the contralateral limb [20]. Typically, strengthening is begun after 8 to 12 weeks in complex fractures. There is no consensus, however, with respect to the ideal dosage and type of strengthening exercises [16]. The American College of Sports Medicine recommends performing 1–3 sets of 6–12 repetitions per exercise, at 80% of the one repetition maximum load that can be lifted by the patient, 3 times per week [24].

2.3.1.3 Rehabilitative Braces

There are several types of elbow braces that may be required during elbow trauma rehabilitation, as follows [25]:

1. Immobilization braces are used to protect the limb by restricting movement. They are used at the beginning of treatment. The amount of time an immobilization brace is worn should be kept to a minimum.
2. Restriction braces allow for early movement, but provide protection by restricting the ROM within a specified range of flexion and extension.
3. Mobilization braces exert forces on soft tissue, and are used to maintain or increase the ROM. These are typically used during Weeks 2–8 of recovery, often to treat stiff elbow.

2.3.2 Specific Rehabilitation Practices

The specific rehabilitation practices and exercises performed depend on the type of injury to the elbow. This section describes recommended practices with respect to common elbow traumas.

2.3.2.1 Radial Head Fractures

Radial head fractures are the most common type of elbow fractures. Rehabilitation is similar for both operative and nonoperative treatments. The ROM exercises performed typically include forearm rotation with the elbow at 90 degrees of flexion, and elbow extension and flexion with the forearm in pronation. ROM exercises are performed at a frequency of 10–15 repetitions per hour. Strengthening exercises begin after 8 weeks. Elbow flexion–extension with the forearm in pronation is performed, with the weight gradually increasing [16].

2.3.2.2 Elbow Dislocations

Elbow dislocation rehabilitation focuses on protecting the collateral ligaments and slowly increasing the ROM by performing AROM exercises. Patients are splinted at 90 degrees of flexion for 5–7 days. If the elbow is stable, full active motion is permitted. If the elbow is unstable, full flexion is permitted, and extension is slowly increased each week [16].

2.3.2.3 Arthroscopic Debridement

Arthroscopic surgical procedures are performed for loose body removal, synovectomy, contracture release, radial head excision, and lateral epicondylitis debridement for tennis elbow. Rehabilitation is similar to open surgical procedures in terms of treating pain and edema. The major difference is that rehabilitation can start immediately following the procedure. AROM may be started on the same day as the surgery. Continuous passive motion (CPM) exercises should start as early as possible to improve tissue extensibility [26].

2.3.2.4 Stiff Elbow

The elbow capsule is prone to thickening, contracture formation, and stiffening following trauma [16]. Stiff elbow is a common complication following elbow surgery or injury due to the decreased compliance of the joint capsule. On a biochemical level, the joint capsule experiences structural alterations in collagen crosslinks, decreased proteoglycan content, and decreased water content [20]. However, the viscoelasticity of soft tissue in the elbow allows ligaments to regain their

original length following injury. Stretching forces are exerted on the tissues by progressive splints to stimulate tissue adaptation. PROM and AROM exercises are employed to increase tissue length [27].

2.3.2.5 Bicep Tendon Tears

Distal bicep tendon tears typically result from an acute eccentric load on a flexed elbow. Patients with a distal biceps tear suffer asymmetrical weakness in supination and elbow flexion [28]. Surgery is typically performed to treat the tear, as nonoperative treatments result in reduced strength. There is limited research on the optimal methods of bicep tear rehabilitation following surgery. The current protocol is to maintain the arm in a sling for 3 to 5 days to minimize pain and edema. Afterwards, early ROM exercises are introduced with a weight restriction. After 3 months, flexion and supination exercises are performed [29].

2.3.3 Elbow Rehabilitation Challenges

Ongoing challenges for traditional rehabilitative approaches include a lack of patient adherence to therapy, and the lack of evidence-based rehabilitation methods and objective outcome measures.

2.3.4 Adherence to Therapy

Patient adherence to therapy requires collaboration between the patient and the therapist to produce the therapeutic result [30]. Non-adherence to therapy increases the risk of disability, and reduces the effectiveness of the treatment [6]. Patient education is essential for adherence to treatment during all phases of healing from elbow trauma [22]. Social determinants of health (SDOH) including race, culture, poverty, illiteracy, unemployment, lack of social support, distances from treatment, family problems, and the cost of travel and treatment are associated with factors that affect adherence to long-term therapies [30].

2.3.5 Assessment and Outcome Measures

The most frequent assessment methods used by therapists throughout elbow rehabilitation include: radiographs, ROM, functional performance assessments, strength assessments, and assessments of

the presence of swelling and pain [22].

The outcome measures most commonly used by therapists include: goniometry, dynamometry, and manual muscle testing (MMT) [22]. The current outcome measures often depend on the therapist's perspective. Subjective outcome measures pose difficulties for researchers who aim to assess the effectiveness of a particular therapy.

Patient questionnaires to rate elbow pain and function include the DASH (disabilities of the arm shoulder and hand) outcome measure, in which patients score items on a 5 point scale. The American Shoulder and Elbow Surgeons elbow scale (ASES-e) consists of a patient questionnaire and an assessment from the physician [31]. Finally, the Patient Rated Elbow Evaluation (PREE) allows patients to rate pain, and their ability to perform specific activities and usual activities on an 11 point scale [32].

2.4 Robotic Rehabilitation

The previous section described traditional elbow trauma rehabilitation methods and identified challenges with these methods. Robot-assisted rehabilitation offers potential solutions to the challenges of patient adherence and the development of objective outcome measures. Robotic devices can assist patients with performing multiple repetitions of exercises. Robotic rehabilitation could also lead to more objective outcome measures of patient health. This section describes the prior art and efficacy of robot-assisted rehabilitation.

2.4.1 Prior Art

A number of robotic systems have been developed to assist patients with rehabilitation and movement. These devices were designed for patients with neurological disorders (e.g., stroke) [4]. The key robotic rehabilitation devices are described below.

2.4.1.1 Stationary Robotic Systems

The robotic rehabilitation systems developed for stroke rehabilitation are primarily exoskeletons attached to large stationary workstations. Stroke patients must perform repetitious exercises

during their rehabilitation. Robot-assisted therapy allows patients to repeat exercises many times and remain motivated, while reducing the time burden on the therapist. Table 2.2 summarizes the major rehabilitative upper-limb exoskeleton systems.

Table 2.2: Summary of rehabilitative upper-limb exoskeleton systems.

Name	DOF	Shoulder	Elbow	Wrist	Commercial Availability	Motion Assistance
ARAMIS [33]	6	✓	✓	—	—	✓
ABLE [34]	4	—	✓	✓	—	✓
ArmeoPower [35]	7	✓	✓	✓	✓	✓
ArmeoSpring [36]	8	✓	✓	✓	✓	—
EXO-UL7 [37]	7	✓	✓	✓	—	✓
CAREX [38]	7	✓	✓	✓	—	✓
IntelliArm [39]	6	✓	✓	✓	—	✓
BOTAS [40]	6	✓	✓	✓	—	✓
ALEX [41]	6	✓	✓	✓	—	✓
L-Exos [42]	4	✓	✓	✓	—	✓

Major commercially available upper-limb exoskeletons for stroke rehabilitation include the ArmeoPower robot (commercial version of the ARMin III [35]) and the ArmeoSpring (commercial version of the T-WREX [36]), both distributed by Hocoma [43]. The ArmeoPower is a 7 degree of freedom (DOF) exoskeleton that assists with movement in the shoulder, elbow, and wrist. Angular sensors and a grip pressure sensor determine when the patient is unable to perform an exercise so that assistance-as-needed can be provided in response to individual requirements. The ArmeoPower was designed for stroke patients in early stages of rehabilitation, and enables the patient to perform repetitive therapeutic exercises to relearn motor function. Games are integrated into the system to provide motivation during training [43]. The ArmeoSpring is an 8 DOF system designed for an intermediate stage of recovery from stroke. The ArmeoSpring allows for simultaneous training of the shoulder, elbow, wrist, and hand. Games are also incorporated into the device to improve patient motivation [43].

Stationary exoskeleton systems are beneficial because they provide a more controlled environment for patient movement, which allows for multiple DOF to be safely implemented into the system, enabling patients to perform movements that closely approximate natural motion. However, the rehabilitative exercises can only be performed at a clinic [4]. Wearable rehabilitation

devices could assist patients with performing the activities of daily living, and allow rehabilitation exercises to be performed at home.

2.4.1.2 Wearable Devices

Several wearable robotic rehabilitative devices have been developed (Table 2.3). A key device is the Myomo e100 (MyoPro), a commercial exoskeleton that provides mechanical assistance to patients performing activities of daily living. The MyoPro can also provide resistance training for strengthening exercises during rehabilitative therapy [5]. The MyoPro estimates joint torque using EMG signals from the flexor and extensor muscles of the elbow. The MyoPro provides 1 DOF (flexion–extension). The reduced complexity is necessary to allow for safety and portability.

Table 2.3: Summary of wearable rehabilitative robotic systems.

Name	Description	DOF	Shoulder	Elbow	Wrist	Commercial Availability	Motion Assistance
Myomo [5]	Upper-limb brace with myoelectric input	1	✓	✓	✓	✓	✓
RUPERT IV [44]	Upper-limb, portable exoskeleton	5	✓	✓	✓	—	✓
ArmeoSenso [43]	Enables self-directed upper-limb rehabilitation	6	✓	✓	✓	✓	—
Wear-ME Brace [45]	Upper-limb brace	2	—	✓	—	—	✓

2.4.1.3 Health Monitoring Devices for Rehabilitation

Several devices have also been developed or proposed for monitoring and diagnosing the health of patients undergoing upper-limb rehabilitation for stroke. A major focus has been on using information from EMG, accelerometer, and/or flex sensors to autonomously determine outcome measures of functional independence for stroke patients [46–48]. Stroke outcome measures, such as the Fugl-Meyer assessment and Wolf Motor Function Test, are self-reported or observer-reported, and can therefore be inaccurate. As well, observer-rated measures are time-consuming for the caregiver to perform [47]. However, the Fugl-Meyer and Wolf Motor Function Test are both ordinal scales that cannot accurately describe patient behaviour, therefore there is interest in

using assessment devices to develop new outcome measures [49].

Hocoma supplies the ArmeoSenso device, which monitors patients with mild upper-limb impairments as they undergo self-directed rehabilitation exercises [43]. The 6 DOF system includes motivating exercises and provides summaries of the patient's performance in terms of coordination and reaction time.

2.4.2 Efficacy of Robotic Rehabilitation Therapy

Few clinical studies have been performed to study the efficacy of robot-assisted therapy. The results of these studies are often difficult to compare because outcome measures are often based on therapist opinion [4]. As well, the majority of the studies have used small numbers of participants and/or lacked a control group [50,51].

Robot-assisted rehabilitation could be expected to maximize a patient's effort and adherence to the rehabilitation program and to improve rehabilitation outcomes. The evidence tends to suggest, however, that there are no clinically significant differences in outcome between robot-assisted therapy and intensive therapist-provided rehabilitation [4, 51]. For example, an RCT that compared the efficacy of treatment provided by the ARMin III exoskeleton with conventional stroke therapy found that the increase in the Fugl-Meyer score in patients assigned to robot-assisted therapy was not clinically relevant, and that patients assigned to conventional therapy exhibited larger gains in muscle strength [52]. A pilot trial that compared the efficacy of rehabilitation for stroke patients using the MyoPro with patients who followed a manual regimen provided by a therapist found that both groups of patients had similar increases in their Fugl-Meyer scores [53].

The current rehabilitative robotic devices are therefore unlikely to provide a significant improvement over therapist-assisted rehabilitation, but they can still reduce the burden on therapists by reducing the time spent manually assisting patients, and by allowing patients to participate in rehabilitation more independently. A study that evaluated the efficacy of the ArmeoSpring as a rehabilitation method for patients suffering cervical spinal cord injuries found no significant difference in rehabilitation outcomes, but found that robot-assisted training required therapist involvement for only 25% of the normal time, indicating that robotic devices can greatly improve efficiency [54]. A cost analysis and RCT study conducted in 2010 determined that there was

no significant difference between outcomes of robot-assisted rehabilitation and intensive therapy. The cost of robot-assisted therapy per patient was slightly less than the cost of therapist-assisted therapy (\$5,152 for robot-assisted therapy, \$7,382 for intensive therapist-assisted therapy [55]). Robot-assisted therapy will likely become increasingly desirable, as the cost of robot-assisted rehabilitation therapy is expected to decrease over time [4].

2.4.3 Towards Robotic Systems for Musculoskeletal Rehabilitation

There are currently no commercial robotic systems developed specifically for MSK rehabilitation. Work has been accomplished towards developing mechanisms of sensing patient motion [45], but not towards sensing and identifying patient health. Further research is required to enable wearable devices to identify the muscle health of patients suffering from MSK injuries.

2.5 Muscle Physiology

An understanding of muscle physiology and EMG is necessary in order to develop a system to identify patient muscle health. This section briefly reviews the background knowledge required to understand the physiological basis of the EMG signal.

2.5.0.1 Skeletal Muscle Fibres

Skeletal muscle is composed of numerous parallel fibres. Each muscle fibre is a single long tubular cell. Muscle fibres are composed of fibrils, which are in turn composed of filaments. There are two types of filaments: thick filaments, which are composed of the motor protein myosin-II, and thin filaments, which are primarily composed of actin. The thick filaments and thin filaments overlap and the thin filaments slide over the thick filaments during muscle contraction (Figure 2.2).

2.5.0.2 The Motor System

The central nervous system is arranged in a hierachal structure. Motor programming begins in the premotor cortex. The outputs from the premotor cortex, cerebellum, and basal ganglia converge at the primary motor cortex to excite and inhibit the primary motor cortex neurons.

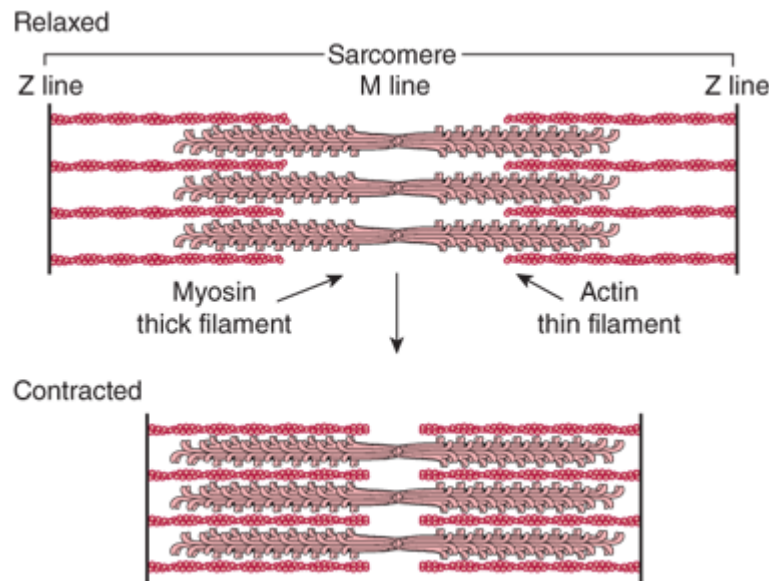


Figure 2.2: Overlapping structure of thick and thin filaments. The thin filaments are composed primarily of actin, and the thick filaments are composed of the double-headed motor protein myosin-II. Reprinted, with permission, from [57] ©2016 McGraw-Hill Education.

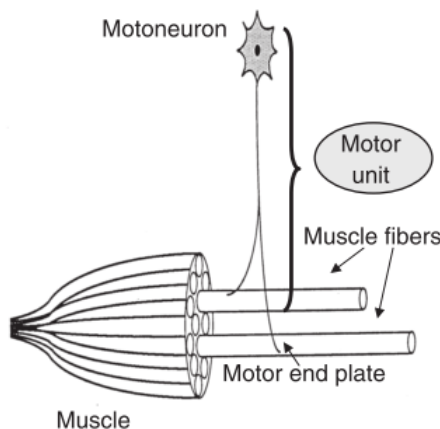


Figure 2.3: Structure of motor unit (MU) and muscle fibres. Reprinted, with permission, from [56].

The outputs from the primary motor cortex influence the neurons of the brain stem and spinal cord. The motoneurons in the spinal cord innervate and activate skeletal muscle fibres. A motor unit (MU) consists of a motoneuron and the muscle fibres that it innervates (Figure 2.3) [56].

2.5.0.3 Action Potentials of Muscle Cells

Nerve and muscle cells are excitable cells that have the ability to generate a propagating wave of depolarization known as the action potential. The action potential is generated following the depolarization of the muscle fibre, and is produced by the flow of ions between the muscle cell and the extracellular matrix (ECM). Voltage-gated ion channels allow ions to move inside and outside of the cell. There are three ions involved in producing an action potential: sodium (Na^+), potassium (K^+), and chloride (Cl^-). Calcium ions (Ca^{2+}) are involved in the process of muscle fibre contraction [58].

The muscle cell has a resting potential of about -80 mV relative to the ECM. If the cell membrane potential is depolarized from -80 mV to -65 mV, voltage-gated Na^+ and K^+ ion channels open. Na^+ ions flow into the cell due to the relative negative charge inside the cell, and due to the concentration gradient. The flow of positive charge rapidly increases the cell membrane potential to +10 mV [59].

Muscle fibre depolarization enables the opening of Ca^{2+} ion channels. Ca^{2+} ions flow into the cell due to the concentration gradient. The influx of Ca^{2+} ions triggers the release of additional Ca^{2+} stored in the sarcoplasmic reticulum of the cell. Ca^{2+} ions enable the formation of cross-bridges between actin and myosin-II, which allows the thin filament to slide across the thick filament [57].

Cell permeability to Na^+ rapidly decreases following depolarization, and permeability to K^+ increases. The outflow of K^+ ions due to the concentration gradient slowly returns the cell membrane potential to resting potential [58].

2.5.0.4 Motor Unit Action Potentials (MUAPs)

The flow of Na^+ ions into the muscle cell is equivalent to a current. The cellular region where the Na^+ ions are drawn to is known as a “current sink,” and the region of the ECM where the Na^+ ions are drawn from is the “current source.” Muscle tissues form a roughly cylindrical shape, therefore, a central negative current sink surrounded by two positive current sources is observed from the outside of the cell. This forms the tripole shape (+ - +) of the action potential (Figure

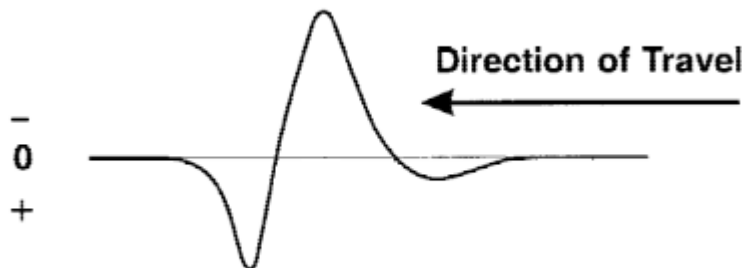


Figure 2.4: Triphasic extracellular action potential waveform. Reprinted, with permission, from [58].

2.4) [58].

Each motoneuron innervates multiple muscle fibres. The summation of the individual potentials of all of the muscle fibres within a motor unit is the motor unit action potential (MUAP) [58].

2.6 Electromyography (EMG)

Electromyography, the study of the currents generated by muscle contraction, is an important tool for studying movement and neuromuscular physiology, and for diagnosing neuromuscular disorders. EMG data can be collected by inserting a needle electrode into the desired muscle. This method allows for individual MUAPs to be recorded, but it is invasive and only useful in a clinical setting.

Surface EMG (sEMG) signals are collected noninvasively by placing electrodes on the surface of the skin. MUAPs produce extracellular currents that extend from the cell membrane to the surface of the skin. The changing potential gradients on the skin will produce electrical currents at the leads of an electrode. Electrodes applied to the skin convert the ionic potentials generated by the muscles into electric potentials. The sEMG signal is the sum of all of the MUAPs produced by the muscle [59]. The sEMG signal is more difficult to interpret than EMG signals obtained from needle electrodes, but it is simple to implement and practical for daily use. sEMG has potential as a noninvasive assessment tool for MSK disease [60].

This section describes common applications of sEMG, including measurement of muscle force, determination of muscle synchronization, and diagnosis of neuromuscular disorders. This section

also discusses the limitations and challenges of sEMG signals.

2.6.1 sEMG and Muscle Force

The sEMG signal is often used to estimate muscle force. Muscle force is regulated by two mechanisms: 1) the recruitment of MUs, and 2) the firing rate of MUs [61]. The amplitude and frequency of the sEMG signal also depend on these two mechanisms, therefore the sEMG signal can be used to estimate the muscle force. However, the relationship between the sEMG signal and muscle force is very complex. The sEMG signal is the summation of the MUAPs, and since the MUAPs are biphasic or triphasic, their summation may be destructive or constructive, whereas the contribution of MUs to force is always constructive. As well, the sEMG signal depends on the distance from the electrode to the MUs. Only superficial MUs contribute to the sEMG signal, whereas all MUs contribute to the force [61]. The sEMG–force relationship also depends on the muscle contraction condition and the joint angle [59]. sEMG activity is higher in concentric contractions compared to isometric contractions, and lower for eccentric contractions of the same force [61].

Furthermore, the sEMG signal is affected by muscle fatigue. During fatiguing isometric contractions, the following events occur [61]:

1. The sEMG amplitude increases
2. There is a shift of signal power towards the lower end of the frequency spectrum (i.e. there is a decrease in high frequency power and an increase in low frequency power).

2.6.2 Muscle Activity Profiles

Muscle activity profiles are developed from sEMG signals to study muscle coordination and muscle activation synergy. A linear envelope is obtained by rectifying the sEMG signal and applying a low pass filter. The cut-off frequency of the low pass filter should retain 95% of the total power of the movement under consideration [62].

Muscle activity profiles should be normalized to a time scale when comparing between trials or individuals. For cyclical behaviour, the time scale can be converted to a percentage of one cycle of the motion. However, this method does not account for variations between individuals in terms

of the ratios spent performing a certain type of behaviour within the motion cycle. To avoid this problem, the motion profile can be normalized to kinematic data [62]. Normalizing the sEMG signal amplitude is also important for comparing between subjects and muscles.

Upper-limb muscle activation patterns have been studied in neurologically intact subjects and in stroke patients performing reaching trajectory tasks to identify muscle health and coordination [63, 64].

2.6.3 Diagnosis of Neuromuscular Disorders

EMG collected by inserting a needle into a single muscle fibre is an established method for the diagnosis of neuromuscular disorders. Individual MUAPs can be classified as normal, neuropathic, or myopathic [9]. Neuropathic muscles have a reduced numbers of MUs, however muscle fibres reorganize to produce larger MUs. MUAPs for neuropathic muscles therefore have higher amplitudes and longer durations. The MUs also fire at a higher rate to compensate for the loss of MUs. Myopathic muscles have reduced numbers of muscle fibres, and exhibit MUAPs with short durations, and low amplitudes [9].

sEMG signals tend to be less reliable than needle EMG signals at identifying neuromuscular health. There is also a great difficulty in correlating observations of sEMG signal qualities with the underlying physiology of the muscle. However, sEMG parameters have been found to exhibit differences between healthy subjects and patients with neuromuscular or muscle disorders including Duchenne muscular dystrophy [65], non-specific arm pain [11], stiff elbow [10], and elbow trauma [12].

2.6.4 Limitations and Challenges of sEMG

sEMG acquisition presents many challenges. The tissue between the muscle and the skin attenuates high-frequency signals, acting as a low pass filter. Surface electrodes placed further away from a signal source have lower signal amplitudes and greater attenuation [66]. sEMG disproportionately represents the signals from superficial muscles. Finally, sEMG may pick up crosstalk recordings from nearby muscles [59].

The sEMG signal is influenced by many factors. Physiological and anatomical features of the

muscle that influence the sEMG signal include the following [59]:

1. Muscle Fibre Length: The distribution of muscle fibres is not uniform in all muscles. Some muscles contain groups of muscle fibres that lie primarily in the proximal or distal end of the muscle. Surface electrodes will only detect the muscle fibres directly underlying the electrode.
2. Muscle Partitioning: Some muscles are partitioned into having different characteristics and functions. For example, the flexor carpi radialis contains three major divisions that activate differently during radial deviation and wrist flexion–extension. An electrode placed without consideration of these specific divisions could lead to a misclassification of the motion being performed.
3. MU Organization: The number of MUs and the number of muscle fibres per MU differs according to the type of muscle. Typically, larger muscles have higher innervation ratios but lower numbers of MUs, while smaller muscles have higher numbers of MUs but lower innervation ratios.
4. Muscle Fibre Organization: The composition of muscle is not uniform, and generally involves fast-twitch fibres closer to the skin, and slow-twitch fibres deeper in the muscle. A surface electrode will be biased towards detecting the fast-twitch fibres closest to the surface of the skin.

Inherent factors that unavoidably influence sEMG signals include noise from ambient electromagnetic radiation, motion artifacts, and the randomness of the MU firing rate. The electrode material and placement are technical factors that should also be considered, and will be discussed in detail in the next section.

2.7 sEMG Acquisition

Since the sEMG signal is inherently affected by various factors, there are several considerations and requirements for the sEMG signal acquisition system. This section describes the recommendations

for the sEMG acquisition system (consisting of the following components: electrodes, amplifiers, filters, and an A/D converter) as well as the procedure for sEMG signal pre-processing.

2.7.1 Electrodes

SENIAM (Surface EMG for the Non-Invasive Assessment of Muscles) was founded in 1996 to provide recommendations for sEMG signal acquisition, electrodes, and electrode placement [60]. Standardization of sEMG acquisition methods between research groups promotes the reproducibility of results and the development of a common body of knowledge. The SENIAM recommendations for electrodes, as well as further recommendations proposed by other research groups, are described in detail below.

2.7.1.1 Electrode Configuration

There are three major electrode configurations used in the literature for sEMG acquisition: bipolar, monopolar, and grid [67].

The monopolar configuration measures the voltage difference between an electrode placed over the muscle of interest and a reference electrode. The reference electrode is placed on a bony area of the body, typically the elbow for upper-body measurements [67].

The bipolar configuration is recommended by SENIAM and is the most commonly used configuration for sEMG acquisition [60]. The sEMG signal is the voltage difference between two electrodes aligned in the direction of the muscle fibres. The bipolar configuration is more tolerant to noise than the monopolar configuration because the electromagnetic interferences common to both electrodes is reduced by determining the voltage difference between the electrodes [59].

Research has been moving towards the use of high density sEMG (HD-sEMG) electrode grids. HD-sEMG provides both temporal and spatial information about muscle activity, and allows for more accurate information about muscle fibre and MU properties, including muscle fibre conduction velocity, muscle fibre length and orientation, MU location, and the decomposition of the sEMG signal into individual MUAPs [66].

2.7.1.2 Inter-electrode Distance

The inter-electrode distance (IED) is the centre-to-centre distance between the conductive areas of two electrodes [60]. The IED determines the “distance volume,” or the volume of muscle tissue that provides a meaningful sEMG signal. The distance volume is approximately a sphere with a radius equal to the IED [59]. When the IED is increased, the sEMG signal exhibits greater amplitudes and lower frequencies [59], however, a larger IED reduces spatial specificity and increases the likelihood of crosstalk from nearby muscles [67].

SENIAM recommends an IED of 20 mm for electrodes in a bipolar configuration [60], however, increasing the IED to 40 mm can improve the tolerance for electrode shifts, and motion classification accuracy [68]. The IED for HD-SEMG configurations should be less than 10 mm to avoid spatial aliasing [69].

2.7.1.3 Electrode Size and Shape

Electrode shape is not thought to have a major influence on the quality of sEMG recordings [60,67]. There are no SENIAM criteria for electrode shape, however most sEMG electrodes are either circular or rectangular [60].

Electrode sizes of 1 cm × 1 cm, 2 cm × 2 cm, and 3 cm × 3 cm have not been found to significantly differ in terms of motion classification accuracy. Larger electrodes are less sensitive to changes caused by electrode shifts [68].

2.7.1.4 Electrode Type

sEMG recordings can be performed with either wet or dry electrodes. Wet electrodes require the application of a conductive electrolyte gel between the electrode and the surface of the skin. Dry electrodes do not require extensive skin preparation [67]. SENIAM recommends the use of Ag/AgCl (silver plated with a thin layer of silver chloride) wet electrodes [60].

Wet electrodes are not optimal for long-term use because the electrolytic gel commonly causes skin irritation as it dries [67]. Applying and removing the electrolytic gel is also time-consuming. Dry electrodes have been observed to achieve signal qualities comparable to wet electrodes [70],

are more comfortable for subjects, and do not require extensive skin preparation [67].

2.7.1.5 Skin Preparation

Skin preparation is necessary for wet electrodes in order to reduce the impedance and noise of the electrode–gel–skin interface. Imbalances between the two electrodes should be reduced by removing body oils and flaky skin layers. SENIAM recommends shaving the skin, cleaning the skin with alcohol, and waiting for the alcohol to dry before applying the sensor. The impedance of the skin should be below $10\text{ k}\Omega$ [60]. With respect to dry electrodes, shaving the skin was demonstrated to improve the sEMG signal quality, however the use of alcohol was found to decrease the signal quality [70].

Electrodes can be fixed to the skin with gel, double-sided adhesive tape, stickers, or elastic bands. The electrode–skin connection should be secure to avoid motion artifacts due to a loss of contact or due to changes in impedance. The electrode cables should be positioned so that they do not tug on the electrodes and affect the sEMG signal [60].

2.7.1.6 Electrode Placement

SENIAM provides recommendations for electrode placements for major muscles [71]. In general, electrodes should be placed over the belly of the muscle between the innervation zone and the tendon, and oriented in the direction of the muscle fibres. Electrodes should not be placed near the innervation zone of the muscle [60].

2.7.2 Amplification

The amplitude of the sEMG signal is usually less than 10 mV. An instrumentation amplifier close to the recording electrodes is used to amplify the sEMG signal by $100\text{--}5000\times$ [67].

2.7.3 Filtering

sEMG signals can be filtered within the hardware prior to A/D conversion or following A/D conversion using software. A high pass filter with a cut-off frequency of 20–50 Hz is typically applied to remove low frequency components due to motion artifacts and the instability of the

electrode–skin interface. The dominant energy of the sEMG signal is limited to frequencies of up to 400–500 Hz, therefore a low pass filter of 400–450 Hz is typically applied to the sEMG signal [67].

Power line interference at frequencies of 60 Hz in North America can corrupt sEMG recordings. A digital notch filter centred at 60 Hz can be applied to the sEMG signal to remove the interference [61]. However, the notch filter may influence the perceived onset of contraction and the mean and median frequencies [72].

2.7.4 A/D Conversion

The final step of the sEMG signal acquisition process is to convert the signal from an analog signal to a digital signal. The Nyquist rule requires the sampling rate for A/D conversion to be at least twice the highest frequency of interest to avoid aliasing. The useful frequencies of the sEMG signal range up to 500 Hz, therefore the sampling rate for sEMG recordings should be at least 1000 Hz [67]. The resolution and range of the A/D converter should be carefully selected to ensure that all of the required information within the sEMG signal is recorded [72].

2.7.5 Normalization of sEMG Signals

Due to the many inherent and technical factors influencing the sEMG signal, when sEMG signal amplitudes are compared between trials, between muscles, or between individuals, signals should be normalized to a reference value. SENIAM recommends that sEMG signals be normalized by dividing the amplitude of the signal by the value of a reference contraction. The amplitude of the signal is then defined as a percentage of the reference value [60]. There are several methods of obtaining a reference contraction, as follows.

2.7.5.1 Maximum Voluntary Contraction (MVC)

The maximum voluntary contraction (MVC) is frequently used as a reference contraction, and is the reference contraction recommended by SENIAM. However, the use of the MVC as a reference contraction has been criticized because values greater than 100% MVC are often observed during rapid and forceful contractions, which indicates that the MVC is not truly representative of maximum muscle activation. Difficulties can also arise in obtaining accurate MVC readings for

older subjects or for subjects with injuries or pathologies [73]. Clarys found that using reference contractions at submaximal values of 80% of the MVC provided a more stable reference value [74].

2.7.5.2 Submaximal Contraction

Isometric submaximal contraction methods provide good reliability. The angle of the contraction does not provide better reliability than using a specific angle, hence it is unnecessary to obtain submaximal MVCs from a range of joint angles [73].

2.7.5.3 Mean and Peak sEMG Amplitude

Normalization can also be performed using the mean or peak sEMG amplitude when performing a task. Mean and peak methods reduce inter-individual variability and should be used if the goal is to reduce the sEMG variability within groups of participants; however, this may not be desirable for all research. Peak and mean methods may not be able to detect alterations in magnitude or patterning of sEMG signals between trials, muscles, or individuals [73].

2.7.6 Detection of Muscle Activation Onset

The detection of the point of the onset of muscle activation in the sEMG signal is important for a variety of applications including motor control analysis, clinical applications, and the control of prosthetic and orthotic devices. Detection can be performed by visually inspecting the signal, or by using algorithms. Visual inspection is time consuming, subjective, and depends on the experience of the examiner. Several algorithms for sEMG onset detection have been proposed [75].

2.7.6.1 Single-threshold Method

The single-threshold method is the most intuitive algorithm. The muscle activation onset is estimated as the point at which the amplitude of the rectified sEMG signal exceeds a predefined threshold. However, the performance of this method depends on the choice of the threshold. The single-threshold method is prone to false alarms [75].

2.7.6.2 Double-threshold Method

The double-threshold method was proposed as an improvement to the single-threshold method in order to decrease the number of false alarms and improve the sensitivity of detection. The double-threshold method detects the muscle activation onset only when a predefined number of consecutive samples exceeds a second threshold [76].

2.7.6.3 Other Methods

Several other methods for muscle activation onset detection have been proposed. The maximum-likelihood method detects the onset of muscle activation by identifying abrupt changes in the variance of the sEMG signal [75, 77]. Merlo *et al.* proposed a real-time onset detection method based on the identification of single MUAPs from an sEMG signal [78].

Computationally complex methods have also been developed for off-line analysis. Drapaa *et al.* proposed a two state detection method. In the first stage the onset is roughly estimated using probability density function estimates of muscle activity and background noise. In the second stage, a more accurate estimate is found by analyzing the neighbourhood of the sample found in the first stage [75].

2.7.6.4 Teager–Kaiser Energy Operator

Regardless of the method of onset detection, the accuracy of detection improves following signal conditioning with the Teager–Kaiser energy operator (TKEO) [79].

The TKEO, $\Psi(\cdot)$, is defined as:

$$\Psi(x_i) = x_i^2 - (x_{i+1} \cdot x_{i-1}) \quad (2.1)$$

where x_i is the i^{th} EMG value.

2.8 Pattern Recognition of EMG Signals

Pattern recognition techniques have been applied to the problems of classifying sEMG signals by motion [80], force [81], neuromuscular health [9], and fatigue [82].

A general procedure for EMG data classification using pattern recognition techniques is summarized in Figure 2.5. The procedure is as follows [83,84]:

1. Data Collection: Data must be collected and preprocessed.
2. Data Windowing: Data are often divided into segments and analyzed in windows of a certain time length to allow for real-time analysis.
3. Feature Extraction: Relevant features are extracted from the data to aid with classification.
4. Feature Selection and/or Reduction: The number of features required should be minimized to reduce the feature extraction time and the information size required for classification. The selection of appropriate features is a critical step, as the features must be able to provide high differentiability between categories.
5. Selection of Classification Model: An appropriate classification model should be selected based on the data. Classifier efficiency may also depend upon the type of features that are used.
6. Training and Evaluation of Classifier: Supervised classifiers must be trained using a set of known data. However, classification models must not be overfitted to a specific set of data, and become unable to classify new data. Therefore, training data must provide a good representation of the data that will be classified.

The performance of a classifier is assessed by attempting to classify a test data set. The effectiveness of a classification model is evaluated based on the system performance as a whole. The computational complexity of the classifier should be evaluated, and a compromise between complexity and performance may be required.

The process of EMG data collection was described in detail in Section 2.6. The remainder of this section describes the subsequent steps of EMG pattern recognition.

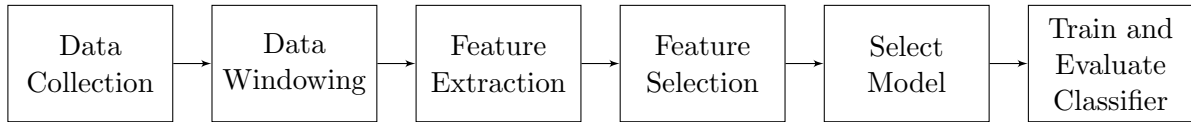


Figure 2.5: Method for pattern recognition.

2.8.1 Data Windowing

The instantaneous EMG signal is not useful for real-time motion classification. EMG features must be extracted from analysis windows of a predefined duration. These windows can be either contiguous or overlapping (Figure 2.6). Window length (T_a) and window increment (T_{inc}) should be selected according to the required classification accuracy and controller delay. There is a trade-off between classification accuracy and delay. Larger window sizes generally provide greater classification accuracies, but lead to larger controller delays that make interactions unintuitive for users [85].

The optimal window length for upper-limb myoelectric devices is within the range of 150–250 ms [85]. Many myoelectric control systems in the literature follow the recommendations of Englehart and Hudgins [86], who state that the longest acceptable controller delay is 300 ms. Englehart and Hudgins also recommend that T_{inc} is set equal to the processing delay, T_d , to maximize the density of the processing stream [86]. Oskoei and Hu [87] found that using 200 ms windows with increments of 50 ms resulted in four times faster control without a significant degradation of the motion classification accuracy. They also observed that classification accuracies do not differ significantly with window size, as long as the window size remains between 50–500 ms.

2.8.2 EMG Feature Extraction

Following data segmentation, the next step of pattern recognition is feature extraction. Over forty features for sEMG analysis have been described in the literature. sEMG features can be categorized by the type of information about the EMG signal that they provide.

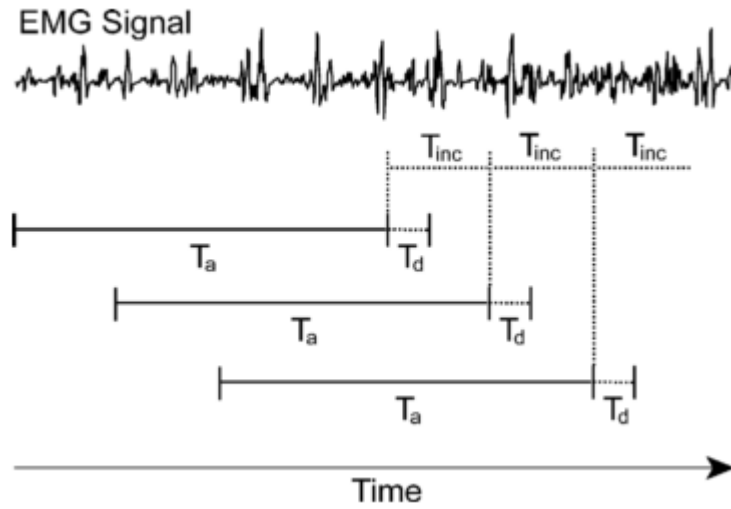


Figure 2.6: EMG signal with overlapping windows. T_a is the duration of the window, T_{inc} is the duration of the increment of new data added to each window, and T_d is the processing time. Reprinted, with permission, from [85] ©2011 IEEE.

2.8.2.1 Time Domain Features

Time domain features are frequently used for real-time applications because they provide high motion classification accuracies at a low computational cost. EMG features extracted from the time domain can provide information about the energy, frequency, and information complexity of the signal. Multiple time domain features can be generated per window.

2.8.2.2 Time Domain: Energy

Time domain features derived from the amplitude of the EMG signal provide information about the energy of the signal. The mean absolute value (MAV) is one of the most popular features for motion recognition. Modifications to the MAV feature have been proposed to improve robustness to noise. The modified MAV Type 1 (MMAV1) feature applies a discrete weighted window function to the MAV feature, and the modified MAV Type 2 (MMAV2) applies a continuous window function [80].

The integrated EMG (IEMG) signal is commonly used for muscle activation onset detection, particularly in clinical settings. The simple square integral (SSI) feature is an energy index. The variance of EMG (VAR) feature is the average of the square values of the standard deviation of

the signal. The root mean square (RMS) is used to estimate the muscle force in non-fatiguing contractions. Finally, the log detector (LOG) feature also provides an estimate of the muscle contraction force [80]. Definitions for these features are provided in Table 2.4.

2.8.2.3 Time domain: Information Complexity

The waveform length (WL), average amplitude change (AAC), and difference absolute standard deviation value (DASDV) describe the information complexity of the sEMG signal. Table 2.5 provides the definitions of these features. The WL feature is the cumulative length of the sEMG signal over a time segment. The AAC feature is similar to the WL feature, but averages the waveform length over the time segment. The DASDV feature provides a standard deviation value of the waveform length [80].

2.8.2.4 Time domain: Frequency

Mathematical definitions of time domain features that describe the frequency of the EMG signal are provided in Table 2.6. The zero crossing (ZC) feature is the number of times the sEMG signal crosses zero. The slope sign change (SSC) is the number of times that the slope of the EMG signal changes sign [86]. A threshold function may be applied to both of these features to reduce the background noise [80].

The myopulse percentage rate (MYOP) is the average number of times the EMG signal exceeds a threshold value. The Willison amplitude (WAMP) is the number of times the difference in EMG amplitude between two adjoining segments exceeds a threshold value. It is related to the firing of MUAPs, and the muscle contraction force [80].

The optimum threshold values for these features are data and subject dependent [88]. Threshold values are typically selected between 50 μ V and 100 mV [80]. A threshold value of 0 mV for the ZC and SSC features was found to be the most generalizable to various data sets and subjects [88].

2.8.2.5 Time domain: Multiple features

The value of time domain features can be improved by deriving multiple features for each window segment. Time domain features that provide multiple values per window include the histogram of

Table 2.4: Definitions of time domain features that describe EMG signal energy [80]. N is the length of the EMG signal and x_i is the i^{th} sample of the EMG signal.

Feature	Definition
Mean Absolute Value (MAV)	$MAV = \frac{1}{N} \sum_{i=1}^N x_i $
Modified Mean Absolute Value 1 (MMAV1)	$MMAV1 = \frac{1}{N} \sum_{i=1}^N W_i x_i $ $W_i = \begin{cases} 1, & \text{if } 0.25N \leq i \leq 0.75N \\ 0.5, & \text{otherwise} \end{cases}$
Modified Mean Absolute Value (MMAV2)	$MMAV2 = \frac{1}{N} \sum_{i=1}^N W_i x_i $ $W_i = \begin{cases} 1, & \text{if } 0.25N \leq i \leq 0.75N \\ 4i/N, & \text{elseif } i < 0.25N \\ 4(i-N)/N, & \text{otherwise} \end{cases}$
Integrated EMG (IEMG)	$IEMG = \sum_{i=1}^N x_i $
Simple Square Integral (SSI)	$SSI = \sum_{i=1}^{N-1} x_i^2$
Variance of EMG (VAR)	$VAR = \frac{1}{N-1} \sum_{i=1}^{N-1} x_i^2$
Root Mean Square (RMS)	$RMS = \sqrt{\frac{1}{N} \sum_{i=1}^N x_i^2}$
Log Detector (LOG)	$LOG = e^{\frac{1}{N} \sum_{i=1}^N \log_{10}(x_i)}$

Table 2.5: Definitions of time domain features that describe EMG information complexity [80]. N is the length of the EMG signal and x_i is the i^{th} sample of the EMG signal.

Feature	Definition
Waveform Length (WL)	$WL = \sum_{i=1}^{N-1} x_{i+1} - x_i $
Average Amplitude Change (AAC)	$AAC = \frac{1}{N} \sum_{i=1}^{N-1} x_{i+1} - x_i $
Difference Absolute Standard Deviation Value (DASDV)	$DASDV = \sqrt{\frac{1}{N-1} \sum_{i=1}^{N-1} (x_{i+1} - x_i)^2}$

EMG (HIST), mean absolute value slope (MAVS), and multiple window (MW) features.

The HIST feature is an extension of the ZC and WAMP features. The EMG signal is divided into voltage bins symmetrical about the signal baseline. The number of times that the EMG voltage falls within each of the voltage bins is calculated. Nine voltage bins are recommended for EMG signals [89]. HIST features were applied to motion classification in several older papers [89, 90], however Phinyomark *et al.* [80] reported more recently that HIST provides poor classification performances.

The MAVS is calculated as the difference between two MAV values calculated over adjacent time windows [90]. The MW features are created by applying a windowing function to the EMG signal, and using the energy within each window as a feature. The Hamming windowing function and the trapezoidal windowing function are typically used [91]. Table 2.7 provides the definitions for the MAVS and MW features.

2.8.2.6 Frequency Domain Features

Frequency domain features (Table 2.8) are used to study muscle fatigue and MU recruitment [80]. They have also been used for motion recognition with some success. Frequency domain features are primarily calculated from the power spectral density of the EMG signal.

Table 2.6: Definitions of time domain features that describe EMG signal frequency [80]. N is the length of the EMG signal, x_i is the i^{th} sample of the EMG signal, and ϵ is a predefined threshold value.

Feature	Definition
ZC (zero crossing)	$ZC = \sum_{i=2}^{N-1} [(-\text{sgn}[x_i \cdot x_{i+1}]) \cap (x_i - x_{i+1} \leq \epsilon)]$ $\text{sgn}(x) = \begin{cases} 1, & \text{if } x \geq 0 \\ 0, & \text{otherwise} \end{cases}$
SSC (slope sign change)	$SSC = \sum_{i=2}^{N-1} [f[(x_i - x_{i-1})(x_i - x_{i+1})]]$ $f(x) = \begin{cases} 1, & \text{if } x \geq \epsilon \\ 0, & \text{otherwise} \end{cases}$
MYOP (myopulse percentage rate)	$MYOP = \frac{1}{N} \sum_{i=1}^N [f(x_i)]$ $f(x) = \begin{cases} 1, & \text{if } x \geq \epsilon \\ 0, & \text{otherwise} \end{cases}$
WAMP (Willison amplitude)	$WAMP = \sum_{i=1}^{N-1} [f(x_i - x_{i+1})]$ $f(x) = \begin{cases} 1, & \text{if } x \geq \epsilon \\ 0, & \text{otherwise} \end{cases}$

Table 2.7: Definitions of time domain features that involve multiple features per window [80]. K is the number of windows and x_i is the i^{th} sample of the EMG signal.

Feature	Definition
Mean Absolute Value Slope (MAVS)	$MAVS = MAV_{k+1} - MAV_k \quad k = 1, \dots, K$
Multiple Window (MW)	$MW_k = \sum_{i=0}^{N-1} (x_i W_{i-i_k})^2, \quad k = 1, \dots, K$

where W_i is the i^{th} value of the windowing function.

The mean frequency (MNF) and median frequency (MDF) can be used for motion recognition [87]. Mean frequency was found to be a highly robust feature when the EMG signal was contaminated with white Gaussian noise [92].

The peak frequency (PKF) is the frequency at which the maximum power occurs. The mean power (MNP) and the total power (TPP) are other frequency features [80].

The first three spectral moments of the signal (SM1, SM2, SM3) can be used as features. The variance of central frequency (VCF) is an important characteristic of the power spectrum and is calculated using the spectral moments [80].

Frequency features can be generated by determining ratios of frequency components within the power spectrum. The frequency ratio (FR) is used to distinguish between muscle contraction and relaxation by using a ratio of low frequency and high frequency components of the signal. The upper and lower cut-off frequencies of the low frequency band and high frequency band must be determined. Typically the value can be assigned using the mean frequency. The power spectrum ratio (PSR) extends the FR feature. It is the ratio of the energy near the maximum of the EMG power spectrum and the whole energy of the power spectrum [80].

2.8.2.7 Prediction Model Coefficients

Feature vectors consisting of coefficients from the autoregressive (AR) prediction model have been implemented as EMG features. The EMG spectrum changes with muscle contraction state, which results in changes in the prediction model coefficients.

The AR model represents each sample of the EMG signal as the linear combination of the previous p samples and a white noise error term. The AR equation is as follows:

$$x_i = \sum_{p=1}^P a_p x_{i-p} + w_i \quad (2.2)$$

where P is the order of the model, w_i is white noise, and a_p is the p^{th} AR coefficient.

The fourth order AR model (AR4) is most commonly used for EMG signals, but the second order AR coefficients (AR2) have also been successful for motion classification when combined with the RMS time domain feature [87]. The AR model coefficients are estimated using the Yule-Walker

Table 2.8: Definitions of frequency domain features [80]. P_j is the EMG power spectrum at bin j , f_j is the frequency of the spectrum at bin j , and M is the length of the frequency bin.

Feature	Definition
Mean Frequency (MNF)	$MNF = \sum_{j=1}^M f_j P_j \Bigg/ \sum_{j=1}^M P_j$
Median Frequency (MDF)	$\sum_{j=1}^{MDF} P_j = \sum_{j=MDF}^M P_j$
Peak Frequency (PKF)	$PKF = f_{\max(P_j)}, \quad j = 1, \dots, M$
Mean Power (MNP)	$MNP = \sum_{j=1}^M P_j \Bigg/ M$
Total Power (TPP)	$TPP = \sum_{j=1}^M P_j = SM0$
Spectral Moments (SM0, SM1, SM2)	$SM_s = \sum_{j=1}^M P_j f_j^s$
Variance of Central Frequency (VCF)	where s is the order of the spectral moment. $VCF = \frac{SM2}{SM0} - \left(\frac{SM1}{SM0} \right)^2$
Frequency Ratio (FR)	$FR = \sum_{j=LLC}^{ULC} P_j \Bigg/ \sum_{j=LHC}^{UHC} P_j$ where ULC and LLC are the upper and lower cut-off frequency of the low frequency band and UHC and LHC are the upper and lower cut-off frequency of the high frequency band respectively.
Power Spectrum Ratio (PSR)	$PSR = \frac{P_0}{P} = \sum_{j=f_0-n}^{f_0+n} P_j \Bigg/ \sum_{j=-\infty}^{\infty} P_j$ where f_0 is the frequency at which the maximum power occurs, and n is the integral limit (typically set to 20).

method [93].

Cepstral analysis is the inverse Fourier transform of the logarithm of the power spectrum magnitude of the EMG signal. The coefficients of cepstral analysis (CC) can be derived using the coefficients from the AR model as follows:

$$\begin{aligned} c_1 &= -a_1 \\ c_p &= -a_p - \sum_{l=1}^{p-1} \left(1 - \frac{l}{p}\right) a_p c_{p-l} \end{aligned} \quad (2.3)$$

where c_p represents the coefficient of the cepstral analysis and $1 \leq l \leq P$, where P is the order of the model. This eliminates the requirement of computing the Fourier transform. The fourth order model is typically used for determining the CC features. AR features have been observed to perform slightly better than CC features in terms of recognition of upper-limb motions [94].

2.8.2.8 Entropy Features

Another category of feature that has been applied to EMG signals consists of features that describe non-linear entropy. Entropy is a measure of the complexity and randomness of a system. The approximate entropy (ApEn) and sample entropy (SampleEn) are entropy features that have been applied to EMG analysis for motion classification [95, 96].

The approximate entropy (ApEn) describes the self-similarity of a time-series, and is a measure of system complexity [97]. ApEn represents the likelihood that patterns of observations will not be followed by similar observations. A less predictable system has a higher ApEn. ApEn requires two parameters: a positive integer, m , representing the sequence length to be compared, and a positive real number, r , the tolerance for matching the similarity between sequences. These parameters are typically set to $m = 2$ and $r = 0.2 \times \sigma$, where σ is the standard deviation of the signal, for EMG analysis [98].

ApEn is calculated by producing a sequence of vectors $\mathbf{u}_1, \mathbf{u}_2, \dots, \mathbf{u}_{N-m+1}$ in \mathbb{R}^m , where N is the length of the sEMG signal and $\mathbf{u}_i = [x_i, x_{i+1}, \dots, x_{i+m-1}]$, where x_i is the i^{th} sample of the sEMG signal.

For each i when $1 \leq i \leq (N - m + 1)$, the value of $C_i^m(r)$, the probability that any vector \mathbf{u}_i is

within a distance of r of vector \mathbf{u}_j where $1 \leq j \leq (N - m + 1)$, is calculated as follows:

$$C_i^m(r) = \frac{\text{number of } j \text{ such that } d[\mathbf{u}_i, \mathbf{u}_j] \leq r}{N - m + 1} \quad (2.4)$$

where:

$$d[\mathbf{u}_i, \mathbf{u}_j] = \max_{k=1,2,\dots,m} (|x_{i+k-1} - x_{j+k-1}|) \quad (2.5)$$

Next, the following function is defined:

$$\Phi^m(r) = (N - m + 1)^{-1} \sum_{i=1}^{N-m+1} \ln C_i^m(r) \quad (2.6)$$

ApEn is then defined as follows [97]:

$$\text{ApEn}(m, r) = \Phi^m(r) - \Phi^{m+1}(r) \quad (2.7)$$

The ApEn feature is subject to a self-matching bias because each vector is counted as being a distance less than r from itself [99]. SampleEn is a refinement of ApEn that eliminates this bias, and improves the consistency of comparisons between data sets.

SampleEn is calculated by first defining:

$$B_i^m(r) = \frac{\text{number of times } d_1[\mathbf{u}_i, \mathbf{u}_j] \leq r}{N - m + 1} \quad 1 \leq j \leq N - m, j \neq i \quad (2.8)$$

$$A_i^m(r) = \frac{\text{number of times } d_2[\mathbf{u}_i, \mathbf{u}_j] \leq r}{N - m + 1} \quad 1 \leq j \leq N - m, j \neq i \quad (2.9)$$

where:

$$d_1[\mathbf{u}_i, \mathbf{u}_j] = \max_{k=1,2,\dots,m} (|x_{i+k-1} - x_{j+k-1}|) \quad (2.10)$$

$$d_2[\mathbf{u}_i, \mathbf{u}_j] = \max_{k=1,2,\dots,m+1} (|x_{i+k-1} - x_{j+k-1}|) \quad (2.11)$$

The averages of the $B_i^m(r)$ and $A_i^m(r)$ values are then calculated as follows:

$$B^m(r) = (N - m)^{-1} \sum_{i=1}^{N-m} B_i^m(r) \quad (2.12)$$

$$A^m(r) = (N - m)^{-1} \sum_{i=1}^{N-m} A_i^m(r) \quad (2.13)$$

$B^m(r)$ is the probability that two sequences match for m points, and $A^m(r)$ is the probability that two sequences match for $m + 1$ points. Finally, SampleEn is defined as [99]:

$$\text{SampleEn}(m, r) = -\ln \frac{A^m(r)}{B^m(r)} \quad (2.14)$$

SampleEn has been used for muscle activation onset detection and motion recognition. SampleEn is useful for identifying bursts of EMG activity with low sensitivity to individual spikes [96].

2.8.2.9 Fractal Dimension (FD) Features

Fractal dimension (FD) features provide information about the morphology, spectrum, and variance of the EMG signal. The FD is a measurement of the non-linear property of a signal, and is related to muscle size and complexity, but is unrelated to the strength of muscle contraction. FD is useful for classifying motions using single EMG channels, and low-level muscle activations [94]. Several FD features have been proposed for the classification of EMG signals.

Higuchi's Fractal Dimension (HFD) is one of the most popular fractal time-series algorithms. HFD first constructs a new EMG time series, \mathbf{X}_m^k , as follows:

$$\mathbf{X}_m^k = [x_m, x_{m+k}, x_{m+2k}, \dots, x_{m+\lfloor \frac{N-m}{k} \rfloor k}] \quad (2.15)$$

where the integer k is the time interval between points, the integer $m = 1, 2, \dots, k$ represents the initial time value, and $\lfloor \frac{N-m}{k} \rfloor$ is the integer part of $\frac{N-m}{k}$. The length of each curve, $L_m(k)$ is then defined as follows:

$$L_m(k) = \frac{1}{k} \left[\frac{N-1}{\lfloor \frac{N-m}{k} \rfloor k} \times \sum_{i=1}^{\lfloor \frac{N-m}{k} \rfloor} |x_{m+ik} - x_{m+(i-1)k}| \right] \quad (2.16)$$

$L(k)$, the length of the curve for time interval k , is calculated as the average length of the m curves as follows:

$$L(k) = \frac{\sum_{m=1}^k L_m(k)}{k} \quad (2.17)$$

$L(k)$ vs. k is plotted on a log-log graph and the HFD is estimated by finding the negative slope of the line relating $\log(L(k))$ and $\log(k)$ [94].

Another common FD feature is the maximum fractal length (MFL), which is applied to the measurement of low-level muscle activation. The MFL is defined as:

$$MFL = \log_{10} \left(\sqrt{\sum_{i=1}^{N-1} (x_{i+1} - x_i)^2} \right) \quad (2.18)$$

where N is the length of the EMG signal and x_i is the i^{th} sample of the EMG signal [94].

Detrended fluctuation analysis (DFA) is a fractal time-series algorithm that was found to perform well for identifying low-level muscle activations in upper-limb EMG signals [94]. The DFA feature uses a self-similarity parameter, α , to represent the FD. A larger value of α corresponds to a smaller FD. The process of calculating the DFA involves first integrating the EMG signal as:

$$y(k) = \sum_{t=1}^k [x_t - \bar{x}_i], k = 1, \dots, N, \quad (2.19)$$

where x_i is the i^{th} sample of the EMG signal, \bar{x}_i is the average value of x_i and N is the length of the EMG signal. The integrated signal is divided into boxes of size ν . Next, a quadratic least-square fit is applied to the signals in each box. The y coordinate of the fitted function, $y_\nu(k)$, is used to calculate the RMS fluctuation of profiles in each box as follows:

$$F(\nu) = \sqrt{\frac{1}{N} \sum_{k=1}^N [y(k) - y_\nu(k)]^2} \quad (2.20)$$

This value is computed for box sizes from $\nu = 4$ to $\nu = N/10$, with the box size incrementing by powers of 2, in order to obtain a relationship between $F(\nu)$ and ν . The value of α is determined by calculating the slope of the line on a log-log graph of $\log(F(\nu))$ vs. $\log(\nu)$ [94].

2.8.2.10 Higher Order Statistics Features

Higher order statistics of EMG signals, such as skewness (SKEW) and kurtosis (KURT) can identify details of the EMG signal that are missed when the signal is assumed to be a Gaussian process. The definitions for these features are provided in Table 2.9.

Table 2.9: Definitions of higher order statistics features. N is the length of the EMG signal, x_i is the i^{th} sample of the EMG signal, \bar{x} is the mean of the EMG signal, and σ is the standard deviation of the signal.

Feature	Definition
Skewness (SKEW)	$SKEW = \left(\frac{1}{N} \sum_{i=1}^N \left(\frac{x_i - \bar{x}}{\sigma} \right)^3 \right)$
Kurtosis (KURT)	$\left(\frac{1}{N} \sum_{i=1}^N \left(\frac{x_i - \bar{x}}{\sigma} \right)^4 \right) - 3$

Skewness is the measure of the degree of symmetry of data around the mean. If the skewness is negative, the data are spread to the left of the mean, and if it is positive, the data are spread to the right of the mean. The skewness of a normal distribution is zero. The SKEW feature has been used for motion classification of facial EMG [100].

Kurtosis describes the peakedness of a probability distribution relative to a normal distribution. Kurtosis values greater than 0 are more prone to outliers (the graph has a “heavy-tailed distribution”), and values less than 0 are less prone to outliers (the graph has a “light-tailed distribution”). The kurtosis of the EMG signal tends to be greater than 0, and to decrease as the contraction level increases. This indicates that as the contraction level increases, the EMG signal begins to approximate a Gaussian distribution [101].

2.8.2.11 Time-Scale Features

The classification accuracies achieved with time domain and frequency domain EMG features may be improved upon by using wavelet methods for time–frequency analysis. Features derived from the wavelet transform have been used to identify MUAPs, determine muscle force and fatigue, and classify motions [102].

The discrete wavelet transform (DWT) is implemented to develop a feature vector, however this process requires a high computational complexity. A wavelet function, typically from the Daubechies wavelet family, is applied to the EMG signal. The EMG signal is transformed into subsets of coefficients, and the original signal is passed through high pass and low pass filters. This

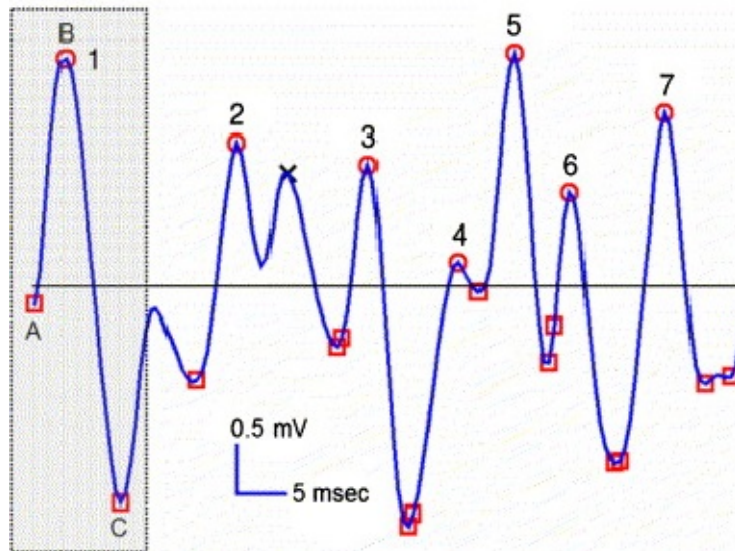


Figure 2.7: Illustration of sEMG spikes and peaks. Spikes are numbered and indicated with red circles. The peak is indicated with a black “x”. Reprinted from [104] ©2007, with permission from Elsevier.

achieves a detailed coefficient subset and an approximation coefficient subset. Each subset can be reconstructed to estimate an EMG component using the inverse DWT [103].

2.8.2.12 Spike Shape Analysis Features

Further information about muscle activation and MU activity can be assessed from the morphology of the sEMG signal with the spike shape analysis (SSA) technique [11]. A spike is defined as a single upward and downward deflection that is greater than a predefined threshold amplitude. The threshold is typically the 95% confidence interval for baseline EMG activity [104]. A peak is defined as an upward and downward deflection within a spike (Figure 2.7).

Table 2.10 provides the definitions for the spike shape features: mean spike amplitude (MSA), mean spike frequency (MSF), mean spike slope (MSS), mean number of peaks per spike (MNPPS), and mean spike duration (MSD). Increased MU recruitment is associated with increases in MSA, MSF, MSS, and MNPPS, and decreases in MSD. Increased MU synchronization is associated with increases in MSA, MSS, and MSD, and decreases in MSF and MNPPS [11].

Spike shape analysis was implemented for identifying and evaluating patients of non-specific

Table 2.10: Definitions of spike shape features [104]. A_x , B_x , C_x , A_y , B_y , and C_y are the x and y coordinates of the points on the spike, indicated in Figure 2.7. NS is the number of spikes, TD is the total duration of the EMG segment, SA is the spike amplitude, SS is the spike slope, and NP is the number of peaks in the EMG segment.

Feature	Definition
Mean Spike Amplitude (MSA)	$SA_i = \frac{(B_y - A_y) + (B_y - C_y)}{2}$ $MSA = \sum_{i=1}^{NS} \frac{SA_i}{NS}$
Mean Spike Frequency (MSF)	$MSF = \frac{NS}{TD}$
Mean Spike Slope (MSS)	$SS_i = \frac{B_y - A_y}{B_x - A_x}$ $MSS = \sum_{i=1}^{NS} \frac{SS_i}{NS}$
Mean Number of Peaks Per Spike (MNPPS)	$MNPPS = \frac{NP}{NS}$
Mean Spike Duration (MSD)	$MSD = \sum_{i=1}^{NS} \frac{C_x - A_x}{NS}$

arm pain. Significant increases in MSA, MSF, MSS, and MNPPS and significant decreases in MSD were observed in the sEMG signals collected from the extensor carpi radialis muscle in subjects with non-specific arm pain compared to controls [11].

2.8.3 Feature Selection and Feature Reduction

EMG features are typically organized into feature sets to improve classification accuracy by incorporating multiple types of information as inputs into a classifier. The number of features in a feature set should be minimized in order to reduce the size of the data set, and computational and

memory requirements.

2.8.3.1 Feature Selection

Features should be selected for inclusion within a feature set according to the following specifications [89]:

1. Class Separability: Clusters of motions or muscle states should have as little overlap as possible within the feature space.
2. Robustness: Class separability should be preserved in noisy environments.
3. Computational complexity: The computational complexity of the features should be low enough for real-time applications and the processing power of small devices, as required for a wearable device.

This section describes algorithms that assist with feature selection and provides a review of the literature concerning the performance of EMG features.

2.8.3.2 Davies–Bouldin Index

The first of these algorithms is the Davies–Bouldin cluster validity index (DB index) [105], which is a measure of cluster separation and is used to determine the class separability of EMG features. Clusters with greater dispersions and smaller distances between them have higher similarities. The similarity between two clusters, R_{ij} , is therefore defined as:

$$R_{ij} = \frac{S_i + S_j}{M_{ij}} \quad (2.21)$$

where S_i and S_j are the dispersions of clusters i and j , and M_{ij} is the distance between the clusters.

The dispersion of a cluster is calculated as follows:

$$S_i = \sqrt{\frac{1}{N_i} \sum_{j=1}^{N_i} (\mathbf{y}_i - \mathbf{m}_i)^T (\mathbf{y}_j - \mathbf{m}_i)} \quad (2.22)$$

where N_i is the number of elements within the i^{th} cluster, \mathbf{y}_i is the i^{th} input vector, and \mathbf{m}_i is the mean vector of cluster i .

The distance, M_{ij} is usually defined as the Euclidean distance between the mean vectors of the clusters as follows:

$$M_{ij} = \sqrt{(\mathbf{m}_i - \mathbf{m}_j)^T (\mathbf{m}_i - \mathbf{m}_j)} \quad (2.23)$$

The DB index, R , is the average of the similarity of each cluster to its most similar cluster, i.e.,

$$R = \frac{1}{\kappa} \sum_{i=1}^k \max(R_{ij}) \quad (2.24)$$

where κ is the number of clusters.

Higher values of R indicate low cluster separation. A good cluster separation measure is considered to be $R < 1$ [106].

The DB index can be used to obtain relative rankings of feature spaces for classifying sEMG signals [89, 106, 107].

2.8.3.3 RELIEFF Algorithm

The importance of individual features in predicting an outcome can be ranked using the RELIEF algorithm. RELIEF works well for features with conditional dependencies, but can only be applied to two-class problems [108].

The RELIEF algorithm provides a weight for each feature based on its predictive ability. Features are first scaled on the interval [0,1]. A set of n instances is randomly selected. For each instance, the RELIEF algorithm searches for the nearest neighbour in the same class (nearest hit) and a different class (nearest miss). A good feature should have high similarity between each instance and the nearest hit, and a low similarity between each instance and the nearest miss. Therefore, the difference between each instance and the nearest hit is added to the feature weight, and the difference between the instance selected and the nearest miss is subtracted from the feature weight as follows:

$$\zeta_i^j = \zeta_i^{j-1} + \frac{\Delta(\mathbf{f}_i - \mathbf{f}_H)}{n} - \frac{\Delta(\mathbf{f}_i - \mathbf{f}_M)}{n} \quad (2.25)$$

where ζ_i^j is the weight for the i^{th} instance at iteration j , \mathbf{f}_i is the feature vector for the i^{th} instance, $\Delta(\cdot)$ is a function that provides the difference between two vectors (typically the Euclidean distance), \mathbf{f}_H is the nearest hit, and \mathbf{f}_M is the nearest miss [108]. The updates are divided by n to ensure that the weights are normalized on the interval [-1, 1].

The RELIEFF algorithm [108] extends the RELIEF algorithm to multi-class data sets. RELIEFF searches for k near misses from each different class and averages them when updating the weight vector.

The RELIEFF algorithm ranks features in decreasing order of importance. The appropriate number of top-ranked features to select for a feature set can then be determined by calculating the DB index for the feature space as each additional feature is added. The optimal cut-off point for adding more features occurs when adding an additional feature leads to no significant improvement in the DB index [48].

2.8.3.4 Individual Feature Evaluation

The DB index has been employed to evaluate the performance of individual EMG features. Of a set of time domain features, HIST and RMS were found to provide the best DB indices when classifying upper-limb motions [89]. Boostani and Moradi used the DB index and a scattering criterion to evaluate the effectiveness of 19 EMG features for the control of a prosthetic hand. Features studied included time domain, frequency domain, cepstral coefficients, and features derived from wavelet and wavelet packet coefficients. A feature vector of wavelet packet coefficients, and a feature vector of cepstral coefficients were found to provide the greatest separabilities [109].

Oskoei and Hu reported that WL, followed by MAV and RMS, offers the best class separability when features are examined individually [87]. Phinyomark *et al.* assessed the performances of EMG features for the classification of upper-limb motions based on the type of information that they provide [80]. WL was found to be the best single feature in terms of classification accuracy, stability, and computation complexity. MAV1 and MAV2 did not provide any more discriminative information than MAV. RMS and VAR had similar performances, with RMS performing slightly better. WAMP, ZC, and SSC were similar in terms of the computation method and performance, with WAMP having the highest performance.

2.8.3.5 Robustness

Phinyomark *et al.* [92] assessed the classification accuracies obtained from features when EMG signals were contaminated with white Gaussian noise. The most robust features were HIST, WL, and MNF. Individually, WL was the best feature for discerning between different upper-limb motions. MAV and WAMP were also found to be useful features. AR features and RMS were useful for noisy situations.

2.8.3.6 Feature Set Evaluation

The Hudgins feature set, developed by Hudgins in 1993, consists of the following five time domain features: MAV, SSC, WL, ZC, and MAVS [90]. MAVS is typically omitted from the Hudgins set in the most recent literature [86]. Many myoelectric devices implement the Hudgins feature set or a variation of the Hudgins feature set because it includes features that are effective for motion classification and are computationally simple to extract [86]. The ZC and SSC features have similar spatial distributions, therefore the Hudgins set can be simplified to include only MAV, WL, and SSC without a large reduction in classification accuracy [80]. Oskoei and Hu [87] determined that the Hudgins feature set worked well for pattern classification, but that a feature set of RMS and AR2 was best for time segments of 200 ms. Phinyomark *et al.* [80] concluded that time domain features are superior to frequency domain features because time domain features achieve similar classification accuracies, but require less computational resources.

Haddara [12] compared six sEMG features (RMS, MAV, MSA, ZC, MDF, MNF) collected from elbow trauma patients and a group of healthy subjects. Statistically significant differences were primarily identified using the RMS and MAV features. The RMS and MAV features collected from the patients at the end of the therapy program were found to more closely resemble the healthy population. The frequency domain features, MDF and MNF, showed no significant differences between the groups.

2.8.3.7 Feature Reduction

Feature reduction is performed to reduce the dimensional space of the feature set, which can improve both the speed of classification and the classification accuracy. The most common feature reduction method applied to EMG signals is principal component analysis (PCA).

2.8.3.8 Principal Component Analysis (PCA)

PCA is a method of representing data in a lower dimensional feature space. PCA develops new features in a lower dimensional space by projecting existing features along the directions of their greatest variances. The feature data are projected onto the most significant eigenvectors of the covariance matrix of the data. PCA is for data representation, not for data classification, therefore PCA is only effective for data classification if the directions of the greatest variances are important for classification [83]. PCA has been successfully applied to several EMG motion recognition problems in order to improve the classification accuracy and increase the classification rate [110].

2.8.4 Classification Models

This section reviews the classifiers commonly used in the literature to develop models for EMG signals. Machine learning classifiers (including linear discriminant analysis (LDA), support vector machines (SVM), k -nearest neighbours (k -NN), and decision tree classifiers), and artificial neural network (ANN) classifiers are described below.

2.8.4.1 Linear Discriminant Analysis (LDA)

LDA uses hyperplanes to separate a feature space into linear decision regions. LDA minimizes the distances between feature vectors of the same class, and maximizes the distances between different classes. Observations within each class are assumed to come from a Gaussian distribution, and the covariance of all classes is assumed to be equal, therefore LDA is best for Gaussian distributions with equal covariance, but can work well for data with other distributions. The LDA decision regions must be spatially contiguous and convex. If the regions are not linearly separable, a linear machine will not work [111].

LDA is a robust classifier and is advantageous for embedded processors involved with real-time applications because it provides fast prediction speeds and small memory usages. LDA has been applied to a variety of EMG classification problems [112], and is generally found to provide acceptable classification accuracies [86] and to provide superior classification accuracies for fluctuating EMG signals [98].

2.8.4.2 Quadratic Discriminant Analysis (QDA)

Quadratic discriminant analysis (QDA) is an extension of LDA that assumes each class has a different covariance matrix. QDA is best for large data sets as it may overfit data sets with a low number of observations and high variance. QDA provides nonlinear quadratic decision boundaries. LDA performance for classifying EMG signals is typically better or comparable to QDA [113,114].

2.8.4.3 Support Vector Machines (SVM)

An extension of the LDA classification method is the SVM classifier, which uses separating hyperplanes to distinguish between two classes of data. An ideal separating hyperplane should be as far away as possible from any sample, to maximize the probability of classifying new data correctly. If a hyperplane cannot be constructed to separate all classes, a margin must be tuned to allow for some violations. The data samples that are closest to a separating hyperplane are called “support vectors”. These data are the most difficult to classify. An optimal SVM separating hyperplane is defined solely by the support vectors. The SVM classifier is robust to observations far from the hyperplane. The SVM method only works for two-class problems, however, multiple SVM classifications can be performed to apply this method to multi-class problems [111].

Pattern classifications in high dimensional space are more likely to be linearly separable than in low dimensional space. Data can be projected into higher dimensions to achieve better classifications. Since these types of functions require high computational power, they can be solved implicitly using kernel functions. Commonly used kernel functions include the polynomial kernel function and the radial basis function [111].

The SVM classifier typically allows for better classifications than LDA, but the prediction speed and memory usage is worse than for LDA. The SVM classifier has been used for many EMG

applications including motion classification [87] and the diagnosis of neuromuscular disorders [115].

2.8.4.4 K-Nearest Neighbours Classification (k -NN)

The k -NN classification method works well on data that are not linearly separable. k -NN is an unsupervised learning method that allows unlabeled data to be organized into “clusters.” Clusters of data should have small inter-cluster distances, and large intra-cluster distances. Data points are assigned to the clusters such that the sum of the squares of the distances of each data point to the centre of the cluster is at a minimum. k -NN classifies each new datum by determining the most common class among the k closest data points. k -NN was found to be very effective for using sEMG forearm signals to distinguish between upper-limb motions [113, 114].

2.8.4.5 Decision Trees

Linear models are simple, but perform poorly if the relationships between features are non-linear. Decision tree classifiers are simple models that provide easily interpretable results, and can outperform linear models when classifying non-linear data. A single decision tree classifier determines an outcome based on a series of splitting rules starting at the top of a tree and continuing into a series of branches. The decision tree stratifies the feature space into regions to provide the prediction.

A single decision tree model is susceptible to over-fitting and a lack of robustness. These problems can be avoided by aggregating many decision trees. The tree bagging method builds hundreds to thousands of decision trees by taking repeated samples from the data set. The most common decision obtained from the trees is used as the final output.

An improvement upon the tree bagging method is the random forest (RF) algorithm, which ensures that decision trees will not be highly correlated due to the influence of a very strong predictor. The RF algorithm prevents decision tree models from considering most of the available predictors at each split (usually the number of predictors considered is the square root of the total number of predictors) [48].

2.8.4.6 Artificial Neural Networks (ANNs)

The ANN is another classification method that works well for non-linear data. ANNs are designed to imitate the networks of neurons in the brain. The most basic ANN is the multilayer perceptron, or feed-forward neural network, which consists of an input layer of neurons, one or more hidden layers, and an output layer. The output of each neuron is determined by a non-linear function of the sum of its inputs.

ANNs have high generalization abilities and can learn directly from large data sets. They work well with data that are not linearly separable, or when the classes of the training data are unknown. ANNs can be also be implemented in real-time.

ANN models have been used for the classification of motions [81]. Often a back-propagation neural network is employed. More sophisticated ANNs such as deep belief networks [116] have been used to classify sEMG signals with greater success than traditional methods such as LDA. ANNs have also been successfully used with needle EMG data to classify neuromuscular disorders [9].

2.8.4.7 Classification Model Evaluation

Classification models, as the ones presented above, should be developed using a training set and a validation set. The model is fitted using the training set, and then the fitted model is used to predict the classes of the validation set and to determine the classification error.

k -fold cross-validation divides the data set into k groups, or folds. The first fold is the validation set and the remaining $k - 1$ folds are the training set. This procedure is repeated k times, and the average of the classification error is obtained [111].

Leave-one-out cross-validation can be used for data sets with a low number of observations. A single observation is used as the validation set, and the remaining observations are used as the training set. This is repeated until each observation has been used as the validation set, and the average of the classification error is obtained. This method decreases the bias in determining the classification error [111].

2.9 Conclusion

This chapter reviewed the anatomy of the elbow, and the motivation and methods for elbow rehabilitation following trauma. The prior art in robot-assisted upper-limb rehabilitation was described. Finally, EMG data acquisition, analysis, and classification methods were reviewed. These topics will be explored in the following section in order to progress towards an EMG model of muscle health.

Chapter 3

Data Collection and Processing

This chapter describes the procedure for EMG data collection and processing. The following section outlines the equipment, patient recruitment, electrode placement, data collection protocol, and signal processing methods implemented to move towards the objective of quantifying health in patients rehabilitating from elbow trauma.

3.1 Equipment

3.1.1 Acquisition System

The sEMG signals were collected with a commercial wireless myoelectric system (Trigno Wireless system, Delsys Inc., USA). The Trigno system includes a base station that interfaces with 16 wireless radio frequency sensors (Figure 3.1). Each $27 \times 37 \times 15$ mm sensor (Figure 3.2) was composed of sEMG electrodes and a triaxial accelerometer. The EMG sampling frequency was 1925.93 Hz and the accelerometer sampling frequency was 148.1 Hz. The signals were amplified 300 \times and filtered on-board with a 20–450 Hz Butterworth bandpass filter. The signals were digitized with a 16 bit A/D converter with 168 nV/bit resolution.

The sEMG detection system consisted of four silver bar electrodes. The electrodes were arranged into two pairs of contacts: 1) a positive signal detection and reference contact, and 2) a negative signal detection and reference contact. This unique electrode configuration was designed to eliminate the need for a separate reference electrode. The stabilizing reference electrodes re-



Figure 3.1: Trigno base station for charging and RF communication with sEMG sensors.

duced motion artifact by limiting the impact of disturbances on the surface of the skin [117]. The contact surface on the skin for each bar was 5×1 mm, and the IED was 10 mm. The sensors were affixed to the skin using Trigno Sensor Skin Interface (SCF03) double-sided adhesive stickers.

The Trigno commercial system was selected for data collection because it promised to mitigate common sEMG signal acquisition difficulties, while fulfilling the requirements for sEMG data collection. The use of a wireless system ensured for more natural movements and eliminated the possibility of motion artifacts due to moving electrical cables. The use of silver electrodes eliminated the need for gel which simplified the data acquisition process, and was more suitable for a prospective wearable application.

3.1.2 Data Recording and Analysis Software

Data were recorded with the Delsys EMGworks 4.3.0 Acquisition software installed on a laptop (Figure 3.3). Delsys EMGworks 4.3.0 Analysis software (Figure 3.4) was used to convert the data to comma-separated format. All off-line data analysis was performed using MATLAB software (The MathWorks Inc., Natick, MA, USA, Version R2017b).

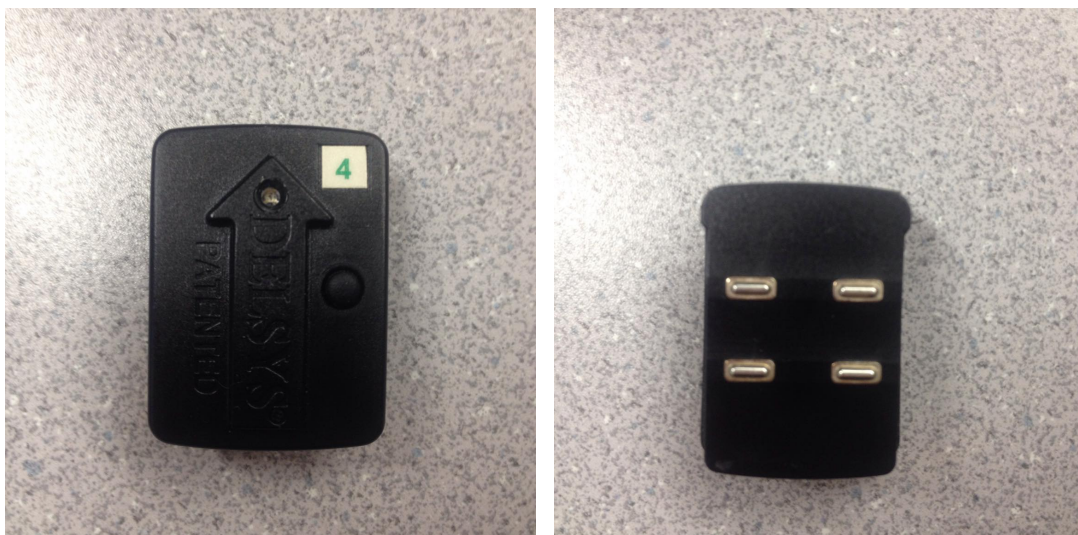


Figure 3.2: Trigno sensor. The front of the sensor (left) includes an arrow to assist with the direction of sensor placement. The arrow should be aligned in the direction of the muscle fibres. The x axis of the accelerometer is parallel to the sensor arrow, and y axis is perpendicular and coplanar to the sensor arrow. The back (right) of the electrode contains 4 bar electrodes.

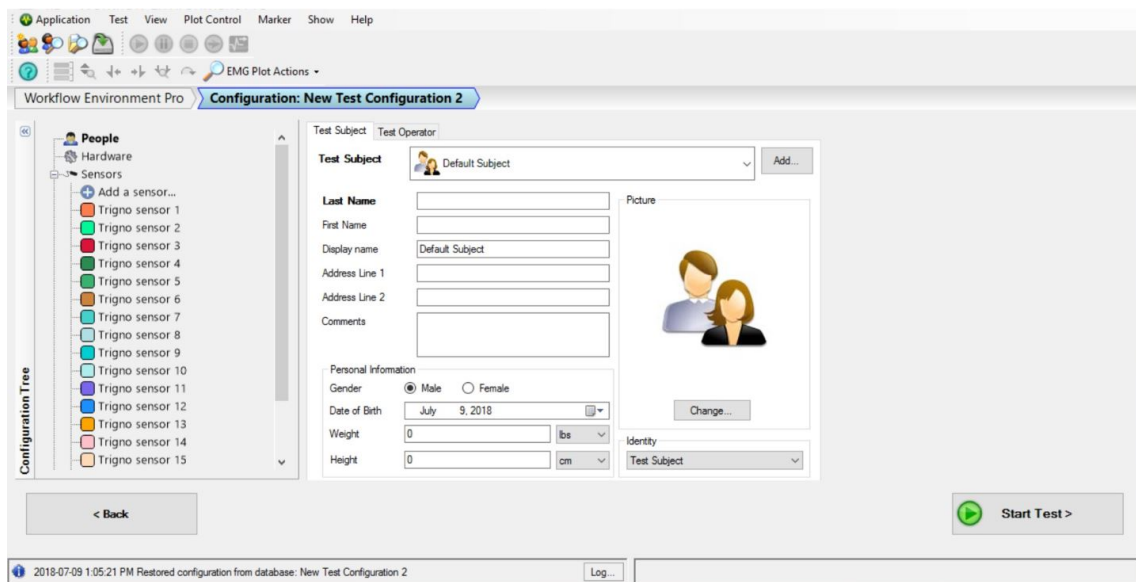


Figure 3.3: Data acquisition software.

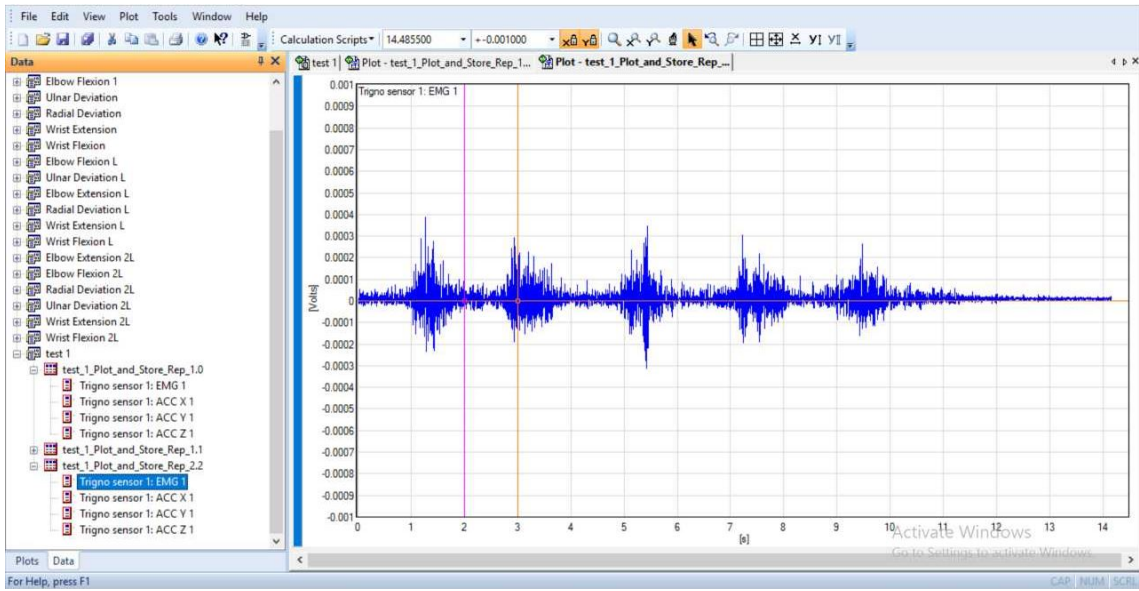


Figure 3.4: Data analysis software.

3.1.3 Load Cell

A load cell (American Archery Products M110 Digital Bow Hang Scale 110 lbs) with an accuracy of 0.05 lbs was used to obtain the peak weight and the holding weight exerted when performing flexion MVC and extension MVC (Figure 3.5).



Figure 3.5: Load cell.

3.2 Patient Recruitment

Trials began after permission was received from the Human Research Ethics Board at Western University. Patients were recruited over a period of 12 months from January to December 2017 from the Roth McFarlane Hand and Upper Limb Centre at St. Joseph's Hospital in London, Ontario. All patient trials were performed at St. Joseph's Hospital. Patients were excluded from the trials if they indicated that they had congenital musculoskeletal defects, or if they had previously experienced elbow trauma on their contralateral limb. The majority of patients (92%) presented with elbow fractures resulting from elbow trauma. Other injuries studied were biceps tendon tears and surgery to treat osteoarthritis. Table 3.1 shows a summary of the patient information.

Table 3.1: Elbow trauma patient information.

Sex	Age (years)	Height (cm)	Weight (kg)	Injured Hand	Time since Injury (weeks)
21 Male 9 Female	45.0 ± 11.5	175 ± 9.8	89.2 ± 20.3	17 Dominant 13 Non-Dominant	9.6 ± 5.9

3.3 Electrode Placement

Electrodes were placed to obtain sEMG recordings from the following muscles:

1. Biceps brachii (BB)
2. Triceps brachii lateral head (TBlat)
3. Triceps brachii long head (TBlong)
4. Pronator teres (PT)
5. Brachioradialis (BRD)
6. Extensor carpi ulnaris (ECU)
7. Flexor carpi ulnaris (FCU)

Electrodes were placed on the skin in accordance to the SENIAM recommendations [71]. The muscle groups not included in SENIAM were placed in the direction of the muscle fibres near the belly of the muscle as recommended by literature guidelines [60]. A sensor was also placed on the inside of the patient's wrist to collect acceleration data. Figure 3.6 and Figure 3.7 indicate the anterior and posterior views of the electrode placement, respectively.

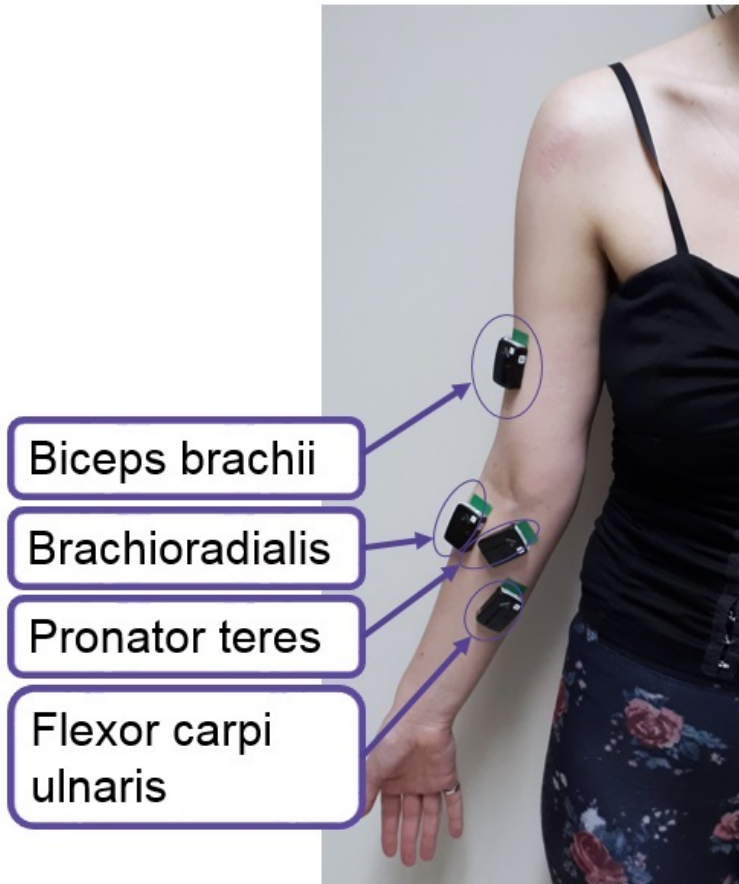


Figure 3.6: sEMG sensor placement (anterior view).

3.4 Motions

This section describes the motions performed during each trial. The motions were selected based on standard elbow rehabilitation exercises. Wrist and hand exercises were included because elbow trauma patients are also encouraged to perform wrist and finger exercises during rehabilitation [16]. The forearm, wrist, and hand exercises were performed with the elbow held at approximately 90

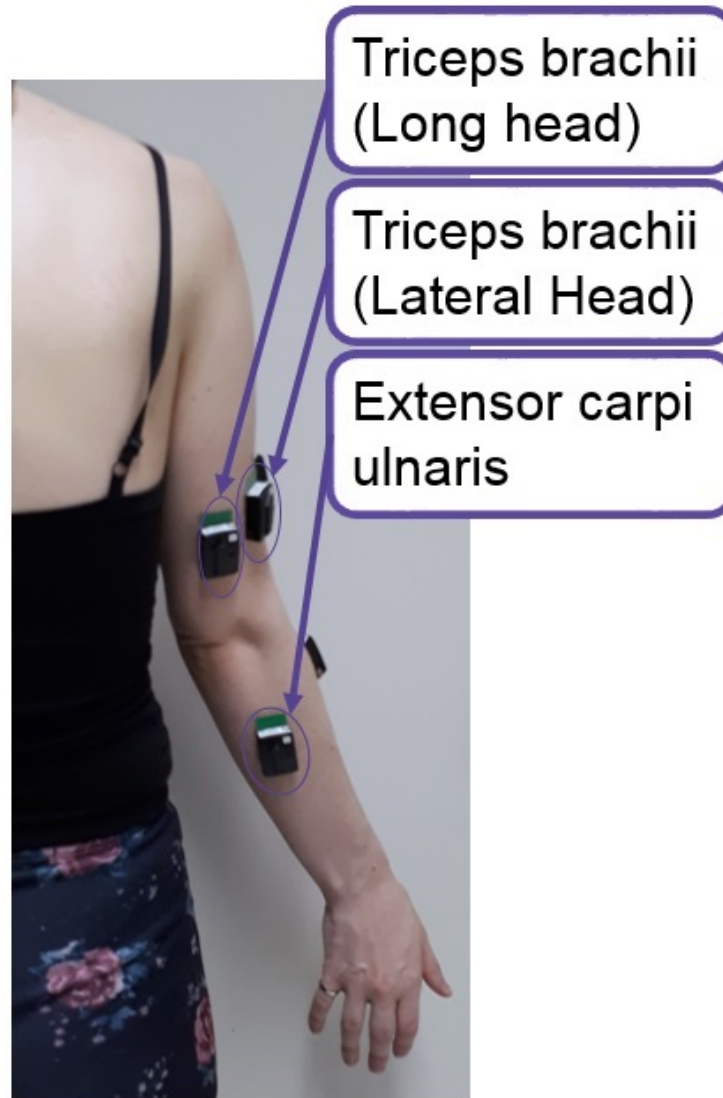


Figure 3.7: sEMG sensor placement (posterior view).

degrees.

1. Elbow Flexion–Extension: Patients were asked to perform elbow flexion (EF) by moving the forearm from approximately 0 degrees to the maximum point of flexion, approximately 120 degrees for healthy subjects [13] (Figure 3.8). Elbow extension (EE) was then performed by moving the arm from the point of maximum possible flexion back to a relaxed position (Figure 3.9). The patients were instructed to keep the wrist at a neutral position while performing this motion.



Figure 3.8: Elbow flexion (EF).



Figure 3.9: Elbow extension (EE).

2. Forearm Pronation–Supination: Patients were asked to perform forearm pronation (P) by rotating the forearm until the palm of the hand faced down (Figure 3.10). Forearm supination (S) was performed by rotating the forearm so that the palm of the hand faced up (Figure 3.11).



Figure 3.10: Forearm pronation (P).

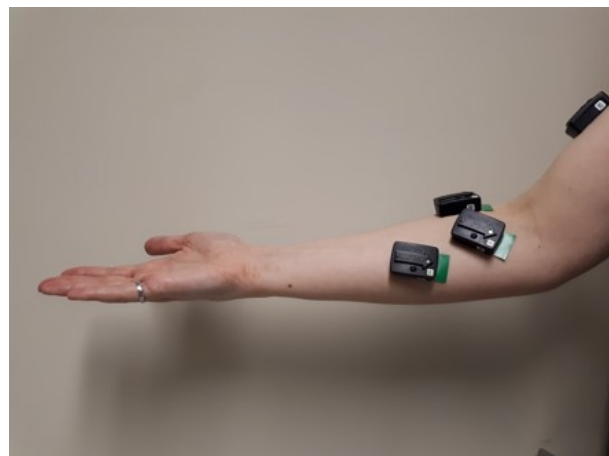


Figure 3.11: Forearm supination (S).

3. Wrist Flexion–Extension: Patients were asked to perform wrist flexion (WF) (Figure 3.12) and wrist extension (WE) (Figure 3.13).



Figure 3.12: Wrist flexion (WF).



Figure 3.13: Wrist extension (WE).

4. Ulnar–Radial Deviation: Patients were asked to perform ulnar deviation (UD) by moving the hand downward towards the ulna (Figure 3.14) and radial deviation (RD) by moving the hand upward towards the radius (Figure 3.15).

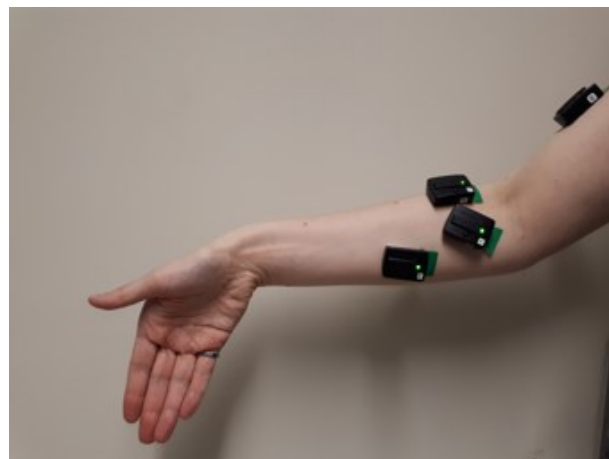


Figure 3.14: Ulnar deviation (UD).



Figure 3.15: Radial deviation (RD).

5. Hand Open–Close: Patients were asked to close their hand into a fist (HC) (Figure 3.16), and then to open their hand with their fingers spread out (HO) (Figure 3.17).



Figure 3.16: Hand close (HC).



Figure 3.17: Hand open (HO).

6. Maximum Voluntary Contraction (MVC): An elbow flexion MVC was performed by having the patient pull up on a band attached to the load cell. An extension MVC was performed by pulling down on the load cell (Figure 3.18). Patients were instructed to avoid using their shoulder to assist with this exertion and to keep the elbow at a 90 degree angle. The EMG signals and the maximum force exerted in pounds were recorded for each MVC.



Figure 3.18: Extension MVC.

3.5 Data Collection Protocol

The following protocol was adopted for all patients. If specific motions were deemed unsafe by the patient's therapist, these motions were not performed.

1. Patients were asked to report the following information:
 - (a) Age
 - (b) Sex

- (c) Height
 - (d) Weight
 - (e) Dominant Hand
 - (f) Type of Injury
 - (g) Date of Injury and/or Surgery
2. The sEMG sensors were placed on the areas specified in Section 3.3 on both the injured and contralateral uninjured limb.
 3. The patient was asked to perform the following sets of motions:
 - (a) Elbow Flexion–Extension (EF–EE)
 - (b) Forearm Pronation–Supination (P–S)
 - (c) Wrist Flexion–Extension (WF–WE)
 - (d) Ulnar–Radial Deviation (UD–RD)
 - (e) Hand Open–Close (HO–HC)

Each motion set was performed with the injured arm three times and with the healthy arm three times. The patient was instructed to perform all motions at a comfortable pace.

4. If agreed upon by the therapist, the patient was asked to perform a static elbow flexion MVC and a static elbow extension MVC with both the injured and uninjured limb. A load cell was used to record the maximum force exerted.

3.6 Data Processing

The EMG signals were further processed and filtered prior to feature extraction. The data processing was performed using MATLAB. The steps of data processing, data segmentation, feature extraction, feature selection, and classification are described in this section.

3.6.1 Data Segmentation

The EMG data were divided into segments representing each motion based on muscle activation. The double-threshold method for detecting EMG onset [75] was used to facilitate segmentation. The first threshold, $th1$, (the amplitude the EMG signal must exceed) was defined as $\bar{b} + 15\sigma$, where b is the baseline value of the EMG signal and σ is the standard deviation of b . The second threshold, $th2$, (the number of consecutive EMG samples that must exceed $th1$) was set to 25 based on trial and error. The signals were conditioned with the Teager–Kaiser energy operator (TKEO) using Equation 2.1 and then rectified and passed through a 2nd order Butterworth 50 Hz low pass filter to improve the robustness and accuracy of muscle activation onset detection [79]. An example of the segmentation output is shown in Figure 3.19.

The segmentations for each EMG recording were verified visually and sets that were not segmented correctly by the algorithm were segmented manually. About 50% of the data sets had to be resegmented manually. Data sets from three subjects were excluded from further analysis after visual inspection indicated that the data were corrupted.

3.6.2 Filtering

The EMG signals were filtered with a 2nd order Butterworth 20–400 Hz band pass filter in order to remove low frequency motion artifacts, and uninformative high-frequency components. The signals were also filtered with a 60 Hz notch filter to reduce power line interference in accordance with literature recommendations [67].

3.6.3 Feature Extraction

Forty EMG features were extracted from each EMG segment. The definitions for these features were provided in Section 2.8.2. These features were also used to develop three preliminary feature sets, as follows:

- Feature Set 1 (FS1) : MAV, SSC, WL, ZC.
- Feature Set 2 (FS2) : RMS, AR2.

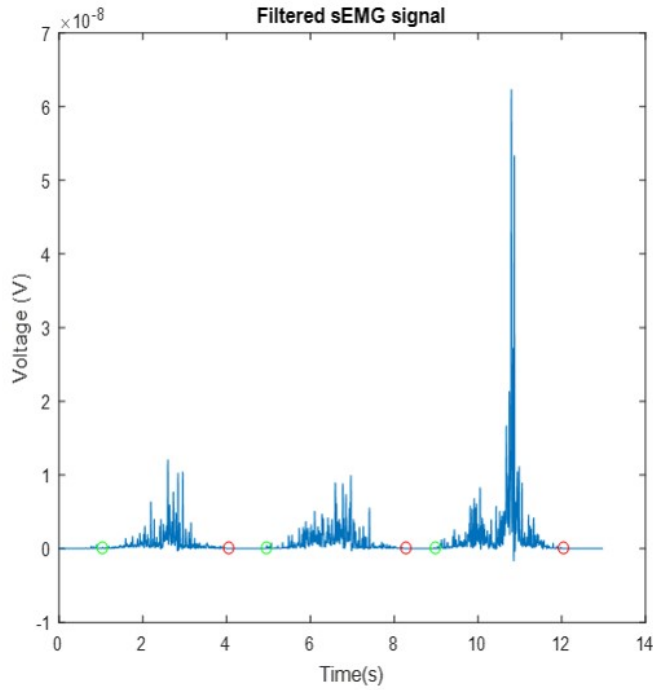


Figure 3.19: Segmentation for EMG signal filtered with TKEO. The green circle indicates the point of muscle activation. The red circle indicates the point of muscle deactivation.

- Feature Set 3 (FS3) : MSA, MSF, MSS, MNPPS, MSD.

FS1 is the Hudgins feature set [90]. FS2 is the feature set developed by Oskeoi and Hu [87] that was observed to perform well for motion classification. FS3 is a feature set consisting of spike shape features [104].

Each feature was calculated from the signal collected over the entire motion. One feature was obtained for each muscle. For example, for FS1 there were $4 \text{ features} \times 7 \text{ EMG muscle channels} = 28$ total features in the feature vector for each segment.

3.6.4 Classification

Classification models were developed and evaluated for each of the ten motions separately. The LDA, SVM, and RF classification models were investigated. The LDA classifier was selected because it is simple, and has been found to be effective for classifying EMG signals in the literature. The SVM classifier was selected as an extension of the LDA classifier. The RF classifier was selected due to its usefulness for classifying stroke rehabilitation outcomes [118]. The RF

classifier was generated from 200 decision trees. Classification models were initially developed to distinguish between healthy and injured limbs. The classification models were also investigated for distinguishing between patients at two different stages of rehabilitation: 0–6 weeks and 7+ weeks.

3.6.5 Evaluation

The classification accuracies were evaluated for each model using a leave-one-patient-out cross-validation method [119]. All of the trials from one patient were used as a test set, and the remaining patients were used as the training set. This process was repeated for each patient. The accuracy was calculated as the number of correct classifications divided by the total number of patients.

3.6.6 Optimization of Feature Sets and Models

Both the feature sets and classification models were further optimized. A majority vote was performed for each patient to combine the outputs of the individual motion models. The majority vote models were further optimized by generating weighted majority vote models.

The process of feature selection was performed in two ways. The best individual features were found by comparing their individual performances in a majority vote model. The RELIEFF algorithm [108] was used with $k=10$ as recommended in [118] to search for the best combinations of features within a feature set.

3.6.7 Identification of Patient Characteristics Influencing the Perception of Patient Health

Following the development and testing of the various classification models, the influence of patient characteristics (sex, age, body mass index (BMI), and the time since injury) on the outcomes of the models was investigated. The patient characteristics were input into the classification models as non-zero ordinal categories, and the models were reevaluated. Decision tree models were explored to determine the patient characteristics that were used for splitting rules.

This chapter described the methods of data collection and processing, feature extraction and selection, and classification model development. The next chapter will describe and discuss the results of the feature selection and the classification model performance.

Chapter 4

Results and Discussion

This chapter describes the results obtained following the execution of the procedure of EMG data collection and analysis described in Chapter 3. First, models were developed to classify between the healthy and injured limbs of subjects. Feature sets based on recommendations in the literature were used for the initial classification. Models were developed for each individual motion, and were then aggregated into majority vote models. New feature sets were developed and optimized based on the performances of individual features. Optimization of the feature sets was performed using the RELIEFF algorithm.

Further explorations were conducted towards improving the classification models. Patient characteristics were added to the models to determine if knowledge of specific characteristics could improve the classification. Time windowing of the EMG data was also investigated. Finally, models were developed to investigate the possibility of classifying between different stages of rehabilitation.

A statistical analysis was performed to identify EMG feature differences between healthy and injured limbs. An analysis was also performed on returning patients to study the changes in EMG features following therapy.

4.1 Healthy–Injured Models

A preliminary goal was to determine if classification models based on EMG features could be developed to distinguish between the healthy and injured limbs of patients. This section describes

the development and evaluation of classification models to differentiate between two levels of health (healthy and injured).

4.1.1 Preliminary Feature Sets

Three preliminary feature sets (FS1–FS3) were developed based on feature set recommendations in the literature. Features were extracted from EMG segments consisting of the entire motion. Classification models were developed for each individual motion. Classification accuracies were obtained using a leave-one-patient-out cross-validation. The classification results for each feature set and motion are shown in Table 4.1.

The models distinguished between the two levels of health with accuracies ranging from 45.9–79.6%, depending on the classification algorithm and the motion. The RF models provided the best classification accuracies for the majority of the motions when used with FS1 and FS2. For example, the RF classification accuracies for FS1 ranged from 56.8–72.2%, while the LDA and SVM classification accuracies ranged from 55.6–69.1% and 54.9–67.9% respectively (Figure 4.1). The better performances of the non-linear RF classifier suggest that many of the relationships between the features in FS1 and FS2 that influence health are non-linear. There was no evident best classifier for FS3, although the best accuracy was obtained with the LDA model for WF, which provided an accuracy of 79.6%.

The performances of the classification models were influenced by the feature sets. When compared to FS1, FS2 had similar performances and performed similarly with the various classifiers, but had an overall worse performance than FS1. FS3 was unique in that there was not a single classifier that was the best, however, FS3 also provided the highest accuracies out of all feature sets. These observations are consistent with the literature, which suggests that feature set selection is more important than classifier selection for obtaining good classification accuracy with EMG signals [67].

The addition of more features in the feature set can improve accuracy, until an asymptote is reached, at which point adding new features will not improve the accuracy [80]. FS1 consisted of four features. FS2 contained two features, although the AR2 feature produced two values per window, providing the FS2 with effectively three features in the feature set. FS3 contained five

Table 4.1: Classification accuracies for each feature set. The best classification result for each motion within each feature set is in bold.

Feature Set	Motion	Classification Accuracy (%)		
		LDA	SVM	RF
FS1 (MAV, SSC, WL, ZC)	EF	62.3	60.5	70.3
	EE	65.4	62.3	71.6
	P	69.1	67.9	67.3
	S	60.5	62.3	68.5
	WF	67.3	56.8	69.1
	WE	55.6	64.8	56.8
	UD	58.6	62.3	71.6
	RD	61.7	65.4	66.0
	HC	64.8	54.9	72.2
FS2 (RMS, AR2)	HO	55.6	61.1	57.4
	EF	59.9	57.4	67.9
	EE	61.7	64.8	69.8
	P	67.3	49.4	71.6
	S	58.6	54.9	69.8
	WF	63.6	59.3	65.4
	WE	60.5	54.3	59.9
	UD	62.3	57.4	63.0
	RD	59.1	45.9	69.2
FS3 (MSA, MSF, MSS, MNPPS, MSD)	HC	63.0	56.2	66.7
	HO	58.6	64.2	63.0
	EF	74.1	61.1	64.8
	EE	61.1	77.8	68.5
	P	72.2	63.0	61.1
	S	50.0	63.0	72.2
	WF	79.6	64.8	75.9
	WE	57.4	66.7	64.8
	UD	72.2	68.5	61.1
	RD	61.1	77.8	57.4
	HC	57.4	59.3	64.8
	HO	48.2	50.0	51.9

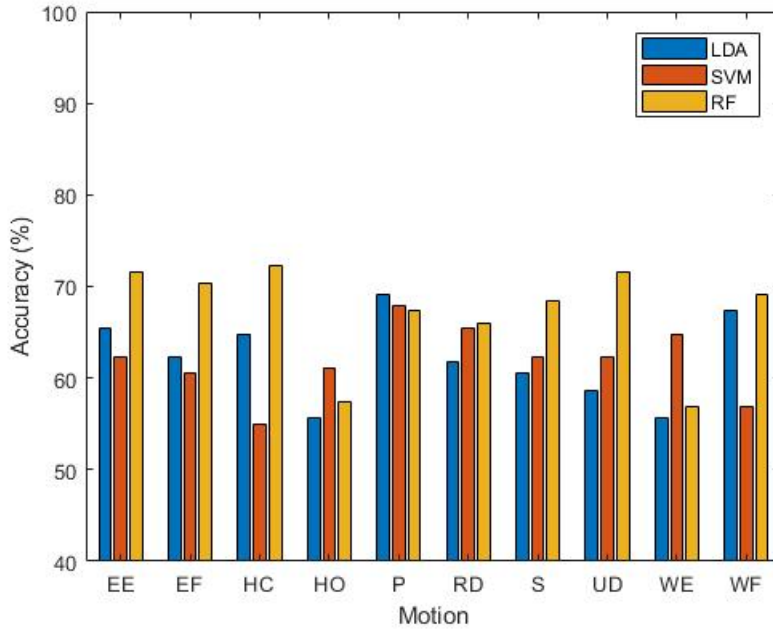


Figure 4.1: Classification accuracies for each motion when using the LDA, SVM, and RF classifiers with FS1. The range of the y axis has been adjusted for clarity. The motions tested were as follows: elbow flexion (EF), elbow extension (EE), forearm pronation (P), forearm supination (S), wrist flexion (WF), wrist extension (WE), ulnar deviation (UD), radial deviation (RD), hand close (HC), and hand open (HO). The RF classifier tended to provide the best accuracy.

features. The inclusion of a greater number of features in FS1 compared to FS2 could account for the better classification performances of FS1. Likewise, FS3 contained the greatest number of features of the three feature sets tested, and displayed higher accuracies than FS1 and FS2.

The initial classification results also suggest that some motions are better than others for classifying patient health. The EE motion provided the range with the highest accuracies overall (62.3–77.8%). The models for the WE and HO motions provided the ranges with the lowest classification accuracies (54.3–66.7% and 48.2–64.2% respectively). All other motions achieved a classification accuracy of at least 72.2% for one of the models, however the RD motion provided classification accuracies below 70% with the exception of only one classification model. Table 4.2 shows the range of classification accuracies for each motion.

The WE, HO, and RD motions are hand and wrist motions, therefore, the performance of these motions may be less impacted by an injury to the elbow. For example, the HO motion involves the

relaxation of the forearm muscles as the hand is released from the closed position, which may be less strenuous on the elbow. The lower classification performances may also be due to the muscles involved in the motion. The primary muscles involved in RD, the extensor carpi radialis and the flexor carpi radialis, were not used as inputs for the classification models. The WE motion is primarily performed by the ECU muscle, which suggests that the activation of the ECU muscle is less informative for assessing elbow health.

The performances of the initial models ranging from 45.9–79.6% were not ideal. This raises the possibility of exploring additional options to improve the performance. The next section will describe the aggregation of the individual motion models into single models in an attempt to improve the classification performances.

Table 4.2: Range of classification accuracies for each motion.

Motion	Classification Accuracy (%)
EF	57.4–74.2
EE	62.3–77.8
P	49.4–72.2
S	50.0–72.2
WF	56.8–79.6
WE	54.3–66.7
UD	57.4–72.2
RD	45.9–77.8
HC	54.9–72.2
HO	48.2–64.2

4.1.2 Majority Vote Models

The classification models for each motion were next aggregated into a majority vote. The decision agreed upon by the majority of the ten individual motion models for each patient was selected as the final classification result. This procedure reduced the effect of errors made by individual motion models. The majority vote models were evaluated using a leave-one-patient-out cross-validation. The results of the majority votes for each feature set and classification model are shown in Table 4.3.

The classification accuracies ranged from 58.6–74.7%. Most of the accuracies obtained with the majority vote models were within the upper range of accuracies that had been achieved with the individual motion models. Two of the majority vote models (SVM with FS1 and LDA with FS2) surpassed the accuracies of all of the individual motion models (see Table 4.1). This indicates that misclassification can be reduced by performing a majority vote, although the motion models often still agree on incorrect classifications.

Table 4.3: Majority vote classification accuracies. Majority vote decisions were developed from all ten motions. The best classification results within each feature set are in bold.

Feature Set	Classification Accuracy (%)		
	LDA	SVM	RF
FS1	67.9	69.8	71.0
FS2	70.4	58.6	69.8
FS3	71.6	74.7	71.6

The majority vote model was further extended by implementing a weighted majority vote decision. The individual motion models were weighted by their respective classification accuracies. For example, when using the LDA classifier with FS1, the weights for each decision model were selected as follows: EF = 62.3, EE = 65.4, P = 69.1, S = 60.5, etc., based on the classification results found in Table 4.1. The sum of the weights of the decision models that identified the patient as healthy was determined, as well as the sum of the weights of the models that identified the patient as injured. The highest sum (representing either healthy or injured) was selected as the final weighted majority vote decision. The classification results for the weighted majority vote are shown in Table 4.4. The weighted majority vote classification accuracies ranged from 64.8–77.2%, and the weighted vote provided improvements to the basic majority vote classification accuracy for all models. This improvement was expected, as the influence of models that were known to be less accurate was reduced. The weighted majority vote provided the highest accuracies when combined with the RF classifier.

The weighted majority vote requires the prior knowledge of how to weight the motion models, and still requires the patient to perform all ten motions. The benefits of using a weighted majority vote could be improved if some of the motions were completely eliminated from consideration in

Table 4.4: Weighted majority vote classification accuracies. The best classification results within each feature set are in bold.

Feature Set	Classification Accuracy (%)		
	LDA	SVM	RF
FS1	72.2	71.0	74.1
FS2	73.5	64.8	75.3
FS3	71.6	73.5	77.2

the vote. This would decrease the number of motions that a patient would be required to perform, as well as the size of the input data sets.

The WE and HO motions provided low ranges of classification accuracies (Table 4.2), so they were eliminated from the majority vote decision. The RD motion was also removed from the majority vote decision because, with the exception of one classification model, the individual motion models provided classification accuracies below 70%. Majority vote decisions based on the outputs of the top motions (EF, EE, P, S, WF, UD, and HC) were weighted equally. The classification results for the majority vote models using only the top motions are shown in Table 4.5.

Table 4.5: Majority vote classification accuracies of majority vote decisions developed from the top motions (EF, EE, P, S, WF, UD, and HC). The best classification results within each feature set are in bold.

Feature Set	Classification Accuracy (%)		
	LDA	SVM	RF
FS1	70.4	69.1	75.3
FS2	69.1	60.5	67.9
FS3	72.2	72.8	74.1

The majority vote classification accuracies ranged from 60.5–75.3% for the top motion models. The highest classification accuracy of 75.3% was achieved using the RF classifier combined with FS1.

The implementation of only the top motion models in the majority vote improved upon the original majority vote. However, out of the three majority vote types investigated, the weighted majority vote provided the best classification accuracies. It should be noted that the improvements

obtained by using the weighted models and the top motion models may have upward bias, as the same set of patient data was used to validate these models.

The majority vote models provided more consistent results than the individual motion models, however, a maximum accuracy of only 77.2% was achieved. Other potential methods of improving performance will be discussed in the following sections.

4.2 Data Windows

The classification models for health must be implemented in a wearable device, which will restrict the computational power and memory of the system. Data windowing would allow for smaller data sets, faster processing times, and lower computational and memory requirements. Data windowing would also be able to provide real-time estimates of patient health. The classification models discussed so far in this chapter were developed from features that were extracted from the entire segment of the EMG signal representing each motion. This section will discuss the effect of applying data windows to the patient data.

The EMG data from each motion were divided into the following segmentation windows of 50% overlap: 250 ms with 125 ms increments, and 125 ms with 75 ms increments. The segmentation window sizes were based on commonly used window sizes in the literature, and the recommended window sizes for myoelectric control [85, 86].

FS1–FS3 were extracted from the data windows. Classification models were developed for each feature set and motion individually, and were evaluated using a leave-one-patient-out cross-validation. The classification results for the 250 ms windows are shown in Table 4.6, and the results for the 125 ms windows are shown in Table 4.7. The accuracies for the 250 ms windows ranged from 52.0–70.8%, and the accuracies for the 150 ms windows ranged from 49.3–69.8%.

The performances of the window sizes depended on both the classifier used and the motions that were performed. Windows consisting of the entire motion tended to provide better results for the RF classifier (Figure 4.2). Windows for the full motion also tended to provide better performances for the EF, EE, P, and WF motions. The 250 ms window worked best for the HO motion. The 150 ms and 250 ms windows both tended to outperform the full window when used

Table 4.6: Classification accuracies for each feature set extracted from window segments of 250 ms with 50% overlap. The best classification result for each motion within each feature set is in bold.

Feature Set	Motion	Classification Accuracy (%)		
		LDA	SVM	RF
FS1 (MAV, SSC, WL, ZC)	EF	62.4	65.0	61.1
	EE	64.6	65.0	67.0
	P	63.1	60.4	65.8
	S	65.8	61.9	68.1
	WF	64.9	61.2	60.4
	WE	62.6	63.6	63.2
	UD	65.8	65.2	63.9
	RD	65.4	63.1	65.1
FS2 (RMS, AR2)	HC	59.0	52.0	68.1
	HO	67.6	65.3	66.0
	EF	62.3	58.2	64.0
	EE	66.4	64.6	65.6
	P	62.3	57.0	59.7
	S	60.9	57.1	64.1
	WF	62.5	56.0	62.9
	WE	67.6	57.6	62.2
FS3 (MSA, MSF, MSS, MNPPS, MSD)	UD	59.7	59.6	65.9
	RD	61.6	57.4	61.6
	HC	62.4	54.3	70.8
	HO	61.4	68.1	64.4
	EF	64.0	67.2	65.0
	EE	63.2	65.0	65.2
	P	63.4	64.2	62.6
	S	69.4	62.6	67.8
	WF	61.1	63.4	60.7
	WE	62.8	65.6	64.6
	UD	65.6	67.2	63.4
	RD	64.5	63.1	70.4
	HC	61.8	53.4	68.0
	HO	64.5	60.0	62.3

Table 4.7: Classification accuracies for each feature set extracted from window segments of 150 ms with 50% overlap. The best classification result for each motion within each feature set is in bold.

Feature Set	Motion	Classification Accuracy (%)		
		LDA	SVM	RF
FS1 (MAV, SSC, WL, ZC)	EF	64.8	63.1	60.8
	EE	64.4	63.6	63.5
	P	61.6	56.9	66.4
	S	68.8	59.2	65.4
	WF	62.0	58.6	61.2
	WE	63.8	60.8	61.1
	UD	65.1	59.5	68.0
	RD	62.7	58.7	69.8
	HC	61.8	52.8	60.8
FS2 (RMS, AR2)	HO	62.1	59.9	59.9
	EF	64.3	60.5	62.8
	EE	65.6	64.8	63.5
	P	61.0	59.6	64.8
	S	62.3	57.3	68.6
	WF	63.7	55.3	63.5
	WE	66.7	60.4	63.2
	UD	63.7	57.5	67.0
	RD	62.3	57.4	67.0
FS3 (MSA, MSF, MSS, MNPPS, MSD)	HC	61.9	57.2	63.4
	HO	57.6	56.9	63.6
	EF	57.5	52.5	59.8
	EE	52.9	48.8	56.2
	P	57.6	50.9	61.9
	S	62.0	59.8	60.8
	WF	61.8	58.4	64.2
	WE	62.9	49.3	63.7
	UD	63.7	53.4	64.4
	RD	57.7	50.2	67.9
	HC	58.1	50.9	56.5
	HO	56.4	49.3	56.8

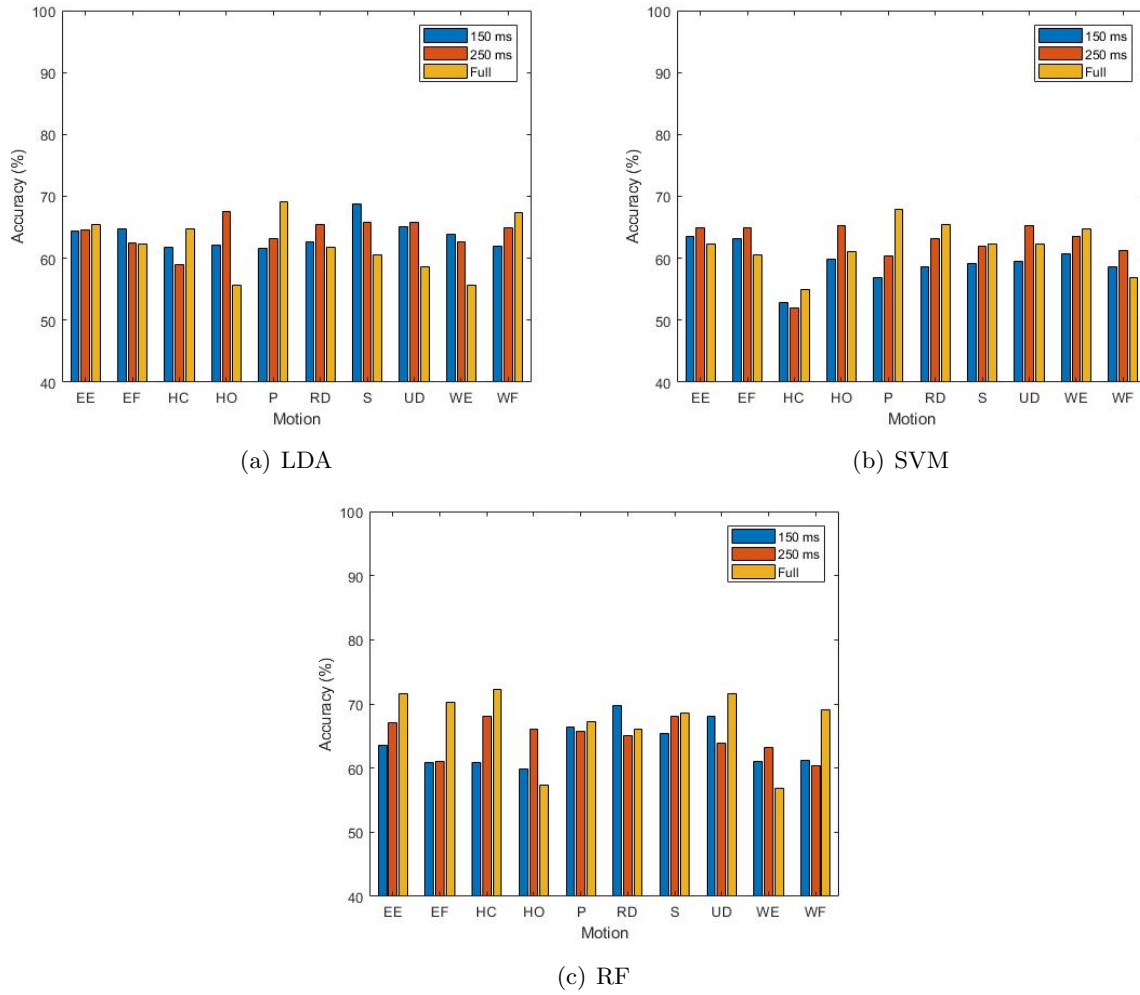


Figure 4.2: FS1 classification accuracies for 150 ms windows, 250 ms windows, and windows consisting of the full motion. The range of the y axis has been adjusted for clarity. The motions tested were as follows: elbow flexion (EF), elbow extension (EE), forearm pronation (P), forearm supination (S), wrist flexion (WF), wrist extension (WE), ulnar deviation (UD), radial deviation (RD), hand close (HC), and hand open (HO).

with the S, WE, RD, and HO motions.

The optimal window size is likely influenced by the average duration of the motions that were performed. Elbow motions (EF, EE, P, and S) typically take more time to perform than wrist and hand motions. The 250 ms and 150 ms window sizes therefore represent a lower proportion of the overall motion for the elbow motions than for the hand and wrist motions.

Changing the window size from 250 ms to 150 ms did not significantly degrade the classification accuracies, which is consistent with Oskoei and Hu's observation that classification accuracies do

not significantly differ if the window size remains between 50–500 ms [87].

The results indicate that there is the possibility of using windowed segments to achieve similar or even better results than using a window representing the full duration of the motion.

4.3 Feature Selection

In order to identify EMG features and feature sets that are useful for differentiating between healthy and injured limbs, the process of feature selection was performed. First, all of the features summarized in Section 2.8 were extracted from the EMG data sets. The performances of each feature were then evaluated individually, and feature sets were developed based on combinations of the best individual features. Feature reduction was performed with the RELIEFF algorithm in order to further optimize feature sets. Classifiers developed using the new feature sets were evaluated.

4.3.1 Individual Feature Performances

The classification performances for individual EMG features were evaluated by developing models for each feature and each motion, combining the motion models into a majority vote, and then evaluating the final models with a leave-one-patient-out cross-validation. The individual feature models classified between healthy and injured limbs with accuracies ranging from 46.3–76.5%. The LDA classifier provided the highest classification accuracy for most individual features. Table 4.8 shows the individual classification performances ranked in order of LDA classification performance.

The individual features were then organized and ranked by classification performance based on the type of information that each feature provides (Table 4.9). The following features were ranked the highest for each feature category: LOG (time domain: energy), DASDV (time domain: information complexity), MYOP (time domain: frequency), MAVS (time domain: multi-window), PSR (frequency domain), AR4 (prediction model coefficients), ApEn (entropy), MFL (fractal dimension), SKEW (higher order statistics), and MSD (spike shape analysis).

Table 4.8: Majority vote classification accuracies for individual features. Features are ordered by LDA classification accuracy. The best classifier result for each feature is in bold.

Feature	LDA	SVM	RF
MFL	76.54	73.45	59.88
MYOP	74.69	66.67	58.64
MSD	74.69	54.94	55.56
AR4	74.07	59.88	50.00
MSF	72.84	72.84	54.94
MNPPS	70.99	64.20	52.47
PSR	70.99	66.67	56.17
ApEn	69.14	65.43	57.41
LOG	69.14	57.41	63.58
MNF	69.14	68.52	54.32
ZC	68.52	62.35	55.56
DASDV	68.52	51.85	61.73
VCF	68.52	57.41	56.17
AAC	67.90	51.85	59.88
MSS	67.90	51.85	56.17
MMAV2	67.38	54.32	61.73
WL	66.05	51.85	56.17
CC4	66.05	51.23	50.62
MDF	65.43	65.43	56.79
SampleEn	65.43	64.81	56.17
SSC	64.81	61.73	51.85
MMAV1	64.81	54.94	62.35
HFD	64.20	62.35	59.88
MAVS	64.20	50.00	56.17
PKF	63.58	67.9	61.11
MAV	63.58	55.60	64.81
MSA	63.58	53.70	62.35
MTW	62.96	50.62	64.20
RMS	62.35	57.41	65.43
MHW	61.73	51.85	62.34
SM3	60.49	61.73	60.49
MNP	59.88	52.47	63.58
TTP	58.79	51.85	64.20
VAR	58.64	52.47	64.20
FR	58.02	67.90	58.02
SM1	58.02	51.85	61.11
SKEW	57.41	53.09	50.00
DFA	56.80	46.30	50.00
SM2	55.56	56.79	59.23
WAMP	54.32	56.17	50.62
KURT	52.47	53.70	50.00

Table 4.9: Individual feature performances organized by feature category.

Feature Type	Ranking	
Time Domain: Energy	1. LOG	4. MAV
	2. MMAV2	5. RMS
	3. MMAV1	6. VAR
Time Domain: Information Complexity	1. DASDV	
	2. AAC	
	3. WL	
Time Domain: Frequency	1. MYOP	
	2. ZC	
	3. SSC	
	4. WAMP	
Time Domain: Multi-Window	1. MAVS	
	2. MTW	
	3. MHW	
Frequency Domain	1. PSR	7. MNP
	2. MNF	8. TTP
	3. VCF	9. FR
	4. MDF	10. SM1
	5. PKF	11. SM2
	6. SM3	
Prediction Model Coefficients	1. AR4	
	2. CC4	
Entropy	1. ApEn	
	2. SampleEn	
Fractal Dimension	1. MFL	
	2. HFD	
	3. DFA	
Higher Order Statistics	1. SKEW	
	2. KURT	
Spike Shape Analysis	1. MSD	
	2. MSF	
	3. MNPPS	
	4. MSS	
	5. MSA	

4.3.2 FS4 and FS5 Feature Set Performances

The individual feature performances were used to inform the development of new feature sets. FS4 consisted of the overall top ranked features. The MFL and MYOP features were selected because adding subsequent features was found to degrade the classification accuracy.

FS5 was developed to include the maximum ranked feature within each feature category. SKEW was excluded because of its low individual performances (below 60% for all classifiers). FS5 ultimately consisted of the following features: LOG, DASDV, MYOP, MAVS, PSR, AR4, ApEn, MFL, MSD.

Feature reduction is necessary in order to improve the performance, speed, and memory usage of the classifiers. FS5 contained nine features, therefore it was desirable to minimize the number of features in this set. The RELIEFF algorithm with $k=10$ was used to rank the top scoring features in FS5. The MSD, PSR, and MFL features were consistently ranked among the best features in FS5 for all motions, and were selected for the optimized feature set.

The classification accuracies for the new feature sets are summarized in Table 4.10. FS4 provided the best ranges of classification accuracies when used with the LDA and SVM classifiers (63.0–78.4% and 60.5–79.6%), however the ranges achieved with the RF classifier were poor (57.4–70.4%). FS5 tended to work better with the SVM and RF classifiers, and tended to have poor classification accuracies when used with the LDA classifier. Following optimization with the RELIEFF algorithm, FS5 tended to achieve higher classification accuracies (Figure 4.3), although the accuracies were degraded for some of the motions and classifiers. The LDA classifier demonstrated the greatest improvement following feature reduction. The RF classification results did not improve following the feature reduction.

The majority vote classification accuracies for FS4 and FS5 are shown in Table 4.11. As was the case with FS1–FS3, the weighted majority vote provided the best results, followed by the majority vote of the top motions, and then the majority vote of all motion models. The highest accuracies were achieved with FS4 using the LDA classifier. FS5 provided higher accuracies following feature reduction with the RELIEFF algorithm.

Both of the new feature sets (FS4, and FS5 optimized with RELIEFF) provided higher clas-

Table 4.10: Classification accuracies for each new feature set. The best classification result for each motion within each feature set is in bold.

Feature Set	Motion	Classification Accuracy (%)		
		LDA	SVM	RF
FS4 (MFL, MYOP)	EF	78.4	70.4	63.6
	EE	68.5	65.4	67.3
	P	71.6	70.4	63.6
	S	72.2	71.0	70.4
	WF	70.3	70.4	70.4
	WE	66.0	60.5	57.4
	UD	77.2	79.6	67.3
	RD	74.7	69.1	67.9
	HC	69.8	69.8	63.6
	HO	63.0	70.4	63.6
FS5 (LOG, DASDV, MYOP, MAVS, PSR, AR4, ApEn, MFL, MSD)	EF	61.7	73.5	71.0
	EE	75.9	72.8	72.8
	P	59.9	66.7	67.9
	S	58.0	71.0	67.9
	WF	64.8	59.9	69.1
	WE	51.9	58.6	63.0
	UD	69.1	74.7	64.8
	RD	61.1	73.5	67.3
	HC	56.2	63.6	67.3
	HO	56.8	64.8	60.5
FS5 Optimized with RELIEFF (PSR, MFL, MSD)	EF	69.8	71.6	64.8
	EE	72.5	72.2	75.9
	P	72.8	70.4	66.0
	S	71.0	72.8	70.4
	WF	56.8	69.1	68.5
	WE	61.7	66.7	64.2
	UD	72.2	76.5	69.1
	RD	67.3	64.8	68.5
	HC	65.4	71.0	61.7
	HO	63.6	66.7	71.6

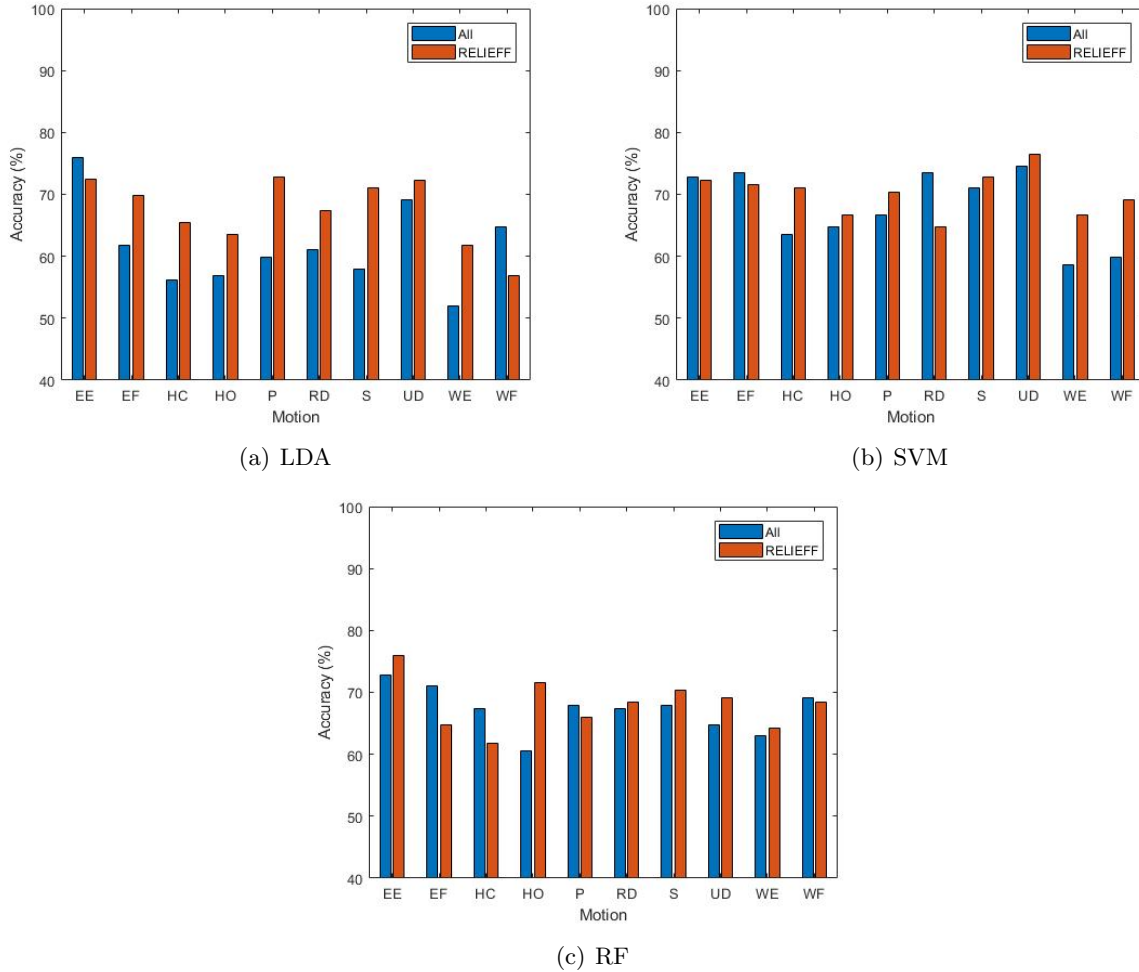


Figure 4.3: FS5 classification accuracies for all features and after feature reduction with RELIEFF. The range of the y axis has been adjusted for clarity. The motions tested were as follows: elbow flexion (EF), elbow extension (EE), forearm pronation (P), forearm supination (S), wrist flexion (WF), wrist extension (WE), ulnar deviation (UD), radial deviation (RD), hand close (HC), and hand open (HO).

Table 4.11: Majority vote classification accuracies for feature sets FS4 and FS5. The best classification result for each feature set is in bold.

Feature Set	Classification Accuracy (%)								
	LDA			SVM			RF		
	All	Weighted	Top	All	Weighted	Top	All	Weighted	Top
FS4	77.8	82.1	79.6	73.4	74.1	77.8	62.3	71.0	64.2
FS5	64.8	67.3	68.5	73.5	75.9	76.5	66.7	75.3	65.4
FS5 Optimized with RELIEFF	74.1	79.6	74.1	78.4	81.5	77.2	63.0	77.2	62.3

sification accuracies than the feature sets developed from the literature (FS1–FS3). These results suggest that the MFL, MYOP, PSR, and MSD features are preferable to the more commonly used EMG features for identifying muscle health.

4.4 Patient Characteristics

Further improvement to the classification models was attempted by introducing patient characteristics into the models. The sex, age, BMI, and time since injury of the patients were included as features in the LDA, SVM, and RF classification models.

These characteristics were input into the classification models as the following feature values:

- Sex:
 - Male: 1
 - Female: 2
- Age (Years):
 - <30: 1
 - 30–45: 2
 - >45: 3
- BMI (kg/m^2):
 - Normal (18.5–25): 1
 - Overweight (25–30): 2
 - Obese (>30): 3
- Time Since Injury:
 - Early (0–6 weeks): 1
 - Late (7–12 weeks): 2
- Injured Limb Dominance:

- Dominant: 1
- Non-Dominant: 2

The patient characteristic features were added to FS1–FS5, and the classification accuracies were obtained using leave-one-patient-out cross-validation (Table 4.12). The results were compared with the classification accuracies obtained from FS1–FS5 without the patient characteristics included. The inclusion of the patient characteristic features did not significantly improve the classification accuracies for any of the motion models. Comparisons of the classification accuracies for FS4 with and without the patient characteristic features are shown in Figure 4.4.

The individual decision tree classification models within the RF classifier were assessed to determine if patient characteristic features were selected as splitting rules. The number of instances that each feature type was selected for a splitting rule was counted for 2000 decision trees (200 per motion model). The average number of times that each patient characteristic feature was used for a splitting rule was calculated and compared to the average number of times that the LOG features were used (Figure 4.5). The features selected for decision branches by the RF algorithm were overwhelmingly EMG features.

Based on this analysis, the patient characteristics of sex, age, BMI, time since injury, and hand dominance do not provide important information for the classifiers tested that could assist with determining the category of muscle health.

4.5 Three-Class Models

Following the development of models with only two categories of health (healthy and injured), models were developed to distinguish between three categories of health: healthy, the early stages of rehabilitation (0–6 weeks of therapy), and the late stages of rehabilitation (7+ weeks of therapy). The rationale behind these divisions was that strengthening rehabilitation exercises begin at 7–8 weeks of therapy [16, 20]. As well, patients in later stages of recovery have been observed to have more similar EMG metrics to healthy subjects [12]. A three-class model could therefore be expected to improve classification over a two-class model if patients in the later stages of rehabilitation were more likely to be misclassified as healthy by the two-class model.

Table 4.12: Classification accuracies for feature sets including patient characteristic features. The best classification result for each motion within each feature set is in bold.

Feature Set	Motion	Classification Accuracy (%)		
		LDA	SVM	RF
FS1 (MAV, SSC, WL, ZC)	EF	65.4	66.7	71.0
	EE	66.0	60.5	74.1
	P	61.1	68.5	67.9
	S	56.8	51.9	67.9
	WF	64.8	59.9	71.6
	WE	55.6	62.3	54.3
	UD	54.9	67.3	68.5
	RD	59.9	66.0	66.0
	HC	63.6	59.9	73.5
FS2 (RMS, AR2)	HO	59.8	60.5	59.9
	EF	61.1	58.0	70.4
	EE	63.6	74.1	70.4
	P	64.8	58.6	69.8
	S	54.9	61.7	73.5
	WF	58.6	63.6	71.0
	WE	61.7	53.7	61.7
	UD	61.1	65.4	68.5
	RD	57.4	57.4	72.8
FS3 (MSA, MSF, MSS, MNPPS, MSD)	HC	66.7	59.9	72.8
	HO	58.0	65.4	66.0
	EF	63.6	64.8	69.8
	EE	66.0	67.3	71.6
	P	67.3	66.0	65.4
	S	58.6	66.0	73.5
	WF	60.5	64.8	71.0
	WE	61.7	71.6	68.5
	UD	61.7	70.4	66.0
FS4 (MFL, MYOP)	RD	59.9	73.5	66.0
	HC	59.3	64.2	67.9
	HO	56.2	56.2	58.6
	EF	71.6	66.0	61.7
	EE	65.4	64.2	67.9
	P	72.2	66.7	63.6
	S	70.4	72.2	71.0
	WF	69.8	66.0	70.4
	WE	60.5	63.6	57.4
FS5 Optimized with RELIEFF (PSR, MFL, MSD)	UD	74.1	77.8	54.2
	RD	71.0	63.0	69.8
	HC	69.8	59.9	64.8
	HO	64.8	72.8	63.0
	EF	64.2	69.1	67.9
	EE	70.4	74.1	75.9
	P	73.5	64.2	70.4
	S	69.8	74.1	72.2
	WF	58.0	69.8	67.9
FS6 Optimized with SVM (PSR, MFL, MSD)	WE	60.5	69.8	69.8
	UD	69.8	76.5	69.8
	RD	70.4	69.1	73.5
	HC	66.0	71.0	63.0
	HO	67.3	67.3	70.4

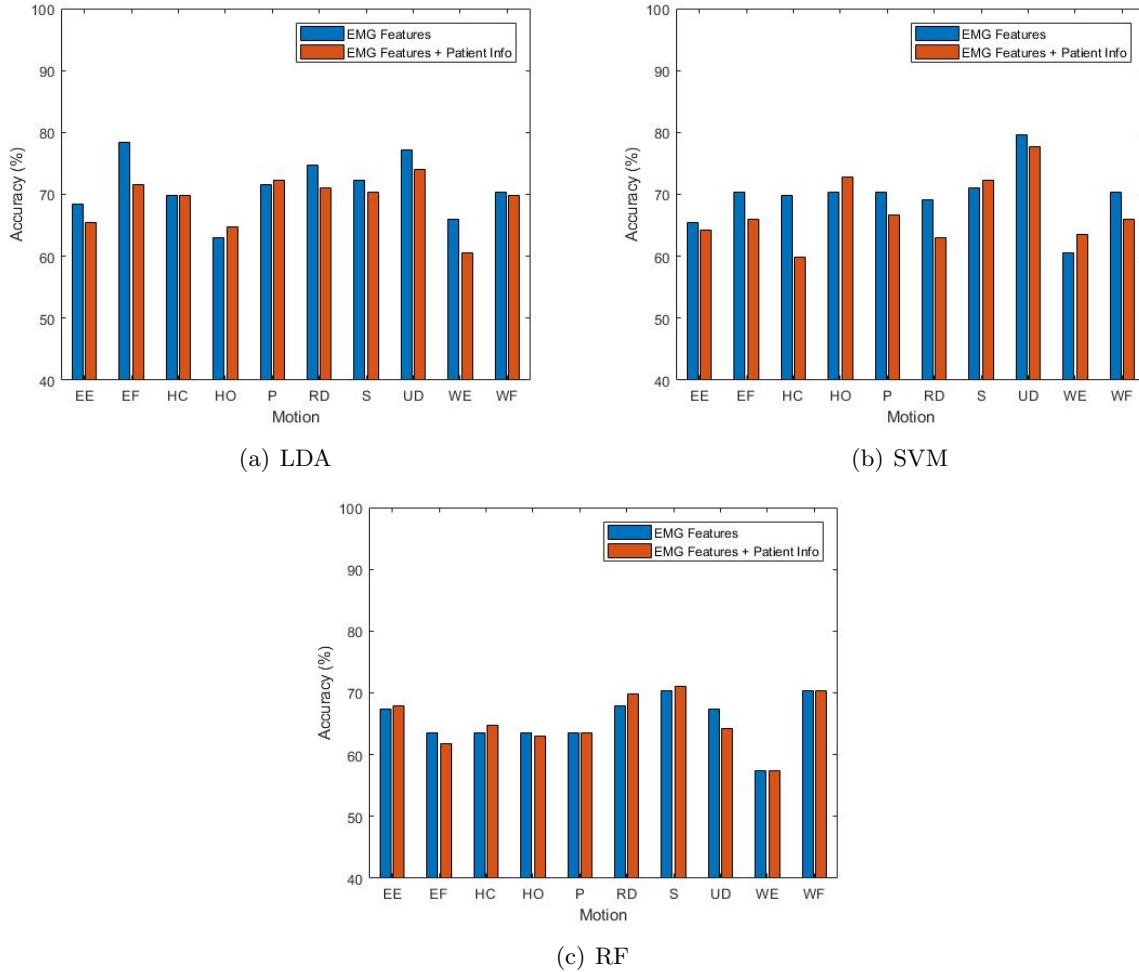


Figure 4.4: FS4 classification accuracies with and without patient information. The range of the y axis has been adjusted for clarity. The motions tested were as follows: elbow flexion (EF), elbow extension (EE), forearm pronation (P), forearm supination (S), wrist flexion (WF), wrist extension (WE), ulnar deviation (UD), radial deviation (RD), hand close (HC), and hand open (HO).

Of the patients evaluated, 13 patients were considered to be in the early stages of injury and 14 patients were considered to be in the later stages. Healthy data sets were collected from the 27 healthy patient arms. In order to prevent imbalance in the number of instances in each class, 12 data sets were randomly selected from each of the three classes for training, and one data set was selected from each category for testing. This process was repeated 10 times, and the average of the accuracies obtained was used as the final result.

The three-class model classification results are shown in Table 4.13 for FS1–FS5. The accuracies

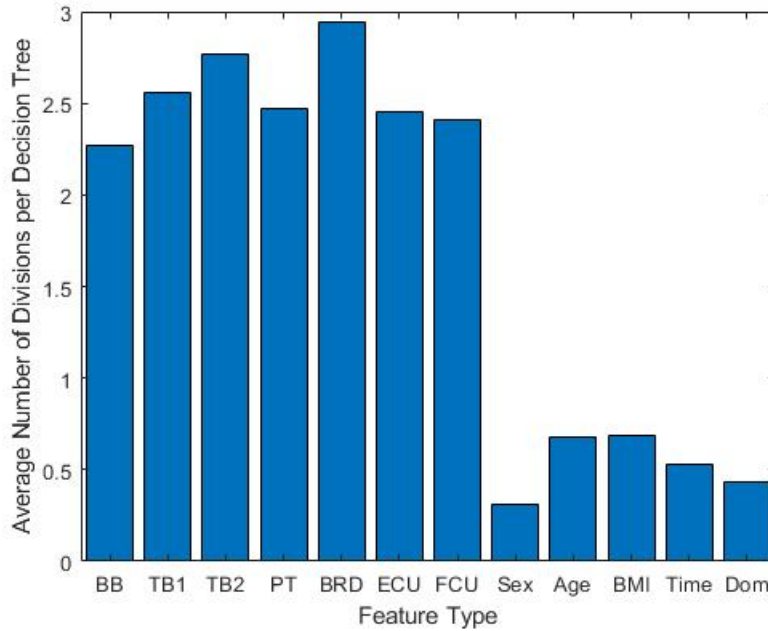


Figure 4.5: Average number of times features were used for decision tree splitting rules in RF classifier.

ranged from 23.3–63.3%. Most results were equal to or slightly greater than the baseline accuracy of 33.3%. These levels of accuracy would not be adequate for determining muscle health.

Confusion matrices were developed to determine if the models tended to have difficulties distinguishing between specific classes. The confusion matrices for the EF and EE motions for the LDA classifier are shown in Table 4.14 and Table 4.15 respectively.

The rows of the confusion matrix represent the actual classes, and the columns represent the predicted classes. Each cell of the confusion matrix represents the percentage of instances within a specific actual class that were classified as a specific predicted class. The ideal confusion matrix for a three-class classification problem would have 33.33% in each of the three cells along the left diagonal of the matrix (representing the correct predictions), and 0% in the remaining cells (representing the incorrect predictions).

In general, the confusion matrices for the classification results tended to indicate that more misclassifications occur between the early and late patient categories than between the early and healthy and the late and healthy categories. The patients included in this study suffered from various types and severities of injuries, hence the number of weeks spent in therapy is likely a poor

Table 4.13: Classification accuracies for three categories of health (baseline accuracy = 33.33%).
The best classification result for each motion within each feature set is in bold.

Feature Set	Motion	Classification Accuracy (%)		
		LDA	SVM	RF
FS1 (MAV, SSC, WL, ZC)	EF	33.3	35.6	36.7
	EE	32.2	38.9	41.1
	P	36.7	37.8	28.9
	S	63.3	47.8	54.4
	WF	51.1	40.0	35.6
	WE	50.0	37.8	35.6
	UD	34.4	33.3	45.6
	RD	50.0	48.9	37.8
	HC	38.9	45.6	43.3
FS2 (RMS, AR2)	HO	34.4	41.1	30.0
	EF	46.7	45.6	53.3
	EE	44.4	41.1	38.9
	P	47.8	35.6	31.1
	S	45.6	48.9	42.2
	WF	43.3	50.0	31.1
	WE	35.6	40.0	34.4
	UD	46.7	37.8	34.4
	RD	55.6	26.7	26.8
FS3 (MSA, MSF, MSS, MNPPS, MSD)	HC	37.8	31.1	54.4
	HO	32.2	57.8	40.0
	EF	38.9	26.7	26.7
	EE	36.7	56.7	36.7
	P	40.0	31.1	36.7
	S	43.3	43.3	37.8
	WF	38.9	33.3	38.9
	WE	41.1	43.3	34.4
	UD	53.3	44.4	41.1
FS4 (MFL, MYOP)	RD	30.0	37.8	35.6
	HC	41.1	58.9	37.8
	HO	34.4	36.7	35.6
	EF	50.0	43.3	33.3
	EE	37.8	61.1	46.7
	P	35.6	36.7	31.1
	S	48.9	53.3	56.7
	WF	35.6	36.7	37.8
	WE	34.4	32.2	26.7
FS5 Optimized with RELIEFF (PSR, MFL, MSD)	UD	48.9	53.3	34.4
	RD	52.2	41.1	38.9
	HC	51.1	50.0	44.4
	HO	40.0	41.1	41.1
	EF	35.6	36.7	33.3
	EE	45.6	41.1	33.3
	P	38.9	30.0	32.2
	S	47.8	51.1	47.8
	WF	33.3	44.4	33.3
	WE	53.3	32.2	34.4
	UD	56.7	61.1	38.9
	RD	47.8	42.2	23.3
	HC	36.7	52.2	43.3
	HO	41.1	45.6	47.8

Table 4.14: Confusion matrix for elbow flexion with LDA classifier. Correct predictions are in bold.

		Predicted			
		Actual	Healthy	Early	Late
Actual	Healthy	15.11%	8.89%	9.33%	
	Early	3.56%	17.78%	12.00%	
	Late	8.89%	16.00%	8.44%	

Table 4.15: Confusion matrix for elbow extension with LDA classifier. Correct predictions are in bold.

		Predicted			
		Actual	Healthy	Early	Late
Actual	Healthy	18.89%	9.33%	5.11%	
	Early	4.22%	18.67%	10.44%	
	Late	12.67%	8.89%	11.78%	

estimate of the patient health, and this is reflected by the poor classification results. The results suggest that the stage of injury was not discernible based on the EMG signals.

4.6 Statistical Analysis of Features

Following the development of classification models, a statistical analysis of the EMG features was conducted in order to identify trends in the EMG data related to patient health. The Statistical Package for Social Sciences v.24 (SPSS) software was used to perform all analyses, and a statistical significance of 0.05 was used.

Paired difference tests were conducted to identify differences between the healthy and injured limbs of the patients. A repeated measures analysis was also conducted for the patients who performed trials at multiple stages of their rehabilitation. This section will discuss the significant

differences found in the results.

4.6.1 Paired Difference Tests

Paired difference tests were performed for the following EMG features: LOG, DASDV, MYOP, PSR, ApEn, MFL, and the spike shape analysis features (MSA, MSF, MSS, MNPPS, MSD). These features were selected for analysis because they had exhibited the highest individual classification performances within their respective feature categories.

The EMG features for each muscle were first averaged over the three repetitions of each motion for each patient. Pairs were then formed between the healthy and injured features for each patient.

The distribution of each EMG feature for each muscle was evaluated for normality using the Shapiro–Wilk test. A paired samples *t*-test was applied to the pairs observed to have normal distributions. A Wilcoxon signed rank test was applied to pairs that were not normally distributed. There were 11 features tested over 7 muscles and 10 different motions, therefore 770 paired difference tests were performed. Using a statistical significance of 0.05, 266 significant differences were identified. The false discovery rate [120] for this dataset was estimated to be 14.5%. The muscles and the motions that exhibited statistically significant differences between healthy and injured limbs are summarized for each feature tested in Tables 4.16–4.25.

The mean values of the healthy LOG features were higher for the healthy muscles for all muscles and motions tested. The significant differences were primarily observed in the forearm muscles (PT, BRD, ECU, FCU), and are listed in Table 4.16. The MFL feature was also observed to have a higher mean in the healthy limb for all muscles and motions. The significant differences are shown in Table 4.17.

The mean MYOP values for the healthy muscles were higher than the mean values for the injured muscles for all instances with significant differences (Table 4.18). The BB and TB1 muscles showed a trend towards having lower mean MYOP values for the healthy limb, although none of these differences were significant.

Fewer significant differences between the healthy and injured means were observed for the DASDV, PSR, and ApEn features. The healthy group had higher mean DASDV values than the injured group for all instances (Table 4.19). The PSR feature was significantly lower for the TB1

Table 4.16: Significant differences for paired difference tests for the LOG feature.

Motion	Muscle	Mean (Healthy - Injured)	Standard Error (Healthy - Injured)	Significance
EF	PT	8.96E-04	3.77E-04	0.005
	BRD	7.92E-03	2.14E-03	<0.001
	ECU	1.01E-03	4.51E-04	0.025
	FCU	1.32E-03	3.21E-04	<0.001
EE	TB2	1.14E-03	9.34E-04	0.006
	PT	1.01E-03	4.39E-04	0.025
	BRD	8.33E-03	2.22E-03	<0.001
	FCU	9.60E-04	2.89E-04	0.008
P	TB2	1.26E-03	4.38E-04	0.004
	PT	1.05E-03	3.10E-04	0.002
	BRD	7.58E-03	1.96E-03	<0.001
	FCU	7.13E-04	2.76E-04	0.006
S	PT	7.19E-04	3.24E-04	0.003
	BRD	7.63E-03	1.87E-03	<0.001
	ECU	1.20E-03	4.50E-04	0.021
	FCU	7.06E-04	2.42E-04	0.007
WF	BRD	5.89E-03	1.82E-03	<0.001
	ECU	2.45E-03	7.91E-04	0.005
WE	PT	6.75E-04	2.12E-04	0.001
	BRD	7.40E-03	1.88E-03	<0.001
	ECU	1.42E-03	5.81E-04	0.017
	FCU	7.09E-04	1.74E-04	<0.001
UD	PT	5.19E-04	2.19E-04	0.015
	BRD	6.86E-03	1.77E-03	<0.001
	ECU	2.10E-03	7.45E-04	0.005
	FCU	1.67E-03	5.32E-04	0.001
RD	PT	8.29E-04	3.00E-04	0.011
	BRD	7.32E-03	2.14E-03	<0.001
	ECU	1.26E-03	5.29E-04	0.020
	FCU	1.28E-03	2.70E-04	<0.001
HC	PT	5.34E-04	1.85E-04	0.001
	BRD	6.55E-03	1.88E-03	<0.001
	ECU	2.20E-03	7.47E-04	0.005
	FCU	1.42E-03	5.68E-04	0.015
HO	PT	4.64E-04	2.03E-04	0.014
	BRD	7.32E-03	1.98E-03	<0.001
	ECU	2.25E-03	7.48E-04	0.004
	FCU	1.00E-03	4.49E-04	0.014

Table 4.17: Significant differences for paired difference tests for the MFL feature.

Motion	Muscle	Mean (Healthy - Injured)	Standard Error (Healthy - Injured)	Significance
EF	PT	4.14E-01	1.31E-01	0.004
	BRD	1.05E+00	2.56E-01	<0.001
	FCU	4.07E-01	1.00E-01	0.001
EE	TB1	3.41E-01	1.42E-01	0.020
	TB2	4.57E-01	1.72E-01	0.006
	PT	4.12E-01	1.78E-01	0.029
	BRD	1.14E+00	2.47E-01	<0.001
	FCU	2.39E-01	1.30E-01	0.021
P	TB2	3.77E-01	1.32E-01	0.019
	PT	4.10E-01	1.24E-01	0.003
	BRD	9.87E-01	2.26E-01	<0.001
S	PT	3.66E-01	1.31E-01	0.010
	BRD	1.10E+00	2.05E-01	<0.001
WF	BRD	8.90E-01	1.91E-01	<0.001
	ECU	5.16E-01	1.98E-01	0.015
WE	PT	3.33E-01	7.65E-02	<0.001
	BRD	8.95E-01	1.43E-01	<0.001
	ECU	4.77E-01	1.67E-01	0.008
	FCU	3.83E-01	8.82E-02	<0.001
UD	TB2	3.11E-01	1.33E-01	0.034
	PT	2.79E-01	7.82E-02	0.002
	BRD	1.00E+00	2.08E-01	<0.001
	ECU	5.24E-01	1.77E-01	0.006
	FCU	5.70E-01	1.36E-01	<0.001
RD	PT	2.89E-01	1.17E-01	0.02
	BRD	8.53E-01	1.96E-01	<0.001
	FCU	4.74E-01	9.56E-02	<0.001
HC	PT	1.96E-01	7.40E-02	0.011
	BRD	7.13E-01	1.74E-01	<0.001
	ECU	4.60E-01	1.32E-01	0.002
	FCU	3.44E-01	1.43E-01	0.023
HO	PT	2.14E-01	7.61E-02	0.008
	BRD	1.02E+00	2.17E-01	<0.001
	ECU	5.97E-01	1.80E-01	0.003

Table 4.18: Significant differences for paired difference tests for the MYOP feature.

Motion	Muscle	Mean (Healthy - Injured)	Standard Error (Healthy - Injured)	Significance
EF	TB2	3.55E-02	6.82E-03	0.010
	PT	1.85E-02	3.56E-03	<0.001
	BRD	3.10E-02	5.97E-03	<0.001
	ECU	3.69E-02	7.10E-03	0.019
	FCU	2.70E-02	5.21E-03	<0.001
EE	BB	2.75E-02	5.30E-03	0.027
	TB1	3.60E-02	6.92E-03	0.045
	TB2	3.31E-02	6.36E-03	<0.001
	PT	4.28E-02	8.25E-03	0.028
	BRD	2.68E-02	5.15E-03	<0.001
	FCU	3.98E-02	7.66E-03	0.020
P	TB2	4.60E-02	8.86E-03	0.001
	PT	2.67E-02	5.14E-03	0.002
	BRD	4.12E-02	7.92E-03	0.009
	FCU	2.72E-02	5.24E-03	0.002
S	TB2	5.27E-02	1.01E-02	0.013
	PT	3.19E-02	6.14E-03	0.015
	BRD	3.52E-02	6.78E-03	0.005
	ECU	2.74E-02	5.28E-03	0.044
	FCU	3.51E-02	6.76E-03	0.044
WF	BRD	3.43E-02	6.61E-03	<0.001
	ECU	3.46E-02	6.66E-03	0.005
WE	PT	2.48E-02	4.77E-03	0.012
	BRD	3.26E-02	6.27E-03	0.002
	FCU	2.65E-02	5.10E-03	0.012
UD	TB2	4.93E-02	9.49E-03	0.005
	PT	2.66E-02	5.12E-03	0.010
	BRD	3.10E-02	5.97E-03	0.010
	FCU	2.62E-02	5.05E-03	0.034
RD	TB2	4.92E-02	9.46E-03	0.002
	PT	2.71E-02	5.21E-03	0.013
	BRD	3.89E-02	7.49E-03	0.020
	FCU	2.48E-02	4.77E-03	0.005
HC	TB2	5.41E-02	1.04E-02	0.009
	PT	2.47E-02	4.76E-03	0.004
	BRD	3.44E-02	6.61E-03	0.004
HO	TB2	5.43E-02	1.05E-02	0.011
	PT	2.78E-02	5.34E-03	0.100
	BRD	3.70E-02	7.13E-03	0.007
	ECU	3.61E-02	6.94E-03	0.026
	FCU	2.82E-02	5.42E-03	0.004

Table 4.19: Significant differences for paired difference tests for the DASDV feature.

Motion	Muscle	Mean (Healthy - Injured)	Standard Error (Healthy - Injured)	Significance
EF	TB1	3.28E-06	1.54E-06	0.016
	PT	7.12E-06	2.77E-06	0.001
	BRD	7.27E-05	2.23E-05	<0.001
	FCU	4.40E-06	1.61E-06	<0.001
EE	BRD	6.30E-05	2.06E-05	<0.001
P	PT	4.68E-06	1.93E-06	0.002
	BRD	5.03E-05	2.00E-05	<0.001
S	BRD	5.44E-05	2.22E-05	<0.001
WF	BRD	3.52E-05	1.49E-05	<0.001
	ECU	1.71E-05	6.17E-06	0.009
WE	PT	1.89E-06	5.65E-07	0.001
	BRD	4.93E-05	1.74E-05	0.001
	FCU	2.38E-06	7.39E-07	0.001
UD	PT	1.37E-06	5.41E-07	0.005
	BRD	4.66E-05	1.68E-05	<0.001
RD	BRD	5.22E-05	1.97E-05	0.001
	FCU	5.69E-06	1.59E-06	<0.001
HC	PT	1.34E-06	4.56E-07	0.007
	BRD	4.28E-05	1.70E-05	0.018
	ECU	1.56E-05	7.02E-06	0.035
HO	PT	8.89E-07	4.18E-07	0.012
	BRD	5.28E-05	1.90E-05	0.001
	ECU	1.34E-05	6.02E-06	0.008

muscle and significantly higher for the BRD muscle in the healthy limb (Table 4.20). The ApEn feature tended to have a lower mean value in healthy muscles (Table 4.21). The ApEn values showed a trend towards higher values in the healthy BB muscle, although these differences were not significant.

All of the spike shape analysis features were investigated because these features provided relatively high individual performance classification accuracies. The MSA (Table 4.22) and MSS (Table 4.23) features primarily exhibited significant differences in the PT and BRD muscles. Higher activations were observed in the healthy muscle groups for all motions.

The MSF feature primarily exhibited significant differences between healthy and injured means

Table 4.20: Significant differences for paired difference tests for the PSR feature.

Motion	Muscle	Mean (Healthy - Injured)	Standard Error (Healthy - Injured)	Significance
EF	TB1	-1.09E-01	3.13E-02	0.002
	BRD	1.83E-01	4.49E-02	<0.001
EE	TB1	-7.33E-02	3.43E-02	0.044
	PT	9.73E-02	4.22E-02	0.029
	BRD	2.63E-01	5.71E-02	<0.001
	FCU	1.35E-01	4.53E-02	0.011
P	TB1	-6.91E-02	3.14E-02	0.037
	BRD	1.77E-01	6.66E-02	0.027
S	TB1	-6.56E-02	2.66E-02	0.021
	BRD	1.73E-01	6.75E-02	0.029
WF	BRD	1.53E-01	6.58E-02	0.021
WE	BRD	1.67E-01	6.33E-02	0.041
UD	TB1	-1.07E-01	3.85E-02	0.010
	BRD	1.55E-01	6.61E-02	0.049
RD	TB1	-1.37E-01	3.22E-02	<0.001
HC	TB1	-7.47E-02	2.74E-02	0.008
HO	TB1	-8.51E-02	3.38E-02	0.018

in the BB, TB1, and BRD muscles. Higher MSF values were observed in the healthy BB and TB1 muscles, and lower values were observed in the BRD and PT muscles (Table 4.24).

Conversely, healthy subjects had lower MSD values for the BB and TB1 muscles, and higher values for the forearm muscles, although only the BRD muscle showed significant differences (Table 4.25).

The MNPPS feature tended to exhibit lower mean values in healthy patients for the TB1 muscle and higher values for the BRD muscle (Table 4.26).

The general trends observed for each feature did not change depending on the specific motions that were performed. This could indicate that the EMG trends for injured and healthy patients are similar regardless of the type of motion performed. However, this could also suggest that factors outside of the muscle activity influence the EMG signals. For example, decreased muscular strength in the injured arm due to a period of inactivity could affect the EMG recordings regardless

Table 4.21: Significant differences for paired difference tests for the ApEn feature.

Motion	Muscle	Mean (Healthy - Injured)	Standard Error (Healthy - Injured)	Significance
EF	PT	-1.25E-01	3.52E-02	0.002
	BRD	-2.66E-01	7.19E-02	0.002
	FCU	-1.24E-01	4.48E-02	0.010
EE	TB2	-9.57E-02	5.21E-02	0.078
	PT	-1.98E-01	5.85E-02	0.002
	BRD	-3.17E-01	6.86E-02	<0.001
P	BRD	-1.69E-01	7.24E-02	0.028
S	TB2	-9.00E-02	4.30E-02	0.011
	BRD	-2.30E-01	7.76E-02	0.004
WF	TB1	1.01E-01	3.04E-02	0.002
	BRD	-1.82E-01	6.30E-02	0.008
WE	BRD	-1.53E-01	4.54E-02	0.002
	ECU	-9.09E-02	3.36E-02	0.012
	FCU	-9.86E-02	3.70E-02	0.013
UD	BRD	-1.79E-01	5.82E-02	0.005
RD	BRD	-1.45E-01	4.64E-02	0.002
	FCU	-8.20E-02	2.35E-02	0.002
HC	BRD	-1.48E-01	4.85E-02	0.005
	FCU	-4.97E-02	2.32E-02	0.042
HO	TB1	6.95E-02	3.30E-02	0.045
	BRD	-1.66E-01	6.49E-02	0.037

of the motion performed.

The EF, EE, WF, and WE motions exhibited the most significant differences between motion pairs, and P and HO had the least significant differences. This is consistent with the P and HO motion models tending to provide lower classification accuracies.

The forearm muscles (PT, BRD, ECU, FCU) tended to provide significant differences between healthy and injured groups for all of the motions performed, with the BRD muscle exhibiting the most differences for all motions. The major elbow flexors and extensors (BB, TB1, and TB2 muscles) tended to exhibit the most differences when the EF, EE, P, S, and WF motions were performed. With the exception of the WF motion, this is consistent with the necessity of the activation of the major elbow muscles to perform the EF, EE, P, and S motions.

Table 4.22: Significant differences for paired difference tests for the MSA feature.

Motion	Muscle	Mean (Healthy - Injured)	Standard Error (Healthy - Injured)	Significance
EF	BRD	8.76E-02	3.06E-02	<0.001
	FCU	2.76E-05	8.66E-06	<0.001
EE	BRD	8.04E-04	2.79E-04	<0.001
P	PT	3.20E-05	1.37E-05	0.002
	BRD	6.14E-04	1.99E-04	0.001
S	BRD	6.06E-04	2.11E-04	<0.001
WF	BRD	4.23E-04	2.01E-04	<0.001
	ECU	1.11E-04	4.05E-05	0.012
WE	PT	1.35E-05	4.65E-06	0.002
	BRD	6.83E-04	2.50E-04	<0.001
	ECU	6.03E-05	2.77E-05	0.009
	FCU	1.30E-05	3.57E-06	0.001
UD	PT	8.78E-06	3.92E-06	0.015
	BRD	5.39E-04	1.80E-04	0.001
	FCU	6.36E-05	3.10E-05	0.002
RD	BRD	7.11E-04	2.96E-04	0.001
	FCU	3.71E-05	1.05E-05	<0.001
HC	PT	9.50E-06	3.96E-06	0.002
	BRD	6.12E-04	2.46E-04	0.001
	ECU	1.10E-04	4.88E-05	0.008
HO	BRD	7.01E-04	2.53E-04	0.001
	ECU	8.93E-05	3.97E-05	0.009

The results of the paired difference tests suggest that there is more activation in healthy muscles compared to injured muscles, particularly in terms of signal energy and information complexity of the EMG signal. MSA and MSS were also always higher in the healthy group, which suggests that there was both higher MU recruitment and synchronization in the healthy muscles. The ApEn feature was lower in most healthy muscles, indicating that the EMG signal had a greater amount of predictability for healthy muscles.

The injured BB and TB1 muscles were observed to have more activity in the MYOP, MSF, and MNPPS features. The PSR feature also demonstrated a higher TB1 activation in the injured subjects. The ApEn and MSD features demonstrated the reverse of this pattern. This suggests

Table 4.23: Significant differences for paired difference tests for the MSS feature.

Motion	Muscle	Mean (Healthy - Injured)	Standard Error (Healthy - Injured)	Significance
EF	TB1	2.11E-03	1.00E-03	0.031
	PT	5.98E-03	2.21E-03	0.007
	FCU	5.05E-03	1.53E-03	<0.001
EE	BRD	7.90E-02	3.00E-02	<0.001
P	PT	6.39E-03	2.39E-03	0.001
	BRD	6.65E-02	2.86E-02	<0.001
S	PT	3.99E-03	1.85E-03	<0.001
	BRD	7.30E-02	3.42E-02	<0.001
WF	ECU	2.64E-02	9.50E-03	0.009
WE	PT	2.74E-03	7.10E-04	<0.001
	BRD	6.71E-02	2.77E-02	0.001
	FCU	2.56E-03	7.07E-04	<0.001
UD	PT	1.57E-03	6.88E-04	0.002
	BRD	5.75E-02	2.51E-02	<0.001
RD	BRD	6.60E-02	2.87E-02	0.002
	FCU	8.23E-03	2.39E-03	<0.001
HC	PT	2.17E-03	8.14E-04	0.002
	BRD	6.03E-02	2.71E-02	0.002
	ECU	2.34E-02	9.88E-03	0.006
HO	BRD	6.91E-02	2.79E-02	0.001
	ECU	1.96E-02	8.61E-03	0.015

that the major elbow flexors and extensors may be more active in injured limbs. The MYOP and PSR features both represent the frequency of the EMG signal, indicating that the EMG frequency is higher for the injured BB and TB1 muscles. The increase in the MSF and MNPPS features and the decrease in the MSD features indicates increased MU recruitment and synchronization.

The results for the LOG, MYOP, MSA, and PSR features are of particular interest because the efficacy of using similar features for assessing elbow muscle health was studied by Haddara [12]. Haddara compared EMG data collected from elbow trauma patients with EMG data collected from healthy subjects performing upper-limb motions. The injured subjects exhibited significantly higher RMS, MAV, ZC, and MSA feature values compared to the healthy subjects. A general trend of higher values for the MNF and MDF frequency domain features was found in the patient

Table 4.24: Significant differences for paired difference tests for the MSF feature.

Motion	Muscle	Mean (Healthy - Injured)	Standard Error (Healthy - Injured)	Significance
EF	BB	1.10E+01	3.23E+00	0.002
	TB1	1.06E+01	4.61E+00	0.029
	PT	-9.09E-02	3.48E+00	0.979
EE	BB	1.49E+01	3.23E+00	0.001
	BRD	-4.05E+01	9.64E+00	0.001
P	BB	1.05E+01	3.75E+00	0.010
	TB1	1.03E+01	3.91E+00	0.014
S	TB1	1.15E+01	2.90E+00	<0.001
	BRD	-2.34E+01	1.01E+01	0.016
WF	BB	1.07E+01	4.69E+00	0.029
	TB1	1.54E+01	4.29E+00	0.002
WE	TB1	1.12E+01	4.96E+00	0.032
	BRD	-2.15E+01	9.15E+00	0.027
UD	TB1	1.48E+01	4.65E+00	0.004
RD	BB	8.35E+00	3.30E+00	0.018
	TB1	1.45E+01	4.36E+00	0.003
HO	TB1	1.27E+01	4.61E+00	0.011

population, however no significant differences were found.

The results of this study were not in agreement with the conclusions made by Haddara. The LOG feature values were higher in the healthy group, which was the opposite of Haddara's observation that injured patients exhibit higher values for the time domain features that describe signal energy (RMS and MAV). Furthermore, with the exception of the BB muscle, the MYOP feature was lower for injured muscles. This was the opposite of Haddara's observations for the ZC feature, which like MYOP is a time domain feature that describes the signal frequency. Finally, several significant differences were observed for the PSR feature in this study, whereas Haddara found that frequency domain features do not demonstrate significant differences.

The differing results between this study and Haddara's study could be due to the differences in the data collection protocols. In this study, control values were obtained from the contralateral healthy arm of the each patient. In Haddara's trials, the healthy controls were obtained from a separate population of subjects. There was no effort to ensure that the healthy subjects resembled

Table 4.25: Significant differences for paired difference tests for the MSD feature.

Motion	Muscle	Mean (Healthy - Injured)	Standard Error (Healthy - Injured)	Significance
EF	BB	-9.68E-04	2.92E-04	0.004
	TB1	-1.05E-03	4.31E-04	0.022
	BRD	2.81E-03	7.83E-04	0.002
EE	BB	-8.81E-04	1.98E-04	<0.001
	BRD	4.54E-03	1.29E-03	0.002
P	BB	-7.62E-04	2.98E-04	0.008
	TB1	-6.30E-04	2.23E-04	0.008
	BRD	3.31E-03	1.48E-03	0.020
S	TB1	-7.55E-04	1.79E-04	<0.001
	BRD	3.15E-03	1.40E-03	0.033
WF	BB	-1.01E-03	4.18E-04	0.022
	TB1	-8.50E-04	2.46E-04	0.002
WE	TB1	-7.12E-04	2.85E-04	0.012
UD	TB1	-9.97E-04	3.06E-04	0.002
RD	BB	-8.50E-04	2.67E-04	0.005
	TB1	-9.13E-04	3.08E-04	0.004
HC	TB1	-6.39E-04	2.65E-04	0.017
HO	TB1	-7.70E-04	2.60E-04	0.003

the characteristics of the elbow trauma patients in terms of age, sex, BMI, etc. Therefore, some of the differences that Haddara observed could have been unrelated to subject health, and due to differences between two groups with different attributes.

However, using the contralateral limb as a control, while avoiding issues with differences in subject characteristics, could also introduce other confounding factors, particularly differences in handedness. As well, patients may have begun to overuse their healthy arm. Therefore, the healthy patient arm may not have represented the state of the patient's healthy arm under normal conditions.

The results indicate that while there are some significant differences between the features, there is often an overlap between healthy and injured EMG feature values. This limits the ability for the classification models to assess patient health. As well, the trends observed in this study differ from the trends observed in a similar EMG study. The collection of more data could ameliorate

Table 4.26: Significant differences for paired difference tests for the MNPPS feature.

Motion	Muscle	Mean (Healthy - Injured)	Standard Error (Healthy - Injured)	Significance
EF	TB1	-8.12E-02	3.11E-02	0.019
	BRD	2.21E-01	5.47E-02	<0.001
EE	BRD	3.33E-01	8.54E-02	0.001
	FCU	7.96E-02	3.70E-02	0.041
P	BB	-6.30E-02	3.03E-02	0.048
	TB1	-6.40E-02	3.06E-02	0.047
S	TB1	-6.04E-02	2.69E-02	0.033
	BRD	2.01E-01	9.65E-02	0.046
WF	TB1	-7.22E-02	3.37E-02	0.041
	FCU	-4.16E-02	1.97E-02	0.045
WE	BRD	1.73E-01	8.04E-02	0.014
UD	TB1	-1.04E-01	4.46E-02	0.027
RD	TB1	-1.17E-01	3.96E-02	0.007
HO	TB1	-7.16E-02	3.34E-02	0.020

the understanding of the differences between healthy and injured limbs.

4.6.2 Returning Patients

A three-level repeated measures comparison was conducted for elbow trauma patients that returned over the course of their therapy to re-perform the trials. Four patients agreed to return. The average time since injury was 5.5 weeks for the initial trial, and 8.5 weeks for the subsequent trial. Repeated measures comparisons were conducted between the three health conditions (healthy, early stage of rehabilitation, and late stage of rehabilitation). Unfortunately, the data sets for one of the patients were compromised during some of the trials, therefore the repeated measures comparisons could only be performed with all four patients for the WF, WE, UD, and RD motions. The LOG, DASDV, MYOP, PSR, MFL, and spike shape analysis features (MSA, MSF, MSS, MNPPS, MSD) were tested for significant differences. Table 4.27 and Table 4.28 summarize the muscles and features that exhibited a significant difference for the WF–WE and UD–RD motions respectively. The false discovery rate was estimated to be 16.8%.

The mean values of the PSR and ApEn features were observed to be higher in the healthy limbs for all muscles and motions tested. The LOG, DASDV, MYOP, and MFL features tended to have higher values for the healthy forearm muscles (PT, BRD, ECU, FCU) than for the injured forearm muscles. The BB muscle exhibited higher feature values in the injured limbs than in the healthy limbs.

Patients re-tested at a later stage of therapy exhibited increases in the PT and BRD muscles features to more closely resemble the values for the healthy muscles. As well, the BB feature values decreased to more closely resemble the observations for the healthy limbs. However, the FCU muscle activity tended to decrease for patients measured at the later stage of rehabilitation, indicating that there was a greater difference between the injured and healthy muscle activity following therapy. Examples for these trends are summarized for the LOG feature and the UD motion in Figure 4.6.

Table 4.27: Repeated measures comparison for wrist flexion and extension for returning subjects. Significant differences are in bold.

Instance	Factor 1	Factor 2	Mean Difference (Factor 1 - Factor 2)	Std Error	Significance
WF					
ApEn BB	Healthy	Early	0.172	0.016	0.002
	Healthy	Late	0.039	0.061	0.564
	Early	Late	-0.133	0.065	0.133
MFL TB1	Healthy	Early	0.695	0.074	0.003
	Healthy	Late	0.414	0.27	0.223
	Early	Late	-0.28	0.201	0.256
MFL PT	Healthy	Early	0.895	0.264	0.043
	Healthy	Late	0.628	0.079	0.004
	Early	Late	-0.267	0.298	0.436
WE					
DASDV ECU	Healthy	Early	1.17E-05	0.000	0.168
	Healthy	Late	1.337E-05	0.000	0.022
	Early	Late	-1.66E-06	0.000	0.662
MYOP ECU	Healthy	Early	0.139	0.126	0.352
	Healthy	Late	0.046	0.009	0.016
	Early	Late	-0.093	0.133	0.534
MSA ECU	Healthy	Early	8.85E-05	0.000	0.126
	Healthy	Late	9.842E-05	0.000	0.017
	Early	Late	9.94E-06	0.000	0.709
MSS ECU	Healthy	Early	0.009	0.007	0.328
	Healthy	Late	0.016	0.003	0.039
	Early	Late	0.007	0.004	0.214

The general trends suggest that muscle activation in elbow trauma patients is higher in BB muscles and lower in the TB and forearm muscles. The results also indicate that as the patients progressed in their therapy, the muscle activity of the injured limb tended to approximate the healthy EMG signal patterns, with the exception of the FCU muscle. However, the results are not conclusive, as only four patients were tested.

These results are somewhat similar to the paired difference test observations described in Section 3.6.1, in which muscle activation was observed to be higher in the TB2 and forearm muscles, and lower for some features, particularly in features describing the frequency of the EMG signal, for the BB and TB1 muscles. The paired difference tests and the repeated measures comparisons both indicate that there is a possibility of using EMG signals to measure the progression of patient

Table 4.28: Repeated measures comparison for radial and ulnar deviation for returning subjects.
Significant differences are in bold.

Instance	Factor 1	Factor 2	RD		
			Mean Difference (Factor 1 - Factor 2)	Std Error	Significance
LOG FCU	Healthy	Early	0.001	<0.001	0.82
	Healthy	Late	0.001	<0.001	0.017
	Early	Late	<0.001	<0.001	0.56
DADSV FCU	Healthy	Early	1.554E-06	<0.001	0.54
	Healthy	Late	1.576E-06	<0.001	0.21
	Early	Late	2.218E-08	<0.001	0.917
MYOP FCU	Healthy	Early	0.022	0.01	0.115
	Healthy	Late	0.27	0.003	0.004
	Early	Late	0.006	0.008	0.561
ApEn BB	Healthy	Early	0.209	0.061	0.042
	Healthy	Late	0.069	0.073	0.416
	Early	Late	-0.14	0.127	0.351
UD					
LOG FCU	Healthy	Early	0.002	<0.001	0.015
	Healthy	Late	0.003	<0.001	0.002
	Early	Late	0.001	<0.001	0.137
DADSV FCU	Healthy	Early	1.35E-05	<0.001	0.01
	Healthy	Late	1.65E-05	<0.001	0.001
	Early	Late	2.95E-06	<0.001	0.168
MYOP FCU	Healthy	Early	0.004	0.013	0.791
	Healthy	Late	0.03	0.005	0.008
	Early	Late	0.026	0.011	0.099
MFL TB1	Healthy	Early	0.782	0.186	0.024
	Healthy	Late	0.594	0.403	0.237
	Early	Late	-0.189	0.225	0.464
MFL FCU	Healthy	Early	0.862	0.076	0.001
	Healthy	Late	1.152	0.191	0.009
	Early	Late	0.29	0.205	0.251
MSA FCU	Healthy	Early	7.00E-05	<0.001	0.004
	Healthy	Late	8.73E-05	<0.001	<0.001
	Early	Late	1.73E-05	<0.001	0.216
MSS FCU	Healthy	Early	0.017	0.003	0.011
	Healthy	Late	0.022	0.002	0.001
	Early	Late	0.005	0.002	0.13
MNPPS PT	Healthy	Early	-0.159	0.016	0.002
	Healthy	Late	-0.096	0.007	0.001
	Early	Late	0.063	0.011	0.011
MSD PT	Healthy	Early	-0.001	<0.001	0.027
	Healthy	Late	0.000	<0.001	0.08
	Early	Late	0.001	<0.001	0.089

healing.

There are multiple potential causes for the general trends observed in this study. The lower muscle activations observed in most of the injured muscles could be due to tissue damage. Greater activation in the BB and TB1 muscles, particularly in the frequency domain, could be due to increased MU firing frequency and recruitment required to achieve the motion while injured.

There are other factors that could affect the EMG signals that are indirectly related to the injury. All of the patients tested would have experienced a loss of muscle mass due to immobility, which could have resulted in the decrease in muscle activation observed in most muscles. Immobility during the injury could also increase the amount of fatty tissue on the skin, which could attenuate the signals and provide the appearance of lower muscle activation.

4.7 Conclusion

This concludes the discussion and results section. There is an indication that it is possible to identify trends, and to differentiate between healthy and injured limbs, based on EMG features. The features that indicated the most promise towards this objective were the MFL, MYOP, PSR, and the spike shape analysis features. Statistical analysis revealed that injured subjects generally have lower muscle activity, although higher muscle activity was observed in the BB and TB1 muscles. Patients tested at later stages of their therapy tended to display EMG signals closer to the expected properties of healthy EMG signals. A greater number of patients should be studied and analyzed to validate these results.

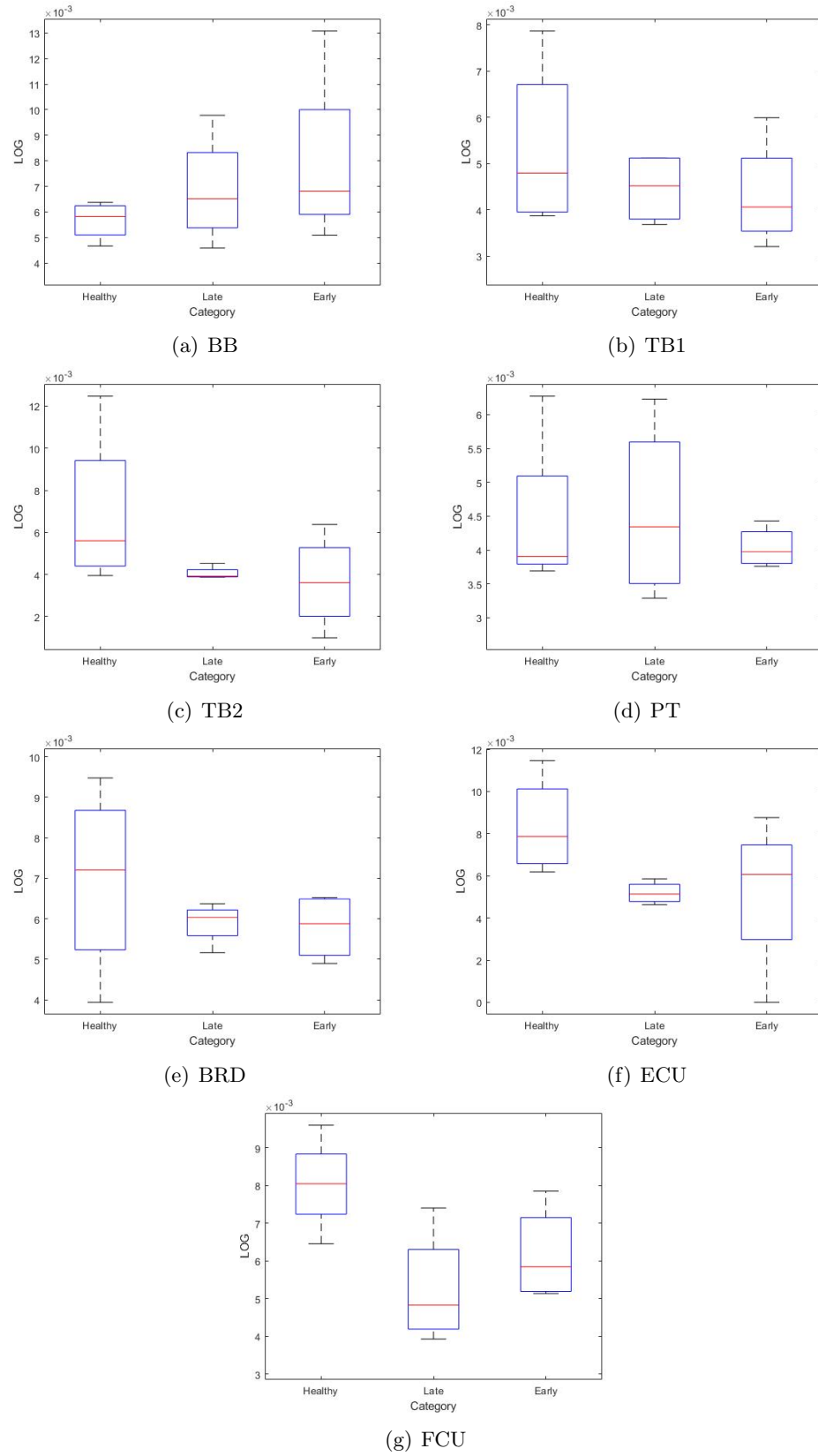


Figure 4.6: LOG feature values for returning subjects. The boxplots are shown for each muscle during the UD motion.

Chapter 5

Concluding Remarks

The work presented in this thesis was towards developing an EMG-based model of muscle health for elbow trauma patients. The purpose of the model was to allow for an objective metric of muscle health to be determined that could identify if a patient was healing. This work was also towards identifying trends in EMG behaviour that reflect muscle health following elbow trauma. A literature review was performed to identify the current challenges in elbow rehabilitation, and the gaps in the development of rehabilitative robotic devices for elbow trauma patients. EMG has been used to study the muscle health of patients with neuromuscular injuries, however, no models have yet been developed to identify and diagnose the muscle health of elbow trauma patients.

EMG features have been applied to the myoelectric control of rehabilitative devices for patients with neuropathologies, and have been used for studying muscle activation and health in certain patients, however, there has not been any significant work done towards an EMG-based model of muscle health for elbow trauma rehabilitation. This study attempted to develop EMG-based classification models to distinguish between the healthy and injured limbs of elbow trauma patients as a precursor to developing a more advanced model of elbow muscle health. EMG data from elbow trauma patients performing elbow, hand, and wrist motions were collected, processed, and analyzed. EMG recordings from the contralateral healthy arm of the patients were collected to provide a control. Feature extraction and selection were performed. Classification models were developed and improved. Majority votes of the motions were studied in order to improve accuracy of the models. Accuracies of up to 82.1% were achieved for these models. However, attempts to

adequately classify the results based on the time that the patient had spent in rehabilitation were unsuccessful with the existing data.

Additionally, a statistical analysis of the EMG features was performed. In general, injured patients tended to show lower muscle activity in most muscles, particularly the forearm muscles. The BB and TB1 muscles in injured subjects tended to exhibit higher activity in some of the features than in healthy limbs. There was some evidence, based on patients who returned to perform the study, that as healing progressed, the behaviour of the injured limbs began to more closely resemble the behaviour of the healthy limb.

This work helped to identify general trends in EMG signals during elbow trauma healing, and some of the best features for identifying patient health. The classification models developed in this thesis achieved results of 48.2–82.1%, and there is much room for improvement.

5.1 Contributions

The contributions of the work presented in this thesis are as follows:

1. A database of sEMG signals was developed from elbow trauma patients and their healthy limbs. This data can be used towards informing the design of future models and control systems for a wearable elbow brace. The patient data are particularly useful because the healthy and injured data sets were collected from the same patient, so that the healthy data sets can be compared to the injured sets, and can allow for a better representation of the population of patients (in terms of age, sex, BMI) presenting at clinics with elbow trauma injuries.
2. EMG features capable of predicting muscle health were identified. An extensive variety of EMG features was investigated. The best individual features were identified to be MFL, MYOP, PSR, and spike shape analysis features, in particular MSD.
3. EMG feature sets were developed and evaluated for efficacy of evaluating muscle health. The spike shape analysis feature set (FS3) provided the best performances of existing feature sets in the literature. New feature sets were proposed based on combinations of features that

performed well individually, and the best feature set overall was a feature set consisting of the MFL and MYOP features.

4. The first classification models to distinguish between healthy and injured limbs of elbow trauma patients based on EMG data were developed. The highest classification accuracy achieved (82.1%) was not ideal, however, this sets a baseline for future comparisons.

5.2 Future Work

The work performed indicates that extensive future work will be necessary in order to develop a practical model of muscle health for a wearable device. The following steps would be required to improve the results of this specific project:

1. *Development of a database of healthy sEMG signals specific to the population for which the elbow brace will be designed.* The average elbow trauma patient recruited for this study was 45 years old and overweight. Only a few studies have examined the muscle activation patterns of subjects representative of middle-aged and elderly populations [63, 121]. There is evidence that the decrease in strength, power, and upper extremity function with age begins around age 40, and subjects over the age of 65 experience decreased ROM. Work by Syczewska *et al.* found that EMG activation patterns in healthy subjects differed between age groups [121]. Further research should be directed towards further understanding the effects of obesity, age, BMI, and handedness on healthy sEMG signals and motion activation patterns.
2. *Recruitment of elbow trauma patients based on the type and severity of elbow injury.* The patient data sets collected in this study varied in terms of the severity of the injury and the treatment for their injury. Most notably, some patients had received only non-surgical treatments, some had received arthroscopic surgery, others had received more extensive surgeries to treat elbow fracture, and one patient underwent multiple surgeries. As well, a variety of injury types were included in the trial including bicep tendon tears, radial head fractures, multiple fractures, and elbow dislocations. In order to obtain a more specific model of muscle health, data sets should be collected from patients who had experienced similar severity and

types of injuries. Due to the limited availability of subjects from where the patients for this study were recruited, a multi-site study would most likely be necessary in order to recruit enough patients in a timely manner.

3. *Improve knowledge of the consistency of therapy treatments.* The patients' schedules sometimes took precedence over therapist recommendations. Some of the patients delayed the start of therapy until up to two weeks after the recommended start time following injury. Patient adherence to home therapy exercises was also not measured. For a few cases, the therapist indicated that they believed that the patient had not followed their exercise regimen. Finally, although the patients in the study were recruited from the same site, they were recruited from different therapists. The treatments recommended to each patient could have varied based on each therapist's opinion. Future studies should attempt to record information about the recommended treatment program and patient adherence.
4. *Collect data from the same patients at multiple stages of recovery.* Unfortunately, it was difficult to convince patients to complete the study multiple times. Only four patients were willing to repeat the study. Issues encountered included the time constraints and availability of the patients, as well as the fact that some of the patients attending the clinic lived several hours away and performed the remainder of their therapy treatments in their hometown. This issue could be diminished if the ease of sEMG acquisition was improved, as described below.
5. *Perform research towards improving the interpretation of sEMG recordings from elbow trauma patients.* The interpretation of sEMG signals is an ongoing challenge. For example, an observed decrease in muscle activity based on sEMG recordings could be due to many underlying factors. Such concerns were observed in a follow-up of patients with Duchenne muscular dystrophy, in which it was unknown if the decrease in muscle activity was due to the loss of muscle fibres or to nonmuscular factors such as the increase of fatty tissues near the skin due to inactivity [65]. Likewise for elbow trauma patients, muscle health will be affected by both the initial injury and by the periods of relative inactivity following the injury.

Over the course of the study, possibilities for future work with sEMG signal acquisition and

analysis were identified that are outside of the scope of the work for this project, but would greatly improve the results of this project. The following issues should be addressed:

1. *Ease of sEMG acquisition and interpretation.* The use of a commercial dry electrode sEMG system greatly improved the ease of recording over the standard wet electrode and wired system, however, the setup for data collection was not without tedium or difficulty. The patients had to agree to move to a separate room to allow for the space and time for 16 electrodes to be correctly placed on their arms by the experimenter. The process required the experimenter to be present at the clinic to perform all of the tests.

The improvement of the ease of use of sEMG acquisition systems could lead to an increase in the amount of data collected for experiments. An acquisition system that is extremely simple to use could allow therapists to collect data from patients during therapy instead of requiring the patient to spend additional time with the experimenter to collect data. An sEMG system that is easy to use could be sent home with the patient, so that data collection could be obtained as the patient performs home exercises. For example, HD-sEMG technology could be applied to this problem to allow patients to place an array of electrodes over the entirety of the desired region, and the experimenter could later assess which electrodes provide the desired signals. The improvement in the ease of acquisition of EMG signals will be critical for the development of a smart brace, as patients will eventually be required to use the device at home without the help of a therapist or researcher.

2. *Improvement of sEMG signal quality.* sEMG signal quality is a major concern for identifying patient muscle health. Care should be taken to ensure that the best signal can be read from the patient. The susceptibility of sEMG signals to noise and motion artifact, as well as the dependency of sEMG signals on environmental factors such as temperature and humidity, will be an ongoing issue. As well, the EMG sensors will need to be placed correctly on each patient's limb while wearing the device. Again, the use of HD-sEMG electrode arrays may assist with these issues.

The purpose of this thesis was to develop and evaluate EMG-based classification models for identifying and monitoring the health of elbow trauma patients. Classification models were de-

veloped that indicated possible to discern between healthy and injured limbs of patients with accuracies of up to 82%. This work also indicated that there are EMG trends that may be used to evaluate patient health. However, the models developed in this thesis are not yet useful for a practical elbow brace. There is the potential for implementing a classification model of health in a rehabilitative elbow brace to assess patients recovering from elbow trauma, however, further work in this direction, including further data collection, validation, optimization, and improvements to the existing state-of-the-art EMG acquisition systems will be necessary to achieve this goal.

References

- [1] GBD 2016 Disease and Injury Incidence and Prevalence Collaborators, “Global, regional, and national incidence, prevalence, and years lived with disability for 328 diseases and injuries for 195 countries, 1990–2016: a systematic analysis for the Global Burden of Disease Study 2016,” *The Lancet*, vol. 390, no. 10100, pp. 1211–1259, 2017.
- [2] Canadian Institute of Musculoskeletal Health and Arthritis. (2014) IMHA Strategic Plan 2014–2018. [Online]. Available: <http://www.cihr-irsc.gc.ca/e/48830.html>
- [3] D. G. Hoy, E. Smith, M. Cross, L. Sanchez-Riera, F. M. Blyth, R. Buchbinder, A. D. Woolf, T. Driscoll, P. Brooks, and L. M. March, “Reflecting on the global burden of musculoskeletal conditions: Lessons learnt from the global burden of disease 2010 study and the next steps forward,” *Annals of the Rheumatic Diseases*, vol. 74, no. 1, pp. 4–7, 2015.
- [4] P. Maciejasz, J. Eschweiler, K. Gerlach-Hahn, A. Jansen-Troy, and S. Leonhardt, “A survey on robotic devices for upper limb rehabilitation,” *Journal of NeuroEngineering and Rehabilitation*, vol. 11, p. 3, 2014.
- [5] Myomo. (2018) Myomo. 2018. [Online] Available: <http://myomo.com>. [Accessed: 18-Jan-2018].
- [6] L. R. Martin, S. L. Williams, K. B. Haskard, and M. R. Dimatteo, “The challenge of patient adherence,” *Therapeutics and Clinical Risk Management*, vol. 1, no. 3, pp. 189–99, 2005.
- [7] D. Stasinopoulos, I. Stasinopoulos, M. Pantelis, and K. Stasinopoulou, “Comparison of effects of a home exercise programme and a supervised exercise programme for the management of lateral elbow tendinopathy,” *Br J Sports Med*, vol. 44, pp. 579–583, 2010.

- [8] H. Gutiérrez-Espinoza, D. Rubio-Oyarzún, C. Olguín-Huerta, R. Gutiérrez-Monclus, S. Pinto-Concha, and G. Gana-Hervias, “Supervised physical therapy vs home exercise program for patients with distal radius fracture: A single-blind randomized clinical study,” *Journal of Hand Therapy*, vol. 30, no. 3, pp. 242–252, 2017.
- [9] J. Yousefi and A. Hamilton-Wright, “Characterizing EMG data using machine-learning tools,” *Computers in Biology and Medicine*, vol. 51, pp. 1–13, 2014.
- [10] C. Page, S. I. Backus, and M. W. Lenhoff, “Electromyographic activity in stiff and normal elbows during elbow flexion and extension,” *J. Hand Ther.*, vol. 16, pp. 5–11, 2003.
- [11] K. M. Calder, D. A. Gabriel, and L. McLean, “Differences in EMG spike shape between individuals with and without non-specific arm pain,” *Journal of Neuroscience Methods*, vol. 178, pp. 148–156, 2009.
- [12] R. Haddara, “Elbow patients’ data collection and analysis: An examination of electromyography healing patterns,” Master’s thesis, The University of Western Ontario, 2016.
- [13] B. Morrey, *The Elbow and its Disorders*, 3rd ed. Philadelphia: W.B. Saunders, 2000.
- [14] S. Fornalski, R. Gupta, and T. Q. Lee, “Anatomy and biomechanics of the elbow joint.” *Techniques in Hand and Upper Extremity Surgery*, vol. 7, no. 4, pp. 168–178, 2003.
- [15] S. Nandi, S. Maschke, P. J. Evans, and J. N. Lawton, “The stiff elbow,” *HAND*, vol. 4, pp. 368–379, 2009.
- [16] S. J. Chinchalkar and M. Szerkeres, “Rehabilitation of elbow trauma,” *Hand Clinics*, vol. 20, pp. 363–374, 2004.
- [17] M. H. Ebrahimzadeh, H. Amadzadeh-Chabock, and D. Ring, “Traumatic Elbow Instability,” *Journal of Hand Surgery*, vol. 35, no. 7, pp. 1220–1225, 2010.
- [18] A. Celli, “Anatomy and biomechanics of the elbow,” in *Treatment of Elbow Lesions*. Trento, Italy: Springer-Verlag, 2008, pp. 1–11.

- [19] D. T. Leonello, I. J. Galley, G. I. Bain, and C. D. Carter, “Brachialis muscle anatomy: A study in cadavers,” *Journal of Bone and Joint Surgery*, vol. 89, no. 6, pp. 1293–1297, 2007.
- [20] I. Fusaro, S. Orsini, S. Stignani Kantar, T. Sforza, M. G. Benedetti, G. Bettelli, and R. Rotini, “Elbow rehabilitation in traumatic pathology,” *Musculoskeletal Surgery*, vol. 98, pp. S95–S102, 2014.
- [21] D. A. Schwartz, “Static progressive orthoses for the upper extremity: a comprehensive literature review,” *HAND*, vol. 7, pp. 10–17, 2012.
- [22] J. C. Macdermid, J. I. Vincent, L. Kieffer, A. Kieffer, J. Demaiter, and S. Macintosh, “A survey of practice patterns for rehabilitation post elbow fracture,” *The Open Orthopaedics Journal*, vol. 6, pp. 429–439, 2012.
- [23] C. E. Nash, S. M. Mickan, C. B. Del Mar, and P. P. Glasziou, “Resting injured limbs delays recovery: a systematic review,” *Journal of Family Practice*, vol. 53, no. 9, pp. 706–712, 2004.
- [24] American College of Sports Medicine, “Progression Models in Resistance Training for Healthy Adults,” *Medicine & Science in Sports & Exercise*, vol. 41, no. 3, pp. 687–708, 2009.
- [25] A. Marinelli, G. Bettelli, E. Guerra, M. Nigrisoli, and R. Rotini, “Mobilization brace in post-traumatic elbow stiffness,” *Musculoskeletal Surgery*, vol. 94, Suppl 1, pp. S37–45, 2010.
- [26] P. Brach and R. J. Goitz, “Elbow Arthroscopy: Surgical Techniques and Rehabilitation,” *Journal of Hand Therapy*, pp. 228–237, 2006.
- [27] S. A. Dávila and K. Johnston-Jones, “Managing the Stiff Elbow: Operative, Nonoperative, and Postoperative Techniques,” *Journal of Hand Therapy*, vol. 19, no. 2, pp. 268–281, 2006.
- [28] D. D. Savin, J. Watson, A. R. Youderian, S. Lee, J. E. Hammarstedt, M. R. Hutchinson, and B. A. Goldberg, “Surgical Management of Acute Distal Biceps Tendon Ruptures,” *The Journal of Bone and Joint Surgery*, vol. 99, pp. 785–796, 2017.
- [29] A. Cil, S. Merten, and S. P. Steinmann, “Immediate active range of motion after modified 2-incision repair in acute distal biceps tendon rupture,” *The American Journal of Sports Medicine*, vol. 37, no. 1, pp. 130–135, 2009.

- [30] L. O'Brien, "Adherence to therapeutic splint wear in adults with acute upper limb injuries: a systematic review," *Hand Therapy*, vol. 15, pp. 3–12, 2010.
- [31] A. S. Dowrick, B. J. Gabbe, O. D. Williamson, and P. A. Cameron, "Outcome instruments for the assessment of the upper extremity following trauma: A review," *Injury*, vol. 36, no. 4, pp. 468–476, 2005.
- [32] J. I. Vincent, J. C. Macdermid, G. J. King, and R. Grewal, "Linking of the Patient Rated Elbow Evaluation (PREE) and the American Shoulder and Elbow Surgeons - Elbow questionnaire (pASES-e) to the International Classification of Functioning Disability and Health (ICF) and hand core sets," *Journal of Hand Therapy*, vol. 28, no. 1, pp. 61–68, 2015.
- [33] L. Pignolo, G. Dolce, G. Basta, L. F. Lucca, S. Serra, and W. G. Sannita, "Upper limb rehabilitation after stroke: ARAMIS a robo-mechatronic innovative approach and prototype," *Proceedings of the IEEE RAS and EMBS International Conference on Biomedical Robotics and Biomechatronics*, pp. 1410–1414, 2012.
- [34] V. Crocher, A. Sahbani, J. Robertson, A. Roby-Brami, and G. Morel, "Constraining upper limb synergies of hemiparetic patients using a robotic exoskeleton in the perspective of neuro-rehabilitation," *IEEE Transactions on Neural Systems and Rehabilitation Engineering*, vol. 20, no. 3, pp. 247–257, 2012.
- [35] T. Nef, M. Guidali, and R. Riener, "ARMin III - arm therapy exoskeleton with an ergonomic shoulder actuation," *Applied Bionics and Biomechanics*, vol. 6, no. 2, pp. 127–142, 2009.
- [36] R. J. Sanchez, J. Liu, S. Rao, P. Shah, R. Smith, T. Rahman, S. C. Cramer, J. E. Bobrow, and D. J. Reinkensmeyer, "Automating arm movement training following severe stroke: Functional exercises with quantitative feedback in a gravity-reduced environment," *IEEE Transactions on Neural Systems and Rehabilitation Engineering*, vol. 14, no. 3, pp. 378–389, 2006.
- [37] M. Simkins, H. Kim, G. Abrams, N. Byl, and J. Rosen, "Robotic unilateral and bilateral upper-limb movement training for stroke survivors afflicted by chronic hemiparesis," in *IEEE*

- International Conference on Rehabilitation Robotics*, Seattle, Washington, June 24–26, 2013, pp. 1–6.
- [38] Y. Mao and S. K. Agrawal, “Design of a cable-driven arm exoskeleton (CAREX) for neural rehabilitation,” *IEEE Transactions on Robotics*, vol. 28, no. 4, pp. 922–931, 2012.
- [39] Y. Ren, S. H. Kang, H. S. Park, Y. N. Wu, and L. Q. Zhang, “Developing a multi-joint upper limb exoskeleton robot for diagnosis, therapy, and outcome evaluation in neurorehabilitation,” *IEEE Transactions on Neural Systems and Rehabilitation Engineering*, vol. 21, no. 3, pp. 490–499, 2013.
- [40] T. Sakurada, T. Kawase, K. Takano, T. Komatsu, and K. Kansaku, “A BMI-based occupational therapy assist suit: Asynchronous control by SSVEP,” *Frontiers in Neuroscience*, vol. 7, no. 7 SEP, pp. 1–10, 2013.
- [41] E. Pirondini, M. Coscia, S. Marcheschi, G. Roas, F. Salsedo, A. Frisoli, M. Bergamasco, and S. Micera, “Evaluation of a new exoskeleton for upper limb post-stroke neuro-rehabilitation: Preliminary results,” in *Replace, Repair, Restore, Relieve – Bridging Clinical and Engineering Solutions in Neurorehabilitation*, W. Jensen, O. K. Andersen, and M. Akay, Eds. New York, NY: Springer, 2014, pp. 637–645.
- [42] A. Frisoli, C. Procopio, C. Chisari, I. Creatini, L. Bonfiglio, M. Bergamasco, B. Rossi, and M. C. Carboncini, “Positive effects of robotic exoskeleton training of upper limb reaching movements after stroke,” *Journal of NeuroEngineering and Rehabilitation*, vol. 9, no. 1, p. 36, 2012.
- [43] Hocoma. (2018) Solutions for Arm & Hand. 2018. [Online] Available: <https://www.hocoma.com/solutions/arm-hand>. [Accessed: 18-Jan-2018].
- [44] S. Balasubramanian, R. Wei, M. Perez, B. Shepard, E. Koeneman, J. Koeneman, and J. He, “Rupert: An exoskeleton robot for assisting rehabilitation of arm functions,” in *2008 Virtual Rehabilitation*, Vancouver, BC, Canada, Aug 25–27, 2008, pp. 163–167.

- [45] T. Desplenter, A. Kyrylova, T. K. Stanbury, A. Escot, S. Chinchalkar, and A. L. Trejos, “A Wearable Mechatronic Brace for Arm Rehabilitation,” in *2014 5th IEEE RAS & EMBS International Conference on Biomedical Robotics and Biomechatronics (BioRob)*, 2014, pp. 491–496.
- [46] R. Bin Ambar, B. M. P. Hazwaj, A. M. B. M. Ali, M. S. Bin Ahmad, and M. M. Bin Abdul Jamil, “Multi-sensor arm rehabilitation monitoring device,” in *2012 International Conference on Biomedical Engineering, ICoBE 2012*, 2012.
- [47] S. H. Roy, M. S. Cheng, S. S. Chang, J. Moore, G. De Luca, S. H. Nawab, and C. J. De Luca, “A combined sEMG and accelerometer system for monitoring functional activity in stroke,” *IEEE Transactions on Neural Systems and Rehabilitation Engineering*, vol. 12, no. 6, 2009.
- [48] S. Patel, R. Hughes, T. Hester, J. Stein, M. Akay, J. G. Dy, and P. Bonato, “A novel approach to monitor rehabilitation outcomes in stroke survivors using wearable technology,” *Proceedings of the IEEE*, vol. 98, no. 3, pp. 450–461, 2010.
- [49] D. J. Reinkensmeyer and V. Dietz, *Neurorehabilitation Technology*, 2nd ed. Switzerland: Springer, 2016.
- [50] L. Bishop and J. Stein, “Three upper limb robotic devices for stroke rehabilitation: A review and clinical perspective,” *NeuroRehabilitation*, vol. 33, no. 1, pp. 3–11, 2013.
- [51] T. Proietti, V. Crocher, A. Roby-Brami, and N. Jarrasse, “Upper-limb robotic exoskeletons for neurorehabilitation: A review on control strategies,” *IEEE Reviews in Biomedical Engineering*, vol. 9, pp. 4–14, 2016.
- [52] V. Klamroth-Marganska, J. Blanco, K. Campen, A. Curt, V. Dietz, T. Ettlin, M. Felder, B. Fellinghauer, M. Guidali, A. Kollmar, A. Luft, T. Nef, C. Schuster-Amft, W. Stahel, and R. Riener, “Three-dimensional, task-specific robot therapy of the arm after stroke: A multicentre, parallel-group randomised trial,” *The Lancet Neurology*, vol. 13, no. 2, pp. 159–166, 2014.

- [53] S. J. Page, V. Hill, and S. White, “Portable upper extremity robotics is as efficacious as upper extremity rehabilitative therapy: a randomized controlled pilot trial,” *Clinical Rehabilitation*, vol. 0, no. 0, 2012.
- [54] J. Zariffa, N. Kapadia, J. L. K. Kramer, P. Taylor, M. Alizadeh-Meghrazi, V. Zivanovic, R. Willms, A. Townson, A. Curt, M. R. Popovic, and J. D. Steeves, “Feasibility and efficacy of upper limb robotic rehabilitation in a subacute cervical spinal cord injury population,” *Spinal Cord*, vol. 50, no. 3, pp. 220–226, 2012.
- [55] A. C. Lo, P. D. Guarino, L. G. Richards, J. K. Haselkorn, G. F. Wittenberg, D. G. Federman, R. J. Ringer, T. H. Wagner, H. I. Krebs, B. T. Volpe, C. T. Bever, D. M. Bravata, P. W. Duncan, B. H. Corn, A. D. Maffucci, S. E. Nadeau, S. S. Conroy, J. M. Powell, G. D. Huang, and P. Peduzzi, “Robot-Assisted Therapy for Long-Term Upper-Limb Impairment after Stroke,” *New England Journal of Medicine*, vol. 362, no. 19, pp. 1772–1783, 2010.
- [56] T. Moritani, D. Stegeman, and R. Merletti, “Basic physiology and biophysics of emg signal generation,” in *Electromyography: Physiology, Engineering, and Noninvasive Applications*. Hoboken, NJ: Wiley, 2004, pp. 1–25.
- [57] “Excitable tissue: Muscle,” in *Ganongs Review of Medical Physiology*, 24th ed., K. E. Barrett, Ed. McGraw-Hill Medical, 2012, ch. 5.
- [58] D. Dumitru, “Physiologic basis of potentials recorded in electromyography,” *Muscle and Nerve*, vol. 23, pp. 1667–1685, 2000.
- [59] G. Kamen and D. A. Gabriel, *Essentials of Electromyography*. Champaign, IL, USA: Human Kinetics, 2010.
- [60] H. J. Hermens, B. Freriks, C. Disselhorst-Klug, and G. Rau, “Development of recommendations for SEMG sensors and sensor placement procedures,” *Journal of Electromyography and Kinesiology*, vol. 10, pp. 361–374, 2000.

- [61] R. Merletti, M. Aventaggiato, A. Botter, A. Holobar, H. Marateb, and T. M. M. Vieira, “Advances in surface EMG: recent progress in detection and processing techniques.” *Critical Reviews in Biomedical Engineering*, vol. 38, no. 4, pp. 305–345, 2010.
- [62] F. Hug, “Can muscle coordination be precisely studied by surface electromyography?” *Journal of Electromyography and Kinesiology*, vol. 21, pp. 1–12, 2011.
- [63] A. M. Hughes, C. T. Freeman, J. H. Burridge, P. H. Chappell, P. L. Lewin, R. M. Pickering, and E. Rogers, “Shoulder and elbow muscle activity during fully supported trajectory tracking in neurologically intact older people,” *Journal of Electromyography and Kinesiology*, vol. 19, no. 6, pp. 1025–1034, 2009.
- [64] A. M. Hughes, C. T. Freeman, J. H. Burridge, P. H. Chappell, P. L. Lewin, and E. Rogers, “Shoulder and elbow muscle activity during fully supported trajectory tracking in people who have had a stroke,” *Journal of Electromyography and Kinesiology*, vol. 20, no. 3, pp. 465–476, 2010.
- [65] J. Y. Hogrel, “Clinical applications of surface electromyography in neuromuscular disorders,” *Neurophysiologie Clinique*, vol. 35, no. 2-3, pp. 59–71, 2005.
- [66] R. Merletti, A. Botter, A. Troiano, E. Merlo, and M. A. Minetto, “Technology and instrumentation for detection and conditioning of the surface electromyographic signal: State of the art,” *Clinical Biomechanics*, vol. 24, pp. 122–134, 2009.
- [67] M. Hakonen, H. Piitulainen, and A. Visala, “Current state of digital signal processing in myoelectric interfaces and related applications,” *Biomedical Signal Processing and Control*, vol. 18, pp. 334–359, 2015.
- [68] A. J. Young, L. J. Hargrove, and T. A. Kuiken, “Improving myoelectric pattern recognition robustness to electrode shift by changing interelectrode distance and electrode configuration,” *IEEE Transactions on Biomedical Engineering*, vol. 59, no. 3, pp. 645–652, 2012.
- [69] B. Afsharipour, K. Ullah, and R. Merletti, “Spatial aliasing and EMG amplitude in time and space: simulated action potential maps,” in *XIII Mediterranean Conference on Medical*

- and Biological Engineering and Computing*, vol. 41, Seville, Spain, Sept 25–28, 2013, pp. 293–296.
- [70] P. Laferriere, E. D. Lemaire, and A. D. C. Chan, “Surface Electromyographic Signals Using Dry Electrodes,” *IEEE Transactions on Instrumentation and Measurement*, vol. 60, no. 10, pp. 3259–3268, 2011.
- [71] SENIAM project, “Seniam,” 2018. [Online] Available: <http://seniam.org>. [Accessed: 02-Feb-2016].
- [72] D. T. Mewett, K. J. Reynolds, and H. Nazeran, “Reducing power line interference in digitised electromyogram recordings by spectrum interpolation,” *Medical and Biological Engineering and Computing*, vol. 42, no. 4, pp. 524–531, 2004.
- [73] A. Burden, “How should we normalize electromyograms obtained from healthy participants? What we have learned from over 25 years of research,” *Journal of Electromyography and Kinesiology*, vol. 20, pp. 1023–1035, 2010.
- [74] J. P. Clarys, “Electromyography in sports and occupational settings: An update of its limits and possibilities,” *Ergonomics*, vol. 43, no. 10, pp. 1750–1762, 2000.
- [75] J. Drapała, K. Brzostowski, A. Szpala, and A. Rutkowska-Kucharska, “Two stage EMG onset detection method,” *Archives of Control Sciences*, vol. 22, no. 4, pp. 427–440, 2012.
- [76] P. Bonato, T. D’Alessio, and M. Knaflitz, “A statistical method for the measurement of muscle activation intervals from surface myoelectric signal during gait,” *IEEE Transactions on Biomedical Engineering*, vol. 45, no. 3, pp. 287–299, 1998.
- [77] J. D. van Putten Jr., “EMG Onset Determination Using a Maximum Likelihood Method,” in *Proceedings of the First Joint BMES/EMBS Conference*, Atlanta, GA, USA, Oct 13–16, 1999, p. 571.
- [78] A. Merlo, D. Farina, and R. Merletti, “A fast and reliable technique for muscle activity detection from surface EMG signals,” *IEEE Transactions on Biomedical Engineering*, vol. 50, no. 3, pp. 316–323, 2003.

- [79] S. Solnik, P. Rider, K. Steinweg, P. Devita, and T. Hortobágyi, “Teager–Kaiser energy operator signal conditioning improves EMG onset detection,” *European Journal of Applied Physiology*, vol. 110, pp. 489–498, 2010.
- [80] A. Phinyomark, P. Phukpattaranont, and C. Limsakul, “Feature reduction and selection for EMG signal classification,” *Expert Systems With Applications*, vol. 39, pp. 7420–7431, 2012.
- [81] E. Scheme and K. Englehart, “Electromyogram pattern recognition for control of powered upper-limb prostheses: State of the art and challenges for clinical use,” *Journal of Rehabilitation Research & Development*, vol. 48, no. 6, pp. 643–660, 2011.
- [82] A. Subasi and M. K. Kiymik, “Muscle fatigue detection in EMG using time-frequency methods, ICA and neural networks,” *Journal of Medical Systems*, vol. 34, no. 4, pp. 777–785, 2010.
- [83] C. M. Bishop, *Pattern Recognition and Machine Learning*. Singapore: Springer, 2006.
- [84] M. A. Oskoei and H. Hu, “Myoelectric control systems—A survey,” *Biomedical Signal Processing and Control*, vol. 2, pp. 275–294, 2007.
- [85] L. H. Smith, L. J. Hargrove, B. A. Lock, and T. A. Kuiken, “Determining the optimal window length for pattern recognition-based myoelectric control: Balancing the competing effects of classification error and controller delay,” *IEEE Transactions on Neural Systems and Rehabilitation Engineering*, vol. 19, no. 2, 2011.
- [86] K. Englehart and B. Hudgins, “A robust, real-time control scheme for multifunction myoelectric control,” *IEEE Transactions on Biomedical Engineering*, vol. 50, no. 7, 2003.
- [87] M. A. Oskoei and H. Hu, “Support Vector Machine-Based Classification Scheme for Myoelectric Control Applied to Upper Limb,” *IEEE Transactions on Biomedical Engineering*, vol. 55, no. 8, pp. 1956–1965, 2008.
- [88] E. N. Kamavuako, E. J. Scheme, and K. B. Englehart, “Determination of optimum threshold values for EMG time domain features; a multi-dataset investigation,” *Journal of Neural Engineering*, vol. 13, p. 046011, 2016.

- [89] M. Zardoshti-Kermani, B. C. Wheeler, K. Badie, and R. M. Hashemi, “Feature Evaluation for Movement Control of Upper Extremity Prostheses,” *IEEE Transactions on Rehabilitation Engineering*, vol. 3, no. 4, pp. 324–333, 1995.
- [90] B. Hudgins, P. Parker, and R. N. Scott, “A New Strategy for Multifunction Myoelectric Control,” *IEEE Transactions on Biomedical Engineering*, vol. 40, no. 1, pp. 82–94, 1993.
- [91] S. Du and M. Vuskovic, “Temporal vs. spectral approach to feature extraction from prehensile EMG signals,” in *Proceedings of the 2004 IEEE International Conference on Information Reuse and Integration*, Las Vegas, NV, USA, Nov 8-10, 2004, pp. 344–350.
- [92] A. Phinyomark, C. Limsakul, and P. Phukpattaranont, “A Novel Feature Extraction for Robust EMG Pattern Recognition,” *Journal of Computing*, vol. 1, no. 1, pp. 71–80, 2009.
- [93] M. R. Bozkurt, A. Subaşı, E. Köklökaya, and M. Yilmaz, “Comparison of AR parametric methods with subspace-based methods for EMG signal classification using stand-alone and merged neural network models,” *Turkish Journal of Electrical Engineering and Computer Sciences*, vol. 24, no. 3, pp. 1547–1559, 2016.
- [94] A. Phinyomark, P. Phukpattaranont, and C. Limsakul, “Fractal analysis features for weak and single-channel upper-limb EMG signals,” *Expert Systems with Applications*, vol. 39, pp. 11 156–11 163, 2012.
- [95] J. Zhao, L. Jiang, H. Cai, H. Liu, and G. Hirzinger, “A novel EMG motion pattern classifier based on wavelet transform and nonlinearity analysis method,” in *2006 IEEE International Conference on Robotics and Biomimetics, ROBIO 2006*, 2006.
- [96] X. Zhang and P. Zhou, “Sample entropy analysis of surface EMG for improved muscle activity onset detection against spurious background spikes,” *Journal of Electromyography and Kinesiology*, vol. 22, no. 6, pp. 901–907, 2012.
- [97] S. M. Pincus, “Approximate entropy as a measure of system complexity,” *Mathematics*, vol. 88, pp. 2297–2301, 1991.

- [98] A. Phinyomark, F. Quaine, S. Charbonnier, C. Serviere, F. Tarpin-Bernard, and Y. Laurillau, “EMG feature evaluation for improving myoelectric pattern recognition robustness,” *Expert Systems with Applications*, vol. 40, pp. 4832–4840, 2013.
- [99] J. S. Richman and J. R. Moorman, “Physiological time-series analysis using approximate entropy and sample entropy,” *American Journal of Physiology-Heart and Circulatory Physiology*, vol. 278, pp. H2039–H2049, 2000.
- [100] E. L. van den Broek, M. H. Schut, J. H. D. M. Westerink, J. van Herk, and K. Tuinenbreijer, “Computing emotion awareness through facial electromyography,” in *Proceedings of international conference on computer vision in human-computer interaction*, 2006, pp. 52–63.
- [101] K. Nazarpour, A. H. Al-Timemy, G. Bugmann, and A. Jackson, “A note on the probability distribution function of the surface electromyogram signal,” *Brain Research Bulletin*, vol. 90, no. 1, pp. 88–91, 2013.
- [102] X. Zhang, Y. Wang, and R. P. Han, “Wavelet transform theory and its application in EMG signal processing,” in *2010 Seventh International Conference on Fuzzy Systems and Knowledge Discovery*, Yantai, China, Aug 10–12, 2010, pp. 2234–2238.
- [103] A. Phinyomark, A. Nuidod, P. Phukpattaranont, and C. Limsakul, “Feature extraction and reduction of wavelet transform coefficients for EMG pattern classification,” *Electronics and Electrical Engineering*, vol. 122, no. 6, pp. 27–32, 2012.
- [104] D. A. Gabriel, S. M. Lester, S. A. Lenhardt, and E. D. J. Cambridge, “Analysis of surface EMG spike shape across different levels of isometric force,” *Journal of Neuroscience Methods*, vol. 159, pp. 146–152, 2007.
- [105] D. L. Davies and D. W. Bouldin, “A Cluster Separation Measure,” *IEEE Transactions on Pattern Analysis and Machine Intelligence*, vol. PAMI-1, no. 2, pp. 224–227, 1979.

- [106] S. Micera, A. M. Sabatini, P. Dario, and B. Rossi, “A hybrid approach to EMG pattern analysis for classification of arm movements using statistical and fuzzy techniques,” *Medical Engineering & Physics*, vol. 21, pp. 303–311, 1999.
- [107] G. Wang, Z. Wang, W. Chen, and J. Zhuang, “Classification of surface EMG signals using optimal wavelet packet method based on Davies-Bouldin criterion,” *Medical and Biological Engineering and Computing*, vol. 44, no. 10, pp. 865–872, 2006.
- [108] I. Kononenko, E. Šimec, and M. Robnik-Šikonja, “Overcoming the myopia of inductive learning algorithms with RELIEFF,” *Applied Intelligence*, vol. 7, pp. 39–55, 1997.
- [109] R. Boostani and M. H. Moradi, “Evaluation of the forearm EMG signal features for the control of a prosthetic hand,” *Physiological Measurement*, vol. 24, pp. 309–319, 2003.
- [110] G. R. Naik, E. Selvan, M. Gobbo, A. Acharyya, H. T. Nguyen, G. R. Naik, and S. E. Selvan, “Principal Component Analysis Applied to Surface Electromyography: A Comprehensive Review,” vol. 4, pp. 4025–4037, 2016.
- [111] G. James, D. Witten, T. Hastie, and R. Tibshirani, *An Introduction to Statistical Learning with Applications in R*. New York: Springer, 2015.
- [112] A. Fougner, E. Scheme, A. D. Chan, K. Englehart, and Ø. Stavdahl, “Resolving the limb position effect in myoelectric pattern recognition,” *IEEE Transactions on Neural Systems and Rehabilitation Engineering*, vol. 19, no. 6, pp. 644–651, 2011.
- [113] F. AlOmari and G. Liu, “Analysis of Extracted Forearm sEMG Signal Using LDA, QDA, K-NN Classification Algorithms,” *The Open Automation and Control Systems Journal*, vol. 6, pp. 108–116, 2014.
- [114] K. S. Kim, H. H. Choi, C. S. Moon, and C. W. Mun, “Comparison of k-nearest neighbor, quadratic discriminant and linear discriminant analysis in classification of electromyogram signals based on the wrist-motion directions,” *Current Applied Physics*, vol. 11, pp. 740–745, 2011.

- [115] A. Subasi, “Classification of EMG signals using PSO optimized SVM for diagnosis of neuromuscular disorders,” *Computers in Biology and Medicine*, vol. 43, pp. 576–586, 2013.
- [116] S. Hyeon-Min and L. Sangmin, “Multi-channel electromyography pattern classification using deep belief networks for enhanced user experience,” *Journal of Central South University of Technology*, vol. 22, pp. 1801–1808, 2015.
- [117] L. D. Gilmore, G. De Luca, and C. J. De Luca, “Biomedical electrode configuration for suppressing movement artifact,” U.S. Patent 12 583 656, Aug 28, 2009.
- [118] S. Patel, R. Hughes, T. Hester, J. Stein, M. Akay, J. Dy, and P. Bonato, “Tracking motor recovery in stroke survivors undergoing rehabilitation using wearable technology,” in *Conf. Proc. IEEE Eng. Med. Biol. Soc.*, Buenos Aires, Argentina, August 31–September 4, 2010, pp. 6858–6861.
- [119] J. Chiang, Z. J. Wang, and M. J. McKeown, “A hidden Markov, multivariate autoregressive (HMM-mAR) network framework for analysis of surface EMG (sEMG) data,” *IEEE Transactions on Signal Processing*, 2008.
- [120] Y. Benjamini and Y. Hochberg, “Controlling the false discovery rate : A practical and powerful approach to multiple testing,” *Journal of the Royal Statistical Society. Series B (Methodological)*, vol. 57, no. 1, pp. 289–300, 1995.
- [121] M. Syczewska, M. Krawczyk, E. Szczerbik, and M. Kalinowska, “Timing of electromyographic activity and ranges of motion during simple motor tasks of upper extremities,” *Biomedical Human Kinetics*, vol. 9, no. 1, pp. 146–157, 2017.
- [122] A. D. C. Chan and G. C. Green, “Myoelectric control development toolbox,” in *30th Conference of the Canadian Medical & Biological Engineering Society*, Toronto, Canada, M0100, 2007.
- [123] K. Lee, “Sample entropy,” 2012. [Online] Available: <https://www.mathworks.com/matlabcentral/fileexchange/35784-sample-entropy>. [Accessed: 01-Jan-2017].

- [124] J. Monge-Álvarez, “Higuchi and katz fractal dimension measures,” 2015.
[Online] Available: <https://www.mathworks.com/matlabcentral/fileexchange/50290-higuchi-and-katz-fractal-dimension-measures>. [Accessed: 01-Jan-2017].

Appendix A

Permissions and Approvals

The following ethics permission statements and forms are presented in this Appendix:

1. Ethics Approval for Trials on Patients from the Research Ethics Board for Health Sciences
Research Involving Human Subjects at the University of Western Ontario
2. Patient Consent Form
3. Patient Trial Form
4. Permissions for Images



**Western
Research**

Western University Health Science Research Ethics Board
HSREB Amendment Approval Notice

Research Ethics

Principal Investigator: Dr. Ana Luisa Trejos

Department & Institution: Unknown,London Health Sciences Centre

Review Type: Full Board

HSREB File Number: 106913

Study Title: Patient Data Collection and Analysis for Elbow Smart Brace

Sponsor: Natural Sciences and Engineering Research Council

HSREB Amendment Approval Date: February 07, 2017

HSREB Expiry Date: October 01, 2017

Documents Approved and/or Received for Information:

Document Name	Comments	Version Date
Instruments	List of Instruments	2017/01/18
Western University Protocol	Rc'd 27Jan2017	
Letter of Information & Consent	LOI/C	2017/01/16

The Western University Health Science Research Ethics Board (HSREB) has reviewed and approved the amendment to the above named study, as of the HSREB Initial Approval Date noted above.

HSREB approval for this study remains valid until the HSREB Expiry Date noted above, conditional to timely submission and acceptance of HSREB Continuing Ethics Review.

The Western University HSREB operates in compliance with the Tri-Council Policy Statement Ethical Conduct for Research Involving Humans (TCPS2), the International Conference on Harmonization of Technical Requirements for Registration of Pharmaceuticals for Human Use Guideline for Good Clinical Practice Practices (ICH E6 R1), the Ontario Personal Health Information Protection Act (PHIPA, 2004), Part 4 of the Natural Health Product Regulations, Health Canada Medical Device Regulations and Part C, Division 5, of the Food and Drug Regulations of Health Canada.

Members of the HSREB who are named as Investigators in research studies do not participate in discussions related to, nor vote on such studies when they are presented to the REB.

The HSREB is registered with the U.S. Department of Health & Human Services under the IRB registration number IRB 00000940.



Letter of Information

Title: Patient Data Collection and Analysis for an Elbow Smart Brace

Dr. Ana Luisa Trejos, Ph.D., P.Eng (Principal Investigator)

Assistant Professor, Department of Electrical and Computer Engineering
[REDACTED]

Associate Scientist, Canadian Surgical Technologies & Advanced Robotics (CSTAR)
[REDACTED]
[REDACTED]

Shrikant Chinchalkar, (Co-Investigator)

Therapist, Schulich School of Medicine and Dentistry
Roth-McFarlane Hand and Upper Limb Centre
[REDACTED]
[REDACTED]

Emma Farago, M.E.Sc. Candidate (Coordinator)

Graduate Student, Electrical and Computer Engineering
[REDACTED]
[REDACTED]

Abelardo Escoto, M.E.Sc. (Coordinator)

Associate Researcher, Canadian Surgical Technologies & Advanced Robotics (CSTAR)
[REDACTED]

Dr. Evan Friedman (Industry Sponsor/Collaborator)

Intronix Technologies Corporation
[REDACTED]
[REDACTED]

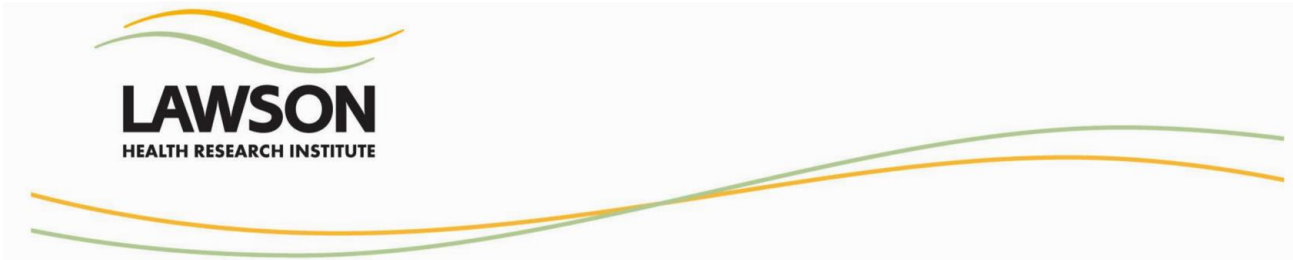
Please Initial: _____

Version 2 (16-01-2017)

Page 1 of 6

The research institute of London Health Sciences Centre and
St. Joseph's Health Care, London.





Sponsor Information:

Intronix Technologies Corporation designs and produces progressive portable medical devices for neuromuscular diagnostics and treatment delivery. Its innovations in injection guidance provide technology that drives clinical solutions to deliver confidence, improve workflow efficiency, and provide a better patient experience. Intronix has extensive experience within the neuromuscular diagnostic and treatment delivery market. Intronix quality system is registered to both ISO 9001:2008 and ISO 13485:2003 (CMDCAS), and is fully USFDA compliant.

For this project, Intronix has lent the WearME Lab their electromyography data collection system and is developing software that will help with improved data collection strategies. All of the data analysis will be performed at the WearMe Lab. Some data samples will need to be sent to Intronix so that they can fine-tune the software to improve the data collection

Conflict of Interest:

There are no real or perceived conflicts of interest in this study.

Details of the Study:

You are being invited to participate in this research study about collecting muscular activity signals because you have a musculoskeletal injury or disorder in your arm.

Musculoskeletal Conditions cost the Canadian health care system over \$17 billion yearly. The purpose of this study is to create a reference base of task-specific bio-signals of people's arm motions in order to inform the development of smart rehabilitation technologies (smart braces). Our smart brace, the WearMe Brace, is a rigid brace in development for the purpose of supporting a patient's weak or deformed arm to enable functional activities. In order to enhance in the development of the brace, muscle activity data will be collected and analyzed to determine how muscle activity changes when the muscles heal. This will provide more intuitive and interpretable information for the control system of the smart brace. The results of the trials will provide valuable information for future improvements of the brace, such that it can provide therapy and assist individuals with upper arm musculoskeletal conditions.

You are being asked to participate because you have a musculoskeletal injury or disorder in your arm. Your usual standard of care will not be altered.

Please Initial: _____

Version 2 (16-01-2017)

Page 2 of 6

The research institute of London Health Sciences Centre and
St. Joseph's Health Care, London.



Up to 300 people will participate in this study and it will take 1 year to complete. It is expected that you will be in this study throughout the length of your treatment, until you fully recover (rehabilitation time is different from patient to patient).

Study Design and Procedures:

The experiments will be conducted at the Hand Therapy Clinic at Saint Joseph's Hospital. If you agree to participate, you will be first asked to sign the consent form. You will also be asked to fill out a self-reported trial form with your personal information as follows: age, gender, weight, height, and hand dominance. After that, a research coordinator will measure the dimensions of your arm. The one-time collection of such personal information is required because muscle activity is intimately related to these characteristics and being able to relate the data to these baseline values is critical for proper analysis.

You will then be asked to sit down on a chair. Surface electrodes (small sensors) will be placed on the skin overlying each muscle or group of muscles in the upper arm and forearm (using sticky pads). These sensors do not obstruct normal movement and are not invasive. The skin where the sensors will be placed will be cleaned with alcohol. As the alcohol vaporizes, two electrodes will be placed on the biceps, four on the triceps, and four on the forearm.

You will then be directed to perform the exercises prescribed by your hand therapist in his or her presence and guidance. The therapy normally provided by the therapist will not be modified. The activity of the arm muscles will be recorded during the tasks using the surface electrodes. A video camera will record the motions of your arm as you are performing the exercises. Your face will not appear in the frame of the camera at any time.

If your other arm is healthy and uninjured, you will be asked to participate in a one-time trial. If you agree, surface electrodes will also be placed on that arm. You will then be asked to put your arm in an adjustable mechanical brace. Your arm will then be secured to the brace using padded straps. The brace limits the arm motion in one of your natural directions of motion. You will be asked to hold a 5-pound weight on your hand and will be instructed to perform elbow flexion-extension tasks (biceps-curls) requiring you to move your lower arm through a specified range at a low speed. You will perform 3 sets of 3 repetitions at 6 different ranges of motion (for a total of 54 repetitions), with a 2-minute break in between sets. We will measure arm motion and muscle activity while you perform these tasks. You will be given a few trial runs to help you

Please Initial: _____

Version 2 (16-01-2017)

Page 3 of 6

The research institute of London Health Sciences Centre and
St. Joseph's Health Care, London.



learn and understand the process and the speed required for the motions. This experiment is a one-time process and you will not be asked to do it again during your next visits. It is estimated to take up to 45 minutes for this one-time experiment.

Your participation in this study is voluntary. You may decide not to be in this study, or to be in the study now and then change your mind later. You may leave the study at any time without affecting your care. We will give you new information that is learned during the study that might affect your decision to stay in the study.

Withdrawal:

If you decide to withdraw from the study, the information that was collected before you leave will still be used in order to help answer the research question. No new information will be collected without your permission.

Risks:

There are no added risks to you since you will be performing what your hand therapist is prescribing you to do.

For the healthy arm, there may be temporary muscle discomfort/fatigue due to the tasks being performed. The mechanical brace will limit your motion in a single plane, which is one of your natural motion directions. The operation can be stopped immediately at any time you wish. The loads for the trial are comparable to the weight of a textbook.

Benefits:

There are no direct benefits to you by participating in this study. Although you may not benefit directly from this study, your participation may contribute to our basic knowledge of human mechanical dynamics, human muscle recruitment, and how to incorporate this knowledge into improving the treatment of musculoskeletal disorders. It will also allow us to advance in the development of a mechatronics-enabled elbow brace in our lab through tuning the system and using the data to allow the brace to provide individualized therapy to its wearers.

Confidentiality:

Confidentiality cannot be 100% guaranteed. All data will be stored in password-protected personal computer ([REDACTED]). Hardcopies of any documents will be stored in locked cabinets in [REDACTED]. The only documents

Please Initial: _____

Version 2 (16-01-2017)

Page 4 of 6

The research institute of London Health Sciences Centre and St. Joseph's Health Care, London.



containing your name will be the Consent Forms, which will not be linked to any of the recorded data. Access to records and data is limited to authorized persons.

Qualified representatives of the following organizations may look at your study records at the site where these records are held, for quality assurance (to check that the information collected for the study is correct and follows proper laws and guidelines).

Examples include:

- Representatives of Lawson Quality Assurance Education Program
- Representatives of University of Western Ontario Health Sciences Research Ethics Board that oversees the ethical conduct of this study.
- Representatives of Health Canada or other regulatory bodies (groups of people who oversee research studies) outside of Canada, such as the United States food and Drug Administration.
- Intronix Technologies Corporation and its affiliated companies

Some of the muscle activity data collected will be transferred to Intronix Technologies Corporation by using an encrypted USB hard drive in order to improve the data collection software. Your anonymity will be protected through the use of alphanumeric codes when analyzing your experimental data.

This project is supported by a Discovery Grant and an Engage grant of the Natural Sciences and Engineering Research Council (NSERC) of Canada, by the Western Strategic Support for NSERC Success Grant, by the Academic Development Fund, Western University, and by the Ontario Centres of Excellence with support from Intronix Technologies Corporation.

If you have any questions or concerns regarding participation in our study, please contact Dr. Ana Luisa Trejos [REDACTED]

If you have any questions about the conduct of this study or your rights as a research subject you may contact Dr. David Hill, Scientific Director, Lawson Health Research Institute at [REDACTED]

[REDACTED] A copy of this information package is yours to keep for your personal records.

Please Initial: _____

Version 2 (16-01-2017)

Page 5 of 6

The research institute of London Health Sciences Centre and
St. Joseph's Health Care, London.





CONSENT FORM

Title of Research: **Title: Patient Data Collection and Analysis for an Elbow Smart Brace**

Principal Investigator: Dr. Ana Luisa Trejos

Co-Investigators: Shrikant Chinchalkar

Collaborators: Emma Farago, Abelardo Escoto, and Intronix Technologies Corporation

For the Participant:

I have read and understand the above information describing this study. I have had the purposes, procedures and technical language of this study explained to me. I have been given sufficient time to consider the above information and to seek advice if I chose to do so. I have had the opportunity to ask questions which have been answered to my satisfaction. I am voluntarily signing this form. I will receive a copy of this consent form for my information.

If at any time I have further questions, problems or adverse events, I can contact Dr. Ana Luisa Trejos, the principal investigator of the project, at [REDACTED] or any of the investigators and collaborators on the project.

If I have any questions about the conduct of this study or your rights as a research subject I may contact Dr. David Hill, Scientific Director, Lawson Health Research Institute at [REDACTED]. By signing this consent form, I am indicating that I agree to participate in this study.

**Name of Participant
(Please print)**

Signature of Participant

Date

**Name of Person Obtaining
Informed Consent**

**Signature of Person Obtaining
Informed Consent**

Date

Please Initial: _____

Version 2 (16-01-2017)

Page 6 of 6

The research institute of London Health Sciences Centre and St. Joseph's Health Care, London.





TRIAL FORM

Title of Research: Patient Data Collection and Analysis for an Elbow Smart Brace

Principal Investigator: Dr. Ana Luisa Trejos

Co-Investigators: Shrikant Chinchalkar

Coordinators: Emma Farago, Abelardo Escoto

To be filled out by the Participant:

If you are not comfortable answering any of these questions you do not have to respond.

Age: _____

Weight: _____

Dominant Hand: R L

Height: _____

Gender: M F

To be measured and entered by the Coordinator:

Upper arm length: _____ mm

Upper arm circumference: _____ mm

Forearm length: _____ mm

Forearm circumference: _____ mm

Hand length: _____ mm

Hand circumference: _____ mm

Subject Code: _____

Version 2

The research institute of London Health Sciences Centre
and St. Joseph's Health Care, London.



Figure 2.1

The screenshot shows the RightsLink® platform interface. At the top left is the Copyright Clearance Center logo. In the center is the RightsLink® logo. At the top right are links for Home, Account Info, Help, and an envelope icon. Below the header, the SAGE logo is prominently displayed. To its right, publication details are listed: Title: The Stiff Elbow; Author: Sumon Nandi, Steven Maschke, Peter J. Evans, et al; Publication: HAND; Publisher: SAGE Publications; Date: 12/01/2009. A copyright notice at the bottom states: Copyright © 2009, © SAGE Publications. On the right side, there is a user session box showing 'Logged in as: Emma Farago Western University' with a 'LOGOUT' button.

Gratis Reuse

Permission is granted at no cost for use of content in a Master's Thesis and/or Doctoral Dissertation. If you intend to distribute or sell your Master's Thesis/Doctoral Dissertation to the general public through print or website publication, please return to the previous page and select 'Republish in a Book/Journal' or 'Post on intranet/password-protected website' to complete your request.

BACK**CLOSE WINDOW**

Copyright © 2018 Copyright Clearance Center, Inc. All Rights Reserved. [Privacy statement](#). [Terms and Conditions](#). Comments? We would like to hear from you. E-mail us at customercare@copyright.com



Hello Emma,

Thank you for your request. I am happy to report that you can consider this email as permission to use the material from the article as detailed below in your upcoming thesis and archiving within your institution's repository. Please note that this permission does not cover any 3rd party material that may be found within the work. include a full academic citation credit the original source, SAGE Publications, Inc.

Please contact us for any further usage of the material and good luck on your thesis!

Figure 2.2

DocuSign Envelope ID: 65C62447-EA9F-4B8F-9470-54301DDB03C8

**PERMISSION LICENSE: EDUCATIONAL PRINT AND ELECTRONIC USE**

Request ID/Invoice Number: EMM621475430-1

Date: June 29, 2018

To: Emma Farago

[REDACTED]
[REDACTED]
[REDACTED]
[REDACTED]
[REDACTED]

McGraw-Hill Education Material

Author: Barrett, et al.

Title: Ganong's Review of Medical Physiology

ISBN: 9780071825108

Edition: 25

Description of material: Figure 5-2 B-C on Page 101 (1 Figure ONLY)

Fee: "Waived"

Purpose of Reproduction

Purpose of use: For use in a master's thesis titled "Development of an EMG-based muscle health model for elbow trauma patients" School: Western University

Professor: Dr. Ana Luisa Trejos

Number of Copies/Number of Users: 3

Semester: 2018

Format: Print and Electronic (Electronic- open access website) Distribution:

One-time educational use for the above purposes only.

Permission for the use described above is granted under the following terms and conditions:

1. McGraw-Hill Education hereby grants Licensee the non-exclusive right to use the McGraw-Hill Education Material as outlined and to reproduce and distribute the

McGraw-Hill Education Material as outlined on condition that the related textbook is the required text for the course identified above. The McGraw-Hill Education Material may be used only as outlined. All use of the McGraw-Hill Education Material is subject to the terms and conditions of this Agreement. This permission will automatically terminate at such time as the related textbook is no longer required.

2. No changes may be made to the McGraw-Hill Education Material without the prior written consent of McGraw-Hill Education.
3. Licensee will provide to McGraw-Hill Education the URL and password for the web site in which the McGraw-Hill Education Material appears (if applicable).
4. McGraw-Hill Education makes no representations or warranties as to the accuracy of any information contained in the McGraw-Hill Education Material, including any warranties of merchantability or fitness for a particular purpose. In no event shall McGraw-Hill Education have any liability to any party for special, incidental, tort, or consequential damages arising out of or in connection with the McGraw-Hill Education Material, even if McGraw-Hill Education has been advised of the possibility of such damages. All persons provided with the McGraw-Hill Education Material must be provided with written notice of this disclaimer and limitation liability, either in an end-user license and/or with an on-screen notice that is visible each time the end-user initiates access to the McGraw-Hill Education Material.
5. A credit to McGraw-Hill Education shall be visible each time the end-user initiates access to any screen or page containing any of the McGraw-Hill Education Material. Such credit shall include the title and author of the work and a copyright notice in the name of McGraw-Hill Education.
6. A SIGNED COPY OF THIS AGREEMENT should be sent to [REDACTED]
[REDACTED].
7. This permission does not cover the use of any third-party copyrighted material, including but not limited to photographs and other illustrations, which appears in the McGraw-Hill Education Material with a credit to other sources. Written permission to use such material must be obtained from the cited source.
8. McGraw-Hill Education shall have the right to terminate this Agreement immediately upon written notice to Licensee if Licensee is in material breach of this Agreement.
9. Licensee shall indemnify McGraw-Hill Education from any damages, lawsuits, claims, liabilities, costs, charges, and expenses, including attorney's fees, relating to its use of the McGraw-Hill Education Material.

DocuSign Envelope ID: 65C62447-EA9F-4B8F-9470-54301DDB03C8

10. This Agreement incorporates the parties' entire agreement with respect to its subject matter. This Agreement may be amended only in writing and signed by both parties and shall be governed by the laws of New York. Licensee may not assign this Agreement or any rights granted hereunder to any third party.

Please sign and return one copy to the address as outlined in Clause 6 of this agreement.

[REDACTED]

[REDACTED]

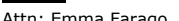
[REDACTED]

[REDACTED]

[REDACTED]

[REDACTED]

Figure 2.3

7/3/2018	RightsLink Printable License
JOHN WILEY AND SONS LICENSE TERMS AND CONDITIONS	
Jul 03, 2018	
<p>This Agreement between Western University -- Emma Farago ("You") and John Wiley and Sons ("John Wiley and Sons") consists of your license details and the terms and conditions provided by John Wiley and Sons and Copyright Clearance Center.</p>	
License Number	4377150051609
License date	Jun 27, 2018
Licensed Content Publisher	John Wiley and Sons
Licensed Content Publication	Wiley Books
Licensed Content Title	Basic Physiology and Biophysics of EMG Signal Generation
Licensed Content Author	T. Moritani, D. Stegeman, R. Merletti
Licensed Content Date	Jan 28, 2005
Licensed Content Pages	25
Type of use	Dissertation/Thesis
Requestor type	University/Academic
Format	Print and electronic
Portion	Figure/table
Number of figures/tables	1
Original Wiley figure/table number(s)	Figure 1.1
Will you be translating?	No
Title of your thesis / dissertation	Development of an EMG-based muscle health model for elbow trauma patients
Expected completion date	Aug 2018
Expected size (number of pages)	180
Requestor Location	[REDACTED]
  	
Publisher Tax ID	Attn: Emma Farago EU826007151
Total	0.00 CAD
Terms and Conditions	

TERMS AND CONDITIONS

This copyrighted material is owned by or exclusively licensed to John Wiley & Sons, Inc. or one of its group companies (each a "Wiley Company") or handled on behalf of a society with which a Wiley Company has exclusive publishing rights in relation to a particular work (collectively "WILEY"). By clicking "accept" in connection with completing this licensing transaction, you agree that the following terms and conditions apply to this transaction (along with the billing and payment terms and conditions established by the Copyright Clearance Center Inc., ("CCC's Billing and Payment terms and conditions"), at the time that

7/3/2018

RightsLink Printable License

you opened your RightsLink account (these are available at any time at <http://myaccount.copyright.com>).

Terms and Conditions

- The materials you have requested permission to reproduce or reuse (the "Wiley Materials") are protected by copyright.
- You are hereby granted a personal, non-exclusive, non-sub licensable (on a standalone basis), non-transferable, worldwide, limited license to reproduce the Wiley Materials for the purpose specified in the licensing process. This license, **and any CONTENT (PDF or image file) purchased as part of your order**, is for a one-time use only and limited to any maximum distribution number specified in the license. The first instance of republication or reuse granted by this license must be completed within two years of the date of the grant of this license (although copies prepared before the end date may be distributed thereafter). The Wiley Materials shall not be used in any other manner or for any other purpose, beyond what is granted in the license. Permission is granted subject to an appropriate acknowledgement given to the author, title of the material/book/journal and the publisher. You shall also duplicate the copyright notice that appears in the Wiley publication in your use of the Wiley Material. Permission is also granted on the understanding that nowhere in the text is a previously published source acknowledged for all or part of this Wiley Material. Any third party content is expressly excluded from this permission.
- With respect to the Wiley Materials, all rights are reserved. Except as expressly granted by the terms of the license, no part of the Wiley Materials may be copied, modified, adapted (except for minor reformatting required by the new Publication), translated, reproduced, transferred or distributed, in any form or by any means, and no derivative works may be made based on the Wiley Materials without the prior permission of the respective copyright owner. **For STM Signatory Publishers clearing permission under the terms of the STM Permissions Guidelines only, the terms of the license are extended to include subsequent editions and for editions in other languages, provided such editions are for the work as a whole in situ and does not involve the separate exploitation of the permitted figures or extracts,** You may not alter, remove or suppress in any manner any copyright, trademark or other notices displayed by the Wiley Materials. You may not license, rent, sell, loan, lease, pledge, offer as security, transfer or assign the Wiley Materials on a stand-alone basis, or any of the rights granted to you hereunder to any other person.
- The Wiley Materials and all of the intellectual property rights therein shall at all times remain the exclusive property of John Wiley & Sons Inc, the Wiley Companies, or their respective licensors, and your interest therein is only that of having possession of and the right to reproduce the Wiley Materials pursuant to Section 2 herein during the continuance of this Agreement. You agree that you own no right, title or interest in or to the Wiley Materials or any of the intellectual property rights therein. You shall have no rights hereunder other than the license as provided for above in Section 2. No right, license or interest to any trademark, trade name, service mark or other branding ("Marks") of WILEY or its licensors is granted hereunder, and you agree that you shall not assert any such right, license or interest with respect thereto
- NEITHER WILEY NOR ITS LICENSORS MAKES ANY WARRANTY OR REPRESENTATION OF ANY KIND TO YOU OR ANY THIRD PARTY,

7/3/2018

RightsLink Printable License

EXPRESS, IMPLIED OR STATUTORY, WITH RESPECT TO THE MATERIALS OR THE ACCURACY OF ANY INFORMATION CONTAINED IN THE MATERIALS, INCLUDING, WITHOUT LIMITATION, ANY IMPLIED WARRANTY OF MERCHANTABILITY, ACCURACY, SATISFACTORY QUALITY, FITNESS FOR A PARTICULAR PURPOSE, USABILITY, INTEGRATION OR NON-INFRINGEMENT AND ALL SUCH WARRANTIES ARE HEREBY EXCLUDED BY WILEY AND ITS LICENSORS AND WAIVED BY YOU.

- WILEY shall have the right to terminate this Agreement immediately upon breach of this Agreement by you.
- You shall indemnify, defend and hold harmless WILEY, its Licensors and their respective directors, officers, agents and employees, from and against any actual or threatened claims, demands, causes of action or proceedings arising from any breach of this Agreement by you.
- IN NO EVENT SHALL WILEY OR ITS LICENSORS BE LIABLE TO YOU OR ANY OTHER PARTY OR ANY OTHER PERSON OR ENTITY FOR ANY SPECIAL, CONSEQUENTIAL, INCIDENTAL, INDIRECT, EXEMPLARY OR PUNITIVE DAMAGES, HOWEVER CAUSED, ARISING OUT OF OR IN CONNECTION WITH THE DOWNLOADING, PROVISIONING, VIEWING OR USE OF THE MATERIALS REGARDLESS OF THE FORM OF ACTION, WHETHER FOR BREACH OF CONTRACT, BREACH OF WARRANTY, TORT, NEGLIGENCE, INFRINGEMENT OR OTHERWISE (INCLUDING, WITHOUT LIMITATION, DAMAGES BASED ON LOSS OF PROFITS, DATA, FILES, USE, BUSINESS OPPORTUNITY OR CLAIMS OF THIRD PARTIES), AND WHETHER OR NOT THE PARTY HAS BEEN ADVISED OF THE POSSIBILITY OF SUCH DAMAGES. THIS LIMITATION SHALL APPLY NOTWITHSTANDING ANY FAILURE OF ESSENTIAL PURPOSE OF ANY LIMITED REMEDY PROVIDED HEREIN.
- Should any provision of this Agreement be held by a court of competent jurisdiction to be illegal, invalid, or unenforceable, that provision shall be deemed amended to achieve as nearly as possible the same economic effect as the original provision, and the legality, validity and enforceability of the remaining provisions of this Agreement shall not be affected or impaired thereby.
- The failure of either party to enforce any term or condition of this Agreement shall not constitute a waiver of either party's right to enforce each and every term and condition of this Agreement. No breach under this agreement shall be deemed waived or excused by either party unless such waiver or consent is in writing signed by the party granting such waiver or consent. The waiver by or consent of a party to a breach of any provision of this Agreement shall not operate or be construed as a waiver of or consent to any other or subsequent breach by such other party.
- This Agreement may not be assigned (including by operation of law or otherwise) by you without WILEY's prior written consent.
- Any fee required for this permission shall be non-refundable after thirty (30) days from receipt by the CCC.

7/3/2018

RightsLink Printable License

- These terms and conditions together with CCC's Billing and Payment terms and conditions (which are incorporated herein) form the entire agreement between you and WILEY concerning this licensing transaction and (in the absence of fraud) supersedes all prior agreements and representations of the parties, oral or written. This Agreement may not be amended except in writing signed by both parties. This Agreement shall be binding upon and inure to the benefit of the parties' successors, legal representatives, and authorized assigns.
- In the event of any conflict between your obligations established by these terms and conditions and those established by CCC's Billing and Payment terms and conditions, these terms and conditions shall prevail.
- WILEY expressly reserves all rights not specifically granted in the combination of (i) the license details provided by you and accepted in the course of this licensing transaction, (ii) these terms and conditions and (iii) CCC's Billing and Payment terms and conditions.
- This Agreement will be void if the Type of Use, Format, Circulation, or Requestor Type was misrepresented during the licensing process.
- This Agreement shall be governed by and construed in accordance with the laws of the State of New York, USA, without regards to such state's conflict of law rules. Any legal action, suit or proceeding arising out of or relating to these Terms and Conditions or the breach thereof shall be instituted in a court of competent jurisdiction in New York County in the State of New York in the United States of America and each party hereby consents and submits to the personal jurisdiction of such court, waives any objection to venue in such court and consents to service of process by registered or certified mail, return receipt requested, at the last known address of such party.

WILEY OPEN ACCESS TERMS AND CONDITIONS

Wiley Publishes Open Access Articles in fully Open Access Journals and in Subscription journals offering Online Open. Although most of the fully Open Access journals publish open access articles under the terms of the Creative Commons Attribution (CC BY) License only, the subscription journals and a few of the Open Access Journals offer a choice of Creative Commons Licenses. The license type is clearly identified on the article.

The Creative Commons Attribution License

The [Creative Commons Attribution License \(CC-BY\)](#) allows users to copy, distribute and transmit an article, adapt the article and make commercial use of the article. The CC-BY license permits commercial and non-

Creative Commons Attribution Non-Commercial License

The [Creative Commons Attribution Non-Commercial \(CC-BY-NC\) License](#) permits use, distribution and reproduction in any medium, provided the original work is properly cited and is not used for commercial purposes.(see below)

Creative Commons Attribution-Non-Commercial-NoDerivs License

The [Creative Commons Attribution Non-Commercial-NoDerivs License](#) (CC-BY-NC-ND) permits use, distribution and reproduction in any medium, provided the original work is properly cited, is not used for commercial purposes and no modifications or adaptations are made. (see below)

7/3/2018

RightsLink Printable License

Use by commercial "for-profit" organizations

Use of Wiley Open Access articles for commercial, promotional, or marketing purposes requires further explicit permission from Wiley and will be subject to a fee. Further details can be found on Wiley Online Library
<http://olabout.wiley.com/WileyCDA/Section/id-410895.html>

Other Terms and Conditions:

v1.10 Last updated September 2015

Questions [REDACTED]

Figure 2.4

7/3/2018 RightsLink Printable License
JOHN WILEY AND SONS LICENSE TERMS AND CONDITIONS
 Jul 03, 2018

This Agreement between Western University -- Emma Farago ("You") and John Wiley and Sons ("John Wiley and Sons") consists of your license details and the terms and conditions provided by John Wiley and Sons and Copyright Clearance Center.

License Number	4377141360992
License date	Jun 27, 2018
Licensed Content Publisher	John Wiley and Sons
Licensed Content Publication	Muscle and Nerve
Licensed Content Title	Physiologic basis of potentials recorded in electromyography
Licensed Content Author	Daniel Dumitru
Licensed Content Date	Oct 23, 2000
Licensed Content Volume	23
Licensed Content Issue	11
Licensed Content Pages	19
Type of use	Dissertation/Thesis
Requestor type	University/Academic
Format	Print and electronic
Portion	Figure/table
Number of figures/tables	1
Original Wiley figure/table number(s)	Figure 1D
Will you be translating?	No
Title of your thesis / dissertation	Development of an EMG-based muscle health model for elbow trauma patients
Expected completion date	Aug 2018
Expected size (number of pages)	180
Requestor Location	[REDACTED]
Publisher Tax ID	Attn: Emma Farago EU826007151
Total	0.00 CAD

Terms and Conditions

TERMS AND CONDITIONS

This copyrighted material is owned by or exclusively licensed to John Wiley & Sons, Inc. or one of its group companies (each a "Wiley Company") or handled on behalf of a society with which a Wiley Company has exclusive publishing rights in relation to a particular work (collectively "WILEY"). By clicking "accept" in connection with completing this licensing transaction, you agree that the following terms and conditions apply to this transaction

7/3/2018

RightsLink Printable License

(along with the billing and payment terms and conditions established by the Copyright Clearance Center Inc., ("CCC's Billing and Payment terms and conditions"), at the time that you opened your RightsLink account (these are available at any time at <http://myaccount.copyright.com>).

Terms and Conditions

- The materials you have requested permission to reproduce or reuse (the "Wiley Materials") are protected by copyright.
- You are hereby granted a personal, non-exclusive, non-sub licensable (on a standalone basis), non-transferable, worldwide, limited license to reproduce the Wiley Materials for the purpose specified in the licensing process. This license, **and any CONTENT (PDF or image file) purchased as part of your order**, is for a one-time use only and limited to any maximum distribution number specified in the license. The first instance of republication or reuse granted by this license must be completed within two years of the date of the grant of this license (although copies prepared before the end date may be distributed thereafter). The Wiley Materials shall not be used in any other manner or for any other purpose, beyond what is granted in the license. Permission is granted subject to an appropriate acknowledgement given to the author, title of the material/book/journal and the publisher. You shall also duplicate the copyright notice that appears in the Wiley publication in your use of the Wiley Material. Permission is also granted on the understanding that nowhere in the text is a previously published source acknowledged for all or part of this Wiley Material. Any third party content is expressly excluded from this permission.
- With respect to the Wiley Materials, all rights are reserved. Except as expressly granted by the terms of the license, no part of the Wiley Materials may be copied, modified, adapted (except for minor reformatting required by the new Publication), translated, reproduced, transferred or distributed, in any form or by any means, and no derivative works may be made based on the Wiley Materials without the prior permission of the respective copyright owner.**For STM Signatory Publishers clearing permission under the terms of the [STM Permissions Guidelines](#) only, the terms of the license are extended to include subsequent editions and for editions in other languages, provided such editions are for the work as a whole in situ and does not involve the separate exploitation of the permitted figures or extracts,** You may not alter, remove or suppress in any manner any copyright, trademark or other notices displayed by the Wiley Materials. You may not license, rent, sell, loan, lease, pledge, offer as security, transfer or assign the Wiley Materials on a stand-alone basis, or any of the rights granted to you hereunder to any other person.
- The Wiley Materials and all of the intellectual property rights therein shall at all times remain the exclusive property of John Wiley & Sons Inc, the Wiley Companies, or their respective licensors, and your interest therein is only that of having possession of and the right to reproduce the Wiley Materials pursuant to Section 2 herein during the continuance of this Agreement. You agree that you own no right, title or interest in or to the Wiley Materials or any of the intellectual property rights therein. You shall have no rights hereunder other than the license as provided for above in Section 2. No right, license or interest to any trademark, trade name, service mark or other branding ("Marks") of WILEY or its licensors is granted hereunder, and you agree that you shall not assert any such right, license or interest with respect thereto
- NEITHER WILEY NOR ITS LICENSORS MAKES ANY WARRANTY OR

7/3/2018

RightsLink Printable License

REPRESENTATION OF ANY KIND TO YOU OR ANY THIRD PARTY, EXPRESS, IMPLIED OR STATUTORY, WITH RESPECT TO THE MATERIALS OR THE ACCURACY OF ANY INFORMATION CONTAINED IN THE MATERIALS, INCLUDING, WITHOUT LIMITATION, ANY IMPLIED WARRANTY OF MERCHANTABILITY, ACCURACY, SATISFACTORY QUALITY, FITNESS FOR A PARTICULAR PURPOSE, USABILITY, INTEGRATION OR NON-INFRINGEMENT AND ALL SUCH WARRANTIES ARE HEREBY EXCLUDED BY WILEY AND ITS LICENSORS AND WAIVED BY YOU.

- WILEY shall have the right to terminate this Agreement immediately upon breach of this Agreement by you.
- You shall indemnify, defend and hold harmless WILEY, its Licensors and their respective directors, officers, agents and employees, from and against any actual or threatened claims, demands, causes of action or proceedings arising from any breach of this Agreement by you.
- IN NO EVENT SHALL WILEY OR ITS LICENSORS BE LIABLE TO YOU OR ANY OTHER PARTY OR ANY OTHER PERSON OR ENTITY FOR ANY SPECIAL, CONSEQUENTIAL, INCIDENTAL, INDIRECT, EXEMPLARY OR PUNITIVE DAMAGES, HOWEVER CAUSED, ARISING OUT OF OR IN CONNECTION WITH THE DOWNLOADING, PROVISIONING, VIEWING OR USE OF THE MATERIALS REGARDLESS OF THE FORM OF ACTION, WHETHER FOR BREACH OF CONTRACT, BREACH OF WARRANTY, TORT, NEGLIGENCE, INFRINGEMENT OR OTHERWISE (INCLUDING, WITHOUT LIMITATION, DAMAGES BASED ON LOSS OF PROFITS, DATA, FILES, USE, BUSINESS OPPORTUNITY OR CLAIMS OF THIRD PARTIES), AND WHETHER OR NOT THE PARTY HAS BEEN ADVISED OF THE POSSIBILITY OF SUCH DAMAGES. THIS LIMITATION SHALL APPLY NOTWITHSTANDING ANY FAILURE OF ESSENTIAL PURPOSE OF ANY LIMITED REMEDY PROVIDED HEREIN.
- Should any provision of this Agreement be held by a court of competent jurisdiction to be illegal, invalid, or unenforceable, that provision shall be deemed amended to achieve as nearly as possible the same economic effect as the original provision, and the legality, validity and enforceability of the remaining provisions of this Agreement shall not be affected or impaired thereby.
- The failure of either party to enforce any term or condition of this Agreement shall not constitute a waiver of either party's right to enforce each and every term and condition of this Agreement. No breach under this agreement shall be deemed waived or excused by either party unless such waiver or consent is in writing signed by the party granting such waiver or consent. The waiver by or consent of a party to a breach of any provision of this Agreement shall not operate or be construed as a waiver of or consent to any other or subsequent breach by such other party.
- This Agreement may not be assigned (including by operation of law or otherwise) by you without WILEY's prior written consent.
- Any fee required for this permission shall be non-refundable after thirty (30) days from receipt by the CCC.

7/3/2018

RightsLink Printable License

- These terms and conditions together with CCC's Billing and Payment terms and conditions (which are incorporated herein) form the entire agreement between you and WILEY concerning this licensing transaction and (in the absence of fraud) supersedes all prior agreements and representations of the parties, oral or written. This Agreement may not be amended except in writing signed by both parties. This Agreement shall be binding upon and inure to the benefit of the parties' successors, legal representatives, and authorized assigns.
- In the event of any conflict between your obligations established by these terms and conditions and those established by CCC's Billing and Payment terms and conditions, these terms and conditions shall prevail.
- WILEY expressly reserves all rights not specifically granted in the combination of (i) the license details provided by you and accepted in the course of this licensing transaction, (ii) these terms and conditions and (iii) CCC's Billing and Payment terms and conditions.
- This Agreement will be void if the Type of Use, Format, Circulation, or Requestor Type was misrepresented during the licensing process.
- This Agreement shall be governed by and construed in accordance with the laws of the State of New York, USA, without regards to such state's conflict of law rules. Any legal action, suit or proceeding arising out of or relating to these Terms and Conditions or the breach thereof shall be instituted in a court of competent jurisdiction in New York County in the State of New York in the United States of America and each party hereby consents and submits to the personal jurisdiction of such court, waives any objection to venue in such court and consents to service of process by registered or certified mail, return receipt requested, at the last known address of such party.

WILEY OPEN ACCESS TERMS AND CONDITIONS

Wiley Publishes Open Access Articles in fully Open Access Journals and in Subscription journals offering Online Open. Although most of the fully Open Access journals publish open access articles under the terms of the Creative Commons Attribution (CC BY) License only, the subscription journals and a few of the Open Access Journals offer a choice of Creative Commons Licenses. The license type is clearly identified on the article.

The Creative Commons Attribution License

The [Creative Commons Attribution License \(CC-BY\)](#) allows users to copy, distribute and transmit an article, adapt the article and make commercial use of the article. The CC-BY license permits commercial and non-

Creative Commons Attribution Non-Commercial License

The [Creative Commons Attribution Non-Commercial \(CC-BY-NC\) License](#) permits use, distribution and reproduction in any medium, provided the original work is properly cited and is not used for commercial purposes.(see below)

Creative Commons Attribution-Non-Commercial-NoDerivs License

The [Creative Commons Attribution Non-Commercial-NoDerivs License](#) (CC-BY-NC-ND) permits use, distribution and reproduction in any medium, provided the original work is properly cited, is not used for commercial purposes and no modifications or adaptations are made. (see below)

7/3/2018

RightsLink Printable License

Use by commercial "for-profit" organizations

Use of Wiley Open Access articles for commercial, promotional, or marketing purposes requires further explicit permission from Wiley and will be subject to a fee.

Further details can be found on Wiley Online Library

<http://olabout.wiley.com/WileyCDA/Section/id-410895.html>

Other Terms and Conditions:

v1.10 Last updated September 2015

Questions? [REDACTED]

Figure 2.6

6/27/2018 Rightslink® by Copyright Clearance Center

 Requesting permission to reuse content from an IEEE publication

Title: Determining the Optimal Window Length for Pattern Recognition-Based Myoelectric Control: Balancing the Competing Effects of Classification Error and Controller Delay
Author: Lauren H. Smith
Publication: Neural Systems and Rehabilitation Engineering, IEEE Transactions on
Publisher: IEEE
Date: April 2011
 Copyright © 2011, IEEE

Logged in as:
 Emma Farago
 Western University
[LOGOUT](#)

Thesis / Dissertation Reuse

The IEEE does not require individuals working on a thesis to obtain a formal reuse license, however, you may print out this statement to be used as a permission grant:

Requirements to be followed when using any portion (e.g., figure, graph, table, or textual material) of an IEEE copyrighted paper in a thesis:

- 1) In the case of textual material (e.g., using short quotes or referring to the work within these papers) users must give full credit to the original source (author, paper, publication) followed by the IEEE copyright line © 2011 IEEE.
- 2) In the case of illustrations or tabular material, we require that the copyright line © [Year of original publication] IEEE appear prominently with each reprinted figure and/or table.
- 3) If a substantial portion of the original paper is to be used, and if you are not the senior author, also obtain the senior author's approval.

Requirements to be followed when using an entire IEEE copyrighted paper in a thesis:

- 1) The following IEEE copyright/ credit notice should be placed prominently in the references: © [year of original publication] IEEE. Reprinted, with permission, from [author names, paper title, IEEE publication title, and month/year of publication]
- 2) Only the accepted version of an IEEE copyrighted paper can be used when posting the paper or your thesis on-line.
- 3) In placing the thesis on the author's university website, please display the following message in a prominent place on the website: In reference to IEEE copyrighted material which is used with permission in this thesis, the IEEE does not endorse any of [university/educational entity's name goes here]'s products or services. Internal or personal use of this material is permitted. If interested in reprinting/republishing IEEE copyrighted material for advertising or promotional purposes or for creating new collective works for resale or redistribution, please go to http://www.ieee.org/publications_standards/publications/rights/rights_link.html to learn how to obtain a License from RightsLink.

If applicable, University Microfilms and/or ProQuest Library, or the Archives of Canada may supply single copies of the dissertation.

[BACK](#) [CLOSE WINDOW](#)

Figure 2.7

6/27/2018	RightsLink Printable License
ELSEVIER LICENSE TERMS AND CONDITIONS	
	Jun 27, 2018
<hr/>	
This Agreement between Western University -- Emma Farago ("You") and Elsevier ("Elsevier") consists of your license details and the terms and conditions provided by Elsevier and Copyright Clearance Center.	
License Number	4377140748584
License date	Jun 27, 2018
Licensed Content Publisher	Elsevier
Licensed Content Publication	Journal of Neuroscience Methods
Licensed Content Title	Analysis of surface EMG spike shape across different levels of isometric force
Licensed Content Author	David A. Gabriel,Steven M. Lester,Sean A. Lenhardt,Edward D.J. Cambridge
Licensed Content Date	Jan 15, 2007
Licensed Content Volume	159
Licensed Content Issue	1
Licensed Content Pages	7
Start Page	146
End Page	152
Type of Use	reuse in a thesis/dissertation
Portion	figures/tables/illustrations
Number of figures/tables/illustrations	1
Format	both print and electronic
Are you the author of this Elsevier article?	No
Will you be translating?	No
Original figure numbers	Figure 3
Title of your thesis/dissertation	Development of an EMG-based muscle health model for elbow trauma patients
Expected completion date	Aug 2018
Estimated size (number of pages)	180
Requestor Location	[REDACTED]
	[REDACTED]

6/27/2018

RightsLink Printable License



Attn: Emma Farago

Publisher Tax ID	GB 494 6272 12
Total	0.00 CAD

Terms and Conditions**INTRODUCTION**

1. The publisher for this copyrighted material is Elsevier. By clicking "accept" in connection with completing this licensing transaction, you agree that the following terms and conditions apply to this transaction (along with the Billing and Payment terms and conditions established by Copyright Clearance Center, Inc. ("CCC"), at the time that you opened your Rightslink account and that are available at any time at <http://myaccount.copyright.com>).

GENERAL TERMS

2. Elsevier hereby grants you permission to reproduce the aforementioned material subject to the terms and conditions indicated.

3. Acknowledgement: If any part of the material to be used (for example, figures) has appeared in our publication with credit or acknowledgement to another source, permission must also be sought from that source. If such permission is not obtained then that material may not be included in your publication/copies. Suitable acknowledgement to the source must be made, either as a footnote or in a reference list at the end of your publication, as follows:

"Reprinted from Publication title, Vol /edition number, Author(s), Title of article / title of chapter, Pages No., Copyright (Year), with permission from Elsevier [OR APPLICABLE SOCIETY COPYRIGHT OWNER]." Also Lancet special credit - "Reprinted from The Lancet, Vol. number, Author(s), Title of article, Pages No., Copyright (Year), with permission from Elsevier."

4. Reproduction of this material is confined to the purpose and/or media for which permission is hereby given.

5. Altering/Modifying Material: Not Permitted. However figures and illustrations may be altered/adapted minimally to serve your work. Any other abbreviations, additions, deletions and/or any other alterations shall be made only with prior written authorization of Elsevier Ltd. (Please contact Elsevier at [REDACTED] No modifications can be made to any Lancet figures/tables and they must be reproduced in full.

6. If the permission fee for the requested use of our material is waived in this instance, please be advised that your future requests for Elsevier materials may attract a fee.

7. Reservation of Rights: Publisher reserves all rights not specifically granted in the combination of (i) the license details provided by you and accepted in the course of this licensing transaction, (ii) these terms and conditions and (iii) CCC's Billing and Payment terms and conditions.

8. License Contingent Upon Payment: While you may exercise the rights licensed immediately upon issuance of the license at the end of the licensing process for the transaction, provided that you have disclosed complete and accurate details of your proposed use, no license is finally effective unless and until full payment is received from you (either by publisher or by CCC) as provided in CCC's Billing and Payment terms and conditions. If full payment is not received on a timely basis, then any license preliminarily granted shall be deemed automatically revoked and shall be void as if never granted.

Further, in the event that you breach any of these terms and conditions or any of CCC's Billing and Payment terms and conditions, the license is automatically revoked and shall be void as if never granted. Use of materials as described in a revoked license, as well as any

6/27/2018

RightsLink Printable License

use of the materials beyond the scope of an unrevoked license, may constitute copyright infringement and publisher reserves the right to take any and all action to protect its copyright in the materials.

9. **Warranties:** Publisher makes no representations or warranties with respect to the licensed material.

10. **Indemnity:** You hereby indemnify and agree to hold harmless publisher and CCC, and their respective officers, directors, employees and agents, from and against any and all claims arising out of your use of the licensed material other than as specifically authorized pursuant to this license.

11. **No Transfer of License:** This license is personal to you and may not be sublicensed, assigned, or transferred by you to any other person without publisher's written permission.

12. **No Amendment Except in Writing:** This license may not be amended except in a writing signed by both parties (or, in the case of publisher, by CCC on publisher's behalf).

13. **Objection to Contrary Terms:** Publisher hereby objects to any terms contained in any purchase order, acknowledgment, check endorsement or other writing prepared by you, which terms are inconsistent with these terms and conditions or CCC's Billing and Payment terms and conditions. These terms and conditions, together with CCC's Billing and Payment terms and conditions (which are incorporated herein), comprise the entire agreement between you and publisher (and CCC) concerning this licensing transaction. In the event of any conflict between your obligations established by these terms and conditions and those established by CCC's Billing and Payment terms and conditions, these terms and conditions shall control.

14. **Revocation:** Elsevier or Copyright Clearance Center may deny the permissions described in this License at their sole discretion, for any reason or no reason, with a full refund payable to you. Notice of such denial will be made using the contact information provided by you. Failure to receive such notice will not alter or invalidate the denial. In no event will Elsevier or Copyright Clearance Center be responsible or liable for any costs, expenses or damage incurred by you as a result of a denial of your permission request, other than a refund of the amount(s) paid by you to Elsevier and/or Copyright Clearance Center for denied permissions.

LIMITED LICENSE

The following terms and conditions apply only to specific license types:

15. **Translation:** This permission is granted for non-exclusive word **English** rights only unless your license was granted for translation rights. If you licensed translation rights you may only translate this content into the languages you requested. A professional translator must perform all translations and reproduce the content word for word preserving the integrity of the article.

16. **Posting licensed content on any Website:** The following terms and conditions apply as follows: Licensing material from an Elsevier journal: All content posted to the web site must maintain the copyright information line on the bottom of each image; A hyper-text must be included to the Homepage of the journal from which you are licensing at <http://www.sciencedirect.com/science/journal/xxxxx> or the Elsevier homepage for books at <http://www.elsevier.com>; Central Storage: This license does not include permission for a scanned version of the material to be stored in a central repository such as that provided by Heron/XanEdu.

Licensing material from an Elsevier book: A hyper-text link must be included to the Elsevier homepage at <http://www.elsevier.com>. All content posted to the web site must maintain the copyright information line on the bottom of each image.

Posting licensed content on Electronic reserve: In addition to the above the following clauses are applicable: The web site must be password-protected and made available only to bona fide students registered on a relevant course. This permission is granted for 1 year only.

6/27/2018

RightsLink Printable License

You may obtain a new license for future website posting.

17. For journal authors: the following clauses are applicable in addition to the above:

Preprints:

A preprint is an author's own write-up of research results and analysis, it has not been peer-reviewed, nor has it had any other value added to it by a publisher (such as formatting, copyright, technical enhancement etc.).

Authors can share their preprints anywhere at any time. Preprints should not be added to or enhanced in any way in order to appear more like, or to substitute for, the final versions of articles however authors can update their preprints on arXiv or RePEc with their Accepted Author Manuscript (see below).

If accepted for publication, we encourage authors to link from the preprint to their formal publication via its DOI. Millions of researchers have access to the formal publications on ScienceDirect, and so links will help users to find, access, cite and use the best available version. Please note that Cell Press, The Lancet and some society-owned have different preprint policies. Information on these policies is available on the journal homepage.

Accepted Author Manuscripts: An accepted author manuscript is the manuscript of an article that has been accepted for publication and which typically includes author-incorporated changes suggested during submission, peer review and editor-author communications.

Authors can share their accepted author manuscript:

- immediately via their non-commercial person
 - homepage or blog
 - by updating a preprint in arXiv or RePEc with the accepted manuscript via
 - their research institute or institutional repository for internal institutional uses or as part of an invitation-only research collaboration work-group
 - directly by providing copies to their students or to research collaborators for their personal use
 - for private scholarly sharing as part of an invitation-only work group on commercial sites with which Elsevier has an agreement
- After the embargo period via non-commercial hosting platforms such as their institutional repository via commercial sites with which Elsevier has an agreement In all cases accepted manuscripts should:
 - link to the formal publication via its DOI bear a
 - CC-BY-NC-ND license - this is easy to do
 - if aggregated with other manuscripts, for example in a repository or other site, be shared in alignment with our hosting policy not be added to or enhanced in any way to appear more like, or to substitute for, the published journal article.

Published journal article (PJA): A published journal article (PJA) is the definitive final record of published research that appears or will appear in the journal and embodies all value-adding publishing activities including peer review co-ordination, copy-editing, formatting, (if relevant) pagination and online enrichment.

Policies for sharing publishing journal articles differ for subscription and gold open access articles:

Subscription Articles: If you are an author, please share a link to your article rather than the full-text. Millions of researchers have access to the formal publications on ScienceDirect, and so links will help your users to find, access, cite, and use the best available version. Theses and dissertations which contain embedded PJsAs as part of the formal submission can be posted publicly by the awarding institution with DOI links back to the formal publications on ScienceDirect.

If you are affiliated with a library that subscribes to ScienceDirect you have additional private sharing rights for others' research accessed under that agreement. This includes use

6/27/2018

RightsLink Printable License

for classroom teaching and internal training at the institution (including use in course packs and courseware programs), and inclusion of the article for grant funding purposes. **Gold Open Access Articles:** May be shared according to the author-selected end-user license and should contain a [CrossMark logo](#), the end user license, and a DOI link to the formal publication on ScienceDirect.

Please refer to Elsevier's [posting policy](#) for further information.

18. **For book authors** the following clauses are applicable in addition to the above:
Authors are permitted to place a brief summary of their work online only. You are not allowed to download and post the published electronic version of your chapter, nor may you scan the printed edition to create an electronic version. **Posting to a repository:** Authors are permitted to post a summary of their chapter only in their institution's repository.

19. **Thesis/Dissertation:** If your license is for use in a thesis/dissertation your thesis may be submitted to your institution in either print or electronic form. Should your thesis be published commercially, please reapply for permission. These requirements include permission for the Library and Archives of Canada to supply single copies, on demand, of the complete thesis and include permission for Proquest/UMI to supply single copies, on demand, of the complete thesis. Should your thesis be published commercially, please reapply for permission. Theses and dissertations which contain embedded PJAs as part of the formal submission can be posted publicly by the awarding institution with DOI links back to the formal publications on ScienceDirect.

Elsevier Open Access Terms and Conditions

You can publish open access with Elsevier in hundreds of open access journals or in nearly 2000 established subscription journals that support open access publishing. Permitted third party re-use of these open access articles is defined by the author's choice of Creative Commons user license. See our [open access license policy](#) for more information.

Terms & Conditions applicable to all Open Access articles published with Elsevier:
Any reuse of the article must not represent the author as endorsing the adaptation of the article nor should the article be modified in such a way as to damage the author's honour or reputation. If any changes have been made, such changes must be clearly indicated. The author(s) must be appropriately credited and we ask that you include the end user license and a DOI link to the formal publication on ScienceDirect.

If any part of the material to be used (for example, figures) has appeared in our publication with credit or acknowledgement to another source it is the responsibility of the user to ensure their reuse complies with the terms and conditions determined by the rights holder.

Additional Terms & Conditions applicable to each Creative Commons user license:

CC BY: The CC-BY license allows users to copy, to create extracts, abstracts and new works from the Article, to alter and revise the Article and to make commercial use of the Article (including reuse and/or resale of the Article by commercial entities), provided the user gives appropriate credit (with a link to the formal publication through the relevant DOI), provides a link to the license, indicates if changes were made and the licensor is not represented as endorsing the use made of the work. The full details of the license are available at <http://creativecommons.org/licenses/by/4.0>.

CC BY NC SA: The CC BY-NC-SA license allows users to copy, to create extracts, abstracts and new works from the Article, to alter and revise the Article, provided this is not done for commercial purposes, and that the user gives appropriate credit (with a link to the formal publication through the relevant DOI), provides a link to the license, indicates if changes were made and the licensor is not represented as endorsing the use made of the work. Further, any new works must be made available on the same conditions. The full details of the license are available at <http://creativecommons.org/licenses/by-nc-sa/4.0>.

CC BY NC ND: The CC BY-NC-ND license allows users to copy and distribute the Article, provided this is not done for commercial purposes and further does not permit distribution of the Article if it is changed or edited in any way, and provided the user gives appropriate credit (with a link to the formal publication through the relevant DOI), provides a link to the

6/27/2018

RightsLink Printable License

license, and that the licensor is not represented as endorsing the use made of the work. The full details of the license are available at <http://creativecommons.org/licenses/by-nc-nd/4.0>. Any commercial reuse of Open Access articles published with a CC BY NC SA or CC BY NC ND license requires permission from Elsevier and will be subject to a fee. Commercial reuse includes:

- Associating advertising with the full text of the Article
- Charging fees for document delivery or access
- Article aggregation
- Systematic distribution via e-mail lists or share buttons

Posting or linking by commercial companies for use by customers of those companies.

20. Other Conditions:

v1.9

Questions? [REDACTED]

Appendix B

MATLAB Code

This appendix includes the MATLAB codes used to conduct the EMG feature extraction and analysis work presented in this thesis. The appendix is divided into sections describing the codes used for segmentation (Section B.1), feature functions (Section B.2), feature extraction (Section B.3), classification (Section B.4), and majority vote classification (Section B.5).

B.1 Segmentation Codes

The first step of EMG analysis was to segment the EMG data into meaningful regions of muscle activation. This section describes the codes used to divide the data into segments representing each motion.

Teager Kaiser Energy Operator (TKEO) Function

The **emgprocessTKEO** function was developed to condition the signals with the Teager Kaiser Energy Operator (TKEO) in order to provide a clearer observation of the onset and offset of muscle contractions during motion.

```
1 function TKEO = emgprocessTKEO(rawsignal, fs)
2 %set EMG baseline to zero
3 y = rawsignal - mean(rawsignal);
4 [l, w] = size(y);
5 %apply TKEO operator to the data
```

```

6 TKE0op = zeros(1,w);
7 for i = 2:l-1
8     for j = 1:w
9         TKE0op(i,j) = y(i,j)^2 - y(i+1,j)*y(i-1,j);
10    end
11 end
12 %rectification
13 rect = abs(TKE0op);
14 %apply a 50Hz LPF to the data for threshold analysis
15 fc = 50;
16 [a,b] = butter (2,fc/(fs/2));
17 TKE0 = filtfilt(a,b,rect);
18 end

```

Automatic Segmentation

The **emgprocessTKEO** function was implemented in the codes used for data segmentation. The automatic segmentation code is shown below.

```

1 p = [331 49 1164 948];
2 set(0, 'DefaultFigurePosition', p)
3 fs=1925.93; % sampling frequency Hz
4 motions = {'EFE', 'PS', 'WFE', 'URD', 'HOC'};
5 muscles = {'bb', 'tb1', 'tb2', 'pt', 'brd', 'ecu', 'fcu'};
6
7 %VARIABLES
8 file_output_motion = 'WF'; %motion to identify
9 health = 1; %health = 0 -> injured, health = 1 -> healthy
10 subjects = {'S137'}; %subject list
11 musc = 1; %muscle of interest
12 mot= 1; %motion of interest
13
14 for s = 1:numel(subjects)
15     filename = strcat('C:\Users\Emma\Documents\Data\', ...
16         subjects{s}, '\',subjects{s},motions{mot}, '.csv');
17     rawdata = xlsread(filename);
18     % IMPORT EMG DATA
19     rawemgdata=zeros(length(rawdata),7);
20     count = 1;

```

```
21     if health ==0
22         cols = 2:8:50;
23     else
24         cols = 66:8:114;
25     end
26     for i = cols
27         rawemgdata(:,count)=rawdata(:,i);
28         count = count+1;
29     end
30
31 % CONDITION EMG DATA WITH TKEO
32 [~,filt] = emgprocessTKEO(rawemgdata,fs);
33
34 % PLOT EMG SIGNAL
35 figure(1)
36 hold off
37 plot(filt(:,musc))
38 title(filename)
39 legend (muscles{musc})
40
41
42
43 % SELECT BASELINE REGION
44 [x_values,~] = ginput;
45 x_values = floor(x_values);
46 baseline = filt(x_values(1):x_values(2),musc);
47
48 % FIND THRESHOLDS
49 h = 15;
50 T1 = mean(baseline)+h*std(baseline);
51 t2 = 25; %starting threshold
52 t3=200; %ending threshold
53
54 %DETERMINE ONSET AND OFFSET
55 divisions = zeros(3,2);
56 start=2;
57 for i = 1:3
58     count = 0;
59     % FIND POINT WHEN T2 CONSECUTIVE SAMPLES EXCEED T1
60     while count <t2
61         if filt(start,musc)>T1 && filt(start-1,musc)>T1
```

```
62         count = count+1;
63     else
64         count = 0;
65     end
66     start=start+1;
67 end
68 divisions(i,1) = start;
69 count = 0;
70 % FIND POINT WHEN T3 CONSECUTIVE SAMPLES ARE BELOW T1
71 while count <t3
72     if filt(start,musc)<T1 && filt(start-1,musc)<T1
73         count = count+1;
74     else
75         count = 0;
76     end
77     start=start+1;
78 end
79 divisions(i,2) = start;
80 end
81
82 % VALIDATE WITH GRAPH
83 figure
84 plot(filt(:,musc))
85 hold on
86 scatter(divisions(:,1),[0,0,0], 'g')
87 scatter(divisions(:,2),[0,0,0], 'r')
88 title (strcat('validation', subjects{s}))
89
90 % SAVE DATA TO FILE
91 if health ==0
92     name = 'Injured';
93 else
94     name = 'Healthy';
95 end
96 for i = 1:3
97     savefilename = strcat('C:\Users\Emma\Documents\Reps',...
98     '\',name,'\',subjects{s},...
99     file_output_motion, '_R',num2str(i),'.csv');
100    A = rawemgdata(divisions(i,1):divisions(i,2),:);
101    csvwrite(savefilename,A)
102 end
```

```
103 end
```

Manual Segmentation

Each segmentation was observed visually in order to determine if the segmentation appeared to be correct based on motion activation. If the segmentation was not conducted appropriately by the automatic method, the segmentation was performed by manually indicating the desired regions to segment using the sEMG voltage vs. time plot. The manual segmentation is shown below.

```
1 p = [331 49 1164 948];
2 set(0, 'DefaultFigurePosition', p)
3 fs=1925.93; % sampling frequency Hz
4 motions = {'EFE', 'PS', 'WFE', 'URD', 'HOC'};
5 muscles = {'bb', 'tb1', 'tb2', 'pt', 'brd', 'ecu', 'fcu'};
6
7 %VARIABLES
8 file_output_motion = 'WF'; %motion to identify
9 health = 1; %health = 0 -> injured, health = 1 -> healthy
10 subjects = {'S137'}; %subject list
11 musc = 1; %muscle of interest
12 mot= 1; %motion of interest
13
14 for s = 1:numel(subjects)
15     filename = strcat('C:\Users\Emma\Documents\Data\', ...
16         subjects{s}, '\', subjects{s}, motions{mot}, '.csv');
17     rawdata = xlsread(filename);
18
19     % IMPORT EMG DATA
20     rawemgdata=zeros(length(rawdata),7);
21     count = 1;
22
23     if health ==0
24         cols = 2:8:50;
25     else
26         cols = 66:8:114;
27     end
28
29     for i = cols
30         rawemgdata(:,count)=rawdata(:,i);
31         count = count+1;
32     end
33
34     % CONDITION EMG DATA WITH TKEO
```

```
32 [~,filt] = emgprocessTKE0(rawemgdata,fs);
33
34 % PLOT DATA
35 figure(1)
36 hold off
37 plot(filt(:,musc))
38 title(filename)
39 legend (muscles{musc})
40
41 % DEFINE FILE NAME
42 if health ==0
43     name = 'Injured';
44 else
45     name = 'Healthy';
46 end
47
48 %SELECT SEGMENTS MANUALLY AND SAVE
49 [x_values,~] = ginput;
50 x_values = floor(x_values);
51 for i = 1:3
52     savefilename = strcat('C:\Users\Emma\Documents\Reps',...
53         name,'\',subjects{s},...
54         file_output_motion, '_R',num2str(i),'.csv');
55     A = rawemgdata(x_values(i*2-1):x_values(i*2),:);
56     csvwrite(savefilename,A)
57 end
58 end
```

B.2 Feature Function Codes

Functions were developed to calculate each EMG feature. Window size and increment could be implemented, if necessary. If window size and increment were not specified in the function inputs, the feature was calculated for the entire EMG signal. This section provides the codes to generate each of the features implemented in this thesis. The feature function codes were developed with assistance from Julian Saldarriaga, and by referring to the Myoelectric Control Development Toolbox [122]. Feature functions for the ApEn and HFD features were developed after referring to codes available on MATLAB Central File Exchange [123, 124].

EMG Feature Function Template

The feature functions are all very similar to each other. The functions first develop data windows based on the window size and increment specified by the user. Features are then extracted from each window segment. The following code is the full feature function code for the MAV feature. This code demonstrates the basic template for the feature functions. Other feature functions were implemented by changing the “feature calculation” region indicated in the MAV function code to the required code for each feature.

```
1 %Mean Amplitude Value (MAV)
2 function feat = mavfeat(X,winsize,wininc)
3 if nargin < 3
4     if nargin < 2
5         winsize = size(X,1);
6     end
7     wininc = winsize;
8 end
9
10 datasize = size(X,1);
11 Nsignals = size(X,2);
12 datawin = ones(winsize,1);
13 numwin = floor((datasize - winsize)/wininc)+1;
14 feat = zeros(numwin,Nsignals);
15 st = 1;
16 en = winsize;
17
```

```

18 for i = 1:numwin
19     curwin = X(st:en,:).*repmat(datawin,1,Nsignals);
20     %feature calculation
21     %%%%%%%%%%%%%%
22     feat(i,:) = mean(abs(curwin));
23     %%%%%%%%%%%%%%
24     st = st + wininc;
25     en = en + wininc;
26 end

```

The “feature calculation” regions for the other feature functions are shown below:

Time Domain: Energy

MMAV1:

```

1 temp = 0;
2 for j = 1:winsize
3     if (0.25*winsize) <= j && j <= (0.75*winsize)
4         w_i = 1;
5     else
6         w_i = 0.5;
7     end
8     temp = temp + w_i*abs(curwin(j,:));
9 end
10 feat(i,:) = temp/winsize;

```

MMAV2:

```

1 temp = 0;
2 for j = 1:winsize
3     if ((0.25*winsize) <= j) && (j <= (0.75*winsize))
4         w_i = 1;
5     elseif j < (0.25*winsize)
6         w_i = 4*j/winsize;
7     else
8         w_i = 4*(j-winsize)/winsize;
9     end
10    temp = temp + w_i*abs(curwin(j,:));
11 end
12 feat(i,:) = temp/winsize;

```

IEMG:

```
1  feat(i,:) = sum((abs(curwin)));
```

SSI:

```
1  temp = 0;
2  for j = 1:winsize
3      temp = temp + curwin(j,:).^2;
4  end
5  feat(i,:) = temp/winsize;
```

VAR:

```
1  temp = 0;
2  for j = 1:winsize
3      temp = temp + curwin(j,:).^2;
4  end
5  feat(i,:) = temp/(winsize-1);
```

RMS:

```
1  temp = 0;
2  for j = 1:winsize
3      temp = temp + curwin(j,:).^2;
4  end
5  feat(i,:) = sqrt(temp/winsize);
```

LOG:

```
1  temp = 0;
2  for j = 1:winsize
3      temp = temp + log10(abs(curwin(j,:)));
4  end
5  feat(i,:) = exp(temp/winsize);
```

Time Domain: Information**WL:**

```
1  temp = 0;
2  for j = 1:winsize-1
3      temp = temp + abs(curwin(j+1,:)-curwin(j,:));
4  end
5  feat(i,:) = temp;
```

AAC:

```

1 temp = 0;
2 for j = 1:winsize-1
3     temp = temp + abs(curwin(j+1,:)-curwin(j,:));
4 end
5 feat(i,:) = temp/winsize;

```

DASDV:

```

1 temp = 0;
2 for j = 1:winsize-1
3     temp = temp + abs((curwin(j+1,:)-curwin(j,:)).^2);
4 end
5 feat(i,:) = sqrt(temp/(winsize-1));

```

Time Domain: Frequency

The time domain features that were related to the frequency also required an optional threshold value to be set. The preliminary part of the feature function was therefore modified for the time domain: frequency features as follows:

```

1 function feat = zcfeat(X,winsize,wininc,threshold)
2 if nargin < 4
3     if nargin < 3
4         if nargin < 2
5             winsize = size(X,1);
6         end
7         wininc = winsize;
8     end
9     threshold = 0;
10 end

```

The feature calculation codes are as follows:

ZC:

```

1 for k = 1:Nsignals
2     temp = 0;
3     for j = 1:winsize-1
4         if sign(curwin(j,k)*curwin(j+1,k)) == -1
5             sgn = 1;
6         else
7             sgn = 0;

```

```

8      end
9      if abs(curwin(j,k)-curwin(j+1,k)) >=threshold
10         check = 1;
11     else
12         check = 0;
13     end
14     if sgn == 1 && check == 1
15         temp = temp + 1;
16     end
17   end
18   feat(i,k) = temp;
19 end

```

SSC:

```

1 for k = 1:Nsignals
2   temp = 0;
3   for j = 2:winsize-1
4     if (curwin(j,k)- curwin(j-1,k)) > threshold
5       f1 = 1;
6     else
7       f1 = 0;
8     end
9     if (curwin(j,k)- curwin(j+1,k)) > threshold
10       f2 = 1;
11     else
12       f2 = 0;
13     end
14     temp = temp + f1*f2;
15   end
16   feat(i,k) = temp;
17 end

```

WAMP:

```

1 for k = 1:Nsignals
2   temp = 0;
3   for j = 1:winsize-1
4     if abs(curwin(j,k)-curwin(j+1,k)) >=threshold
5       temp = temp + 1;
6     else
7       temp = temp + 0;
8     end

```

```

9      end
10     feat(i,k) = temp;
11 end

```

MYOP:

```

1 temp = 0;
2 for k = 1:Nsignals
3     for j = 1:winsize
4         if curwin(j,k)>=threshold
5             temp = temp + 1;
6         end
7     end
8     feat(i,k) = temp/winsize;
9 end

```

Time Domain: Multiple Features

The MAVS function calculates the MAV function for a series of consecutive windows. The feature outputs are the differences between the features.

MAVS:

```

1 function feat = mavsfeat(X,winsize,wininc,k)
2
3 if nargin <4
4     if nargin < 3
5         if nargin < 2
6             winsize = size(X,1);
7         end
8         wininc = winsize;
9     end
10    k=3;
11 end
12 datasize = size(X,1);
13 Nsignals = size(X,2);
14 datawin = ones(winsize,1);
15 numwin = floor((datasize - winsize)/wininc)+1;
16 feat = zeros(numwin,Nsignals*(k-1));
17
18 st = 1;
19 en = winsize;

```

```

20  for i = 1:numwin
21      curwin = X(st:en,:).*repmat(datawin,1,Nsignals);
22      winsize_k = floor(winsize/k);
23      mav = zeros(k,Nsignals);
24      st2 = 1;
25      en2 = winsize_k;
26      for w = 1:k
27          curwin_k = curwin(st2:en2,:);
28          %feature calculation
29          %-----
30          mav(w,:) = mean(abs(curwin_k));
31          %-----
32          st2 = st2 + winsize_k;
33          en2 = en2 + winsize_k;
34      end
35      for i2 = 1:k-1
36          feat(i,i2) = mav(i2+1,:)-mav(i2);
37      end
38      st = st + wininc;
39      en = en + wininc;
40  end

```

MHW:

```

1  %create 3 hamming windows with 30% overlap
2  L = length(curwin);
3  %length hamming
4  LH = floor(5/12*L);
5  w = hamming(LH);
6  for k = 1:Nsignals
7      feat1 = sum((curwin(1:LH,k).*w).^2);
8      feat2 = sum((curwin(floor(LH*.7):floor(LH*.7)+LH-1,k).*w).^2);
9      feat3 = sum((curwin(L-LH+1:L,k).*w).^2);
10     feat (i,(k-1)*3+1:k*3) = [feat1, feat2, feat3];
11 end

```

MTW:

```

1  %create 3 trapezoidal windows with 30% overlap
2  L = length(curwin);
3  %length of window
4  LH = floor(5/12*L);
5  w = trapmf(1:LH,[1 LH/4 LH*3/4 LH]);

```

```

6   for k = 1:Nsignals
7     feat1 = sum((curwin(1:LH,k)'.*w).^2);
8     feat2 = sum((curwin(floor(LH*.7):floor(LH*.7)+LH-1,k)'.*w).^2);
9     feat3 = sum((curwin(L-LH+1:L,k)'.*w).^2);
10    feat (i,(k-1)*3+1:k*3) = [feat1, feat2, feat3];
11  end

```

Prediction Model Coefficients

The prediction model coefficient codes for AR and CC features are shown in full. Both codes were designed to be used for any order, but the default order is 4.

AR:

```

1 function feat = ARfeat( X, winsize,wininc, order)
2 if nargin <4
3   if nargin < 3
4     if nargin < 2
5       winsize = size(X,1);
6     end
7     wininc = winsize;
8   end
9   order = 4;
10 end
11
12 datasize = size(X,1);
13 Nsignals = size(X,2);
14 datawin = ones(winsize,1);
15 numwin = floor((datasize - winsize)/wininc)+1;
16 feat = zeros(numwin,Nsignals,order);
17 st = 1;
18 en = winsize;
19 for i = 1:numwin
20   curwin = X(st:en,:).*repmat(datawin,1,Nsignals);
21   for k = 1:Nsignals
22     %feature calculation
23     %-----
24     temp = -aryule(curwin(:,k),order);
25     feat (i,k,1:order) = temp(2:order+1);
26   end
27   %-----

```

```

28     st = st + wininc;
29     en = en + wininc;
30 end

```

CC4:

```

1 function feat = ccfeat( X, winsize,wininc, order)
2 if nargin <4
3     if nargin < 3
4         if nargin < 2
5             winsize = size(X,1);
6         end
7         wininc = winsize;
8     end
9     order = 4;
10 end
11
12 datasize = size(X,1);
13 Nsignals = size(X,2);
14 datawin = ones(winsize,1);
15 numwin = floor((datasize - winsize)/wininc)+1;
16
17 feat = zeros(numwin,Nsignals*order);
18
19 st = 1;
20 en = winsize;
21 for i = 1:numwin
22     curwin = X(st:en,:).*repmat(datawin,1,Nsignals);
23
24 %feature calculation
25 %-----%
26 for k = 1:Nsignals
27
28     temp = -aryule(curwin(:,k),order);
29     c = zeros(1,order);
30     c(1) = -temp(2);
31     for p = 2:order
32         temp2 = 0;
33         for l = 1:p-1
34             temp2 = temp2+(1-l/p)*temp(p+1)*c(p-1);
35         end
36         c(p) = -temp(p+1)-temp2;

```

```

37         end
38     feat (i,(k-1)*order+1:k*order) = c;
39 end
40 end
41 %-----%
42 st = st + wininc;
43 en = en + wininc;
44 end

```

Frequency Domain Features

MNF:

```

1 fs = 1925.93; %Sampling frequency (Hz)
2 feat(i,:) = meanfreq(curwin)*fs/2/pi;

```

MDF:

```

1 fs = 1925.93;
2 feat(i,:) = medfreq(curwin)*fs/2/pi;

```

PKF:

```

1 %Peak frequency (PKF) feature calculation
2 fs = 1925.93;
3 for k = 1:Nsignals
4     xdft = fft(curwin(:,k));
5     if mod(winsize,2) == 0
6         xdft = xdft(1:winsize/2+1); %even window size
7     else
8         xdft = xdft(1:(winsize+1)/2); %odd window size
9     end
10    %compute power spectral density (PSD)
11    psdx = (1/(2*pi*winsize)) * abs(xdft).^2;
12    psdx(2:end-1) = 2*psdx(2:end-1);
13    freq = 0:fs/winsize:fs/2;
14    [~,b] = max(psdx);
15    feat (i,k) = freq(b);
16 end

```

MNP:

```

1 fs = 1925.93;
2 xdft = fft(curwin);

```

```

3 if mod(winsize,2) == 0
4     xdft = xdft(1:winsize/2+1); %even window size
5 else
6     xdft = xdft(1:(winsize+1)/2); %odd window size
7 end
8 %compute power spectral density (PSD)
9 psdx = (1/(2*pi*winsize)) * abs(xdft).^2;
10 psdx(2:end-1) = 2*psdx(2:end-1);
11 feat (i,:) = sum(psdx)/winsize;

```

TTP:

```

1 fs = 1925.93;
2 xdft = fft(curwin);
3 if mod(winsize,2) == 0
4     xdft = xdft(1:winsize/2+1); %even window size
5 else
6     xdft = xdft(1:(winsize+1)/2); %odd window size
7 end
8 %compute power spectral density (PSD)
9 psdx = (1/(2*pi*winsize)) * abs(xdft).^2;
10 psdx(2:end-1) = 2*psdx(2:end-1);
11 feat (i,:) = sum(psdx);

```

SM1-3:

```

1 fs = 1925.93;
2 xdft = fft(curwin);
3 if mod(winsize,2) == 0
4     xdft = xdft(1:winsize/2+1); %even window size
5 else
6     xdft = xdft(1:(winsize+1)/2); %odd window size
7 end
8 %compute power spectral density (PSD)
9 psdx = (1/(2*pi*winsize)) * abs(xdft).^2;
10 psdx(2:end-1) = 2*psdx(2:end-1);
11 freq = 0:fs/winsize:fs/2;
12 sm1feat (i,:) = freq.*psdx;
13 sm2feat (i,:) = freq.^2.*psdx;
14 sm3feat (i,:) = freq.^3.*psdx;

```

VCF:

```
1 fs = 1925.93;
```

```

2  xdft = fft(curwin);
3  if mod(winsize,2) == 0
4      xdft = xdft(1:winsize/2+1); %even window size
5  else
6      xdft = xdft(1:(winsize+1)/2); %odd window size
7 end
8 %compute power spectral density (PSD)
9 psdx = (1/(2*pi*winsize)) * abs(xdft).^2;
10 psdx(2:end-1) = 2*psdx(2:end-1);
11 freq = 0:fs/winsize:fs/2;
12 M1 = freq*psdx;
13 M0 = sum(psdx);
14 M2 = freq.^2*psdx;
15 feat (i,:) = M2/M0-(M1/M0)^2;

```

FR:

```

1  fs = 1925.93;
2 %Low Frequency Band
3 LLC = 15;
4 ULC = 45;
5 %High Frequency Band
6 LHC = 95;
7 UHC = 500;
8 xdft = fft(curwin);
9 if mod(winsize,2) == 0
10     xdft = xdft(1:winsize/2+1); %even window size
11 else
12     xdft = xdft(1:(winsize+1)/2); %odd window size
13 end
14 %compute power spectral density (PSD)
15 psdx = (1/(2*pi*winsize)) * abs(xdft).^2;
16 psdx(2:end-1) = 2*psdx(2:end-1);
17 freq = 0:fs/winsize:fs/2;
18 %find index
19 %Low Frequency Band
20 [~, LLC_i]= min(abs(freq-LLC));
21 [~, ULC_i]= min(abs(freq-ULC));
22 %High Frequency Band
23 [~, LHC_i]= min(abs(freq-LHC));
24 [~, UHC_i]= min(abs(freq-UHC));
25 lower_band = sum(psdx(LLC_i:ULC_i));

```

```

26 upper_band = sum(psdx(LHC_i:UHC_i));
27 feat (i,:) = lower_band/upper_band;

```

PSR:

```

1 fs = 1925.93;
2 n=20;
3 for k = 1:Nsignals
4     xdft = fft(curwin(:,k));
5     if mod(winsize,2) == 0
6         xdft = xdft(1:winsize/2+1); %even window size
7     else
8         xdft = xdft(1:(winsize+1)/2); %odd window size
9     end
10    %compute power spectral density (PSD)
11    psdx = (1/(2*pi*winsize)) * abs(xdft).^2;
12    psdx(2:end-1) = 2*psdx(2:end-1);
13    freq = 0:fs/winsize:fs/2;
14
15    %find f0
16    [~,b] = max(psdx);
17    f0 = freq(b);
18
19    %Frequency Bands
20    [~, LC_i]= min(abs(freq-10));
21    [~, UC_i]= min(abs(freq-500));
22
23    [~, LC2_i]= min(abs(freq-(f0-n)));
24    [~, UC2_i]= min(abs(freq-(f0+n)));
25    P = sum(psdx(LC_i:UC_i));
26    P0 = sum(psdx(LC2_i:UC2_i));
27
28    feat (i,k) = P0/P;
29 end

```

Entropy Features

The full codes for the entropy features are shown below.

ApEn:

```

1 function feat = ApEnfeat(X,winsize,wininc,m1,r)
2 if nargin <5

```

```
3     if nargin <4
4         if nargin < 3
5             if nargin < 2
6                 winsize = size(X,1);
7             end
8             wininc = winsize;
9         end
10        m1 = 2;
11    end
12    r = 0.2*std(X);
13 end
14 m = m1;
15 datasize = size(X,1);
16 Nsignals = size(X,2);
17 datawin = ones(winsize,1);
18 numwin = floor((datasize - winsize)/wininc)+1;
19
20 feat = zeros(numwin,Nsignals);
21
22 st = 1;
23 en = winsize;
24 for i = 1:numwin
25     curwin1 = X(st:en,:).*repmat(datawin,1,Nsignals);
26     for j = 1:Nsignals
27         curwin = curwin1(:,j);
28         Phi_m = zeros(1,2);
29         %feature calculation
30         %-----
31         for k = 1:2
32             m = m+k-1;
33             count = zeros(1,winsize-m+1);
34             %make the correlation dimension matrix (i.e. matrix of u_i)
35             corr_dim = zeros(m,winsize-m+1);
36             for i2 = 1:m
37                 corr_dim(i2,:) = curwin(i2:winsize-m+i2);
38             end
39
40             %calculate Cm
41             for i3 = 1:winsize-m+1
42                 tempMat = abs(corr_dim - repmat(corr_dim(:,i3),1,winsize-m+1));
43                 boolMat = any(tempMat > r);
```

```

44         count(i3) = sum(~boolMat)/(winsize-m+1);

45     end

46     %calculate Phi_m

47     Phi_m(k) = sum(log(count))/(winsize-m+1);

48 end

49 feat(i,j) = Phi_m(1)-Phi_m(2);

50 m=m1;

51 end

52 %-----  

53 st = st + wininc;
54 en = en + wininc;

55 end

```

SampleEn:

```

1 function feat = SampleEnfeat(X,winsize,wininc,m1,r)
2 if nargin < 5
3     if nargin < 4
4         if nargin < 3
5             winsize = size(X,1);
6         end
7         wininc = winsize;
8     end
9     m1 = 2;
10 end
11 r = 0.2*std(X);
12 end
13 m = m1;
14 datasize = size(X,1);
15 Nsignals = size(X,2);
16 datawin = ones(winsize,1);
17 numwin = floor((datasize - winsize)/wininc)+1;
18
19
20 feat = zeros(numwin,Nsignals);
21
22 st = 1;
23 en = winsize;
24 for i = 1:numwin
25     curwin1 = X(st:en,:).*repmat(datawin,1,Nsignals)
26     for j = 1:Nsignals
27         curwin = curwin1(:,j);

```

```

28     Phi_m = zeros(1,2);
29     %feature calculation
30     %-----
31     for k = 1:2
32         m = m+k-1;
33         count = zeros(1,winsize-m+1);
34         %make the correlation dimension matrix (i.e. matrix of u_i)
35         corr_dim = zeros (m,winsize-m+1);
36         for i2 = 1:m
37             corr_dim(i2,:) = curwin(i2:winsize-m+i2);
38         end
39
40         %calculate Cm
41         for i3 = 1:winsize-m+1
42             tempMat = abs(corr_dim - repmat(corr_dim(:,i3),1,winsize-m+1));
43             boolMat = any(tempMat > r);
44             count(i3) = (sum(~boolMat)-1)/(winsize-m+1);
45         end
46         %calculate Phi_m
47         Phi_m(k) = sum(count)/(winsize-m);
48     end
49     feat(i,j) = -log(Phi_m(2)/Phi_m(1));
50     m=m1;
51 end
52 %-----
53 st = st + wininc;
54 en = en + wininc;
55 end

```

Fractal Dimension Features

The codes for the feature calculations of the fractal features are shown below.

MFL:

```

1 temp = 0;
2 for j = 1:winsize-1
3     temp = temp + (curwin(j+1,:)-curwin(j,:))^2;
4 end
5 feat(i,:) = log10(temp);

```

HFD:

```

1 %get time series
2 kmax = 128;
3 X2 = zeros(kmax,kmax,winsize);
4 for k = 1:kmax
5     for m = 1:k
6         limit = floor((winsize-m)/k);
7         j = 1;
8         for i2 = m:k:(m + (limit*k))
9             X2(k,m,j) = curwin(i2);
10            j = j + 1;
11        end
12    end
13 end
14 L = zeros(1, kmax);
15 for k = 1:kmax
16     L_m = zeros(1,k);
17     for m = 1:k
18         R = (winsize - 1)/(floor((winsize - m)/k) * k);
19         aux = squeeze(X2(k,m,logical(~isnan(X2(k,m,:))))); %We get the sub-serie without
19             the NaNs.
20         for i2 = 1:(length(aux) - 1)
21             L_m(m) = L_m(m) + abs(aux(i2+1) - aux(i2));
22         end
23         L_m(m) = (L_m(m) * R)/k;
24     end
25     L(k) = sum(L_m)/k;
26 end
27 %Compute the HFD:
28 x = 1./(1:kmax);
29 aux = polyfit(log(x),log(L),1);
30 feat(i,n) = aux(1);

```

DFA:

```

1 %Detrended Fluctuation Analysis (DFA) feature calculation
2 for j = 1:Nsignals
3     curwin = curwin1(:,j);
4     %Step 1: Integrate
5     y = zeros(1,winsize);
6     t= 1:1:winsize;
7     for k = 1:winsize
8         y(k) = sum(curwin(1:k));

```

```

9      end
10
11 %Step 2: Calculate Box Sizes
12 boxesize = 4;
13 nmax = winsize/10;
14 while boxesize(end)<nmax
15     boxesize(end+1)=boxesize(end)*2;
16 end
17
18 %Step 3: Fit Each Box to Quadratic Least Squares
19 for n = 1:length(boxesize)
20     temp = 0;
21     p = zeros(1,3);
22     pv = zeros(1,winsize);
23     m = boxesize(n);
24     for i2 = 1:m:winsize-m+1
25         temp = temp+1;
26         p(temp,:)=polyfit(t(i2:i2+m-1),y(i2:i2+m-1),2);
27         pv(i2:i2+m-1) = polyval(p(temp,:),t(i2:i2+m-1));
28
29     end
30 %Step 4: Calculate RMS
31 F(n)= sqrt((1/winsize)*sum(y-pv)^2);
32 end
33
34 %Step 5: Calculate self-similarity parameter, alpha (i.e. the feature)
35 fit = polyfit(log(boxesize),log10(F),1);
36 feat(i,j) = fit(1);
37 end

```

Higher Order Features

The codes for the feature calculations of the higher order features are shown below.

SKEW:

```

1 sigma = std (curwin);
2 mu = mean(curwin);
3 temp = 0;
4 for j = 1:winsize
5     temp = temp + ((curwin(j,:)-mu)/sigma).^3;
6 end

```

```
7  feat(i,:) = temp/winsize ;
```

KURT:

```
1  sigma = std (curwin);
2  mu = mean(curwin);
3  temp = 0;
4  for j = 1:winsize
5      temp = temp + ((curwin(j,:)-mu)/sigma).^4;
6  end
7  feat(i,:) = (temp/winsize)-3; %subtract 3 to get 0 for a normal distribution
```

Spike Shape Analysis Features

The full code to generate all five of the major spike shape analysis features is shown below.

```
1  function feat = spikefeat( X, winsize,wininc, th)
2  if nargin <4
3      if nargin < 3
4          if nargin < 2
5              winsize = size(X,1);
6          end
7          wininc = winsize;
8      end
9      th = 0;
10 end
11
12 datasize = size(X,1);
13 Nsignals = size(X,2);
14 datawin = ones(winsize,1);
15 numwin = floor((datasize - winsize)/wininc)+1;
16
17 feat = zeros(numwin,Nsignals*5);
18
19 st = 1;
20 en = winsize;
21 for i = 1:numwin
22     curwin = X(st:en,:).*repmat(datawin,1,Nsignals);
23     for k = 1:Nsignals
24
25         %feature calculation
26         %-----
```



```
68                     Ax(end+1) = btmlv;
69                     Ay(end+1) = btm(btml);
70                     Cy(end+1) = btm(btmg);
71                     Cx(end+1)= btmhv;
72                     spike_no = spike_no+1;
73             end
74         else
75             [By(end+1),ind] = max(pkss(peaks_index));
76             Bx(end+1) = locs(peaks_index(ind));
77             Ax(end+1) = btmlv;
78             Ay(end+1) = btm(btml);
79             Cy(end+1) = btm(btmg);
80             Cx(end+1)= btmhv;
81             spike_no = spike_no+1;
82         end
83     end
84 end
85
86
87 %calculate single spike amplitudes (SA) and spike slopes (SS)
88 SA = zeros(1,spike_no);
89 SS = SA;
90 SD = SA;
91
92 for j = 1:spike_no
93     SA(j) = (By(j)-Ay(j)) + (By(j)-Cy(j))/2;
94     SS(j) = (By(j)-Ay(j))/(Bx(j)-Ax(j));
95     SD(j) = Cx(j)-Ax(j);
96 end
97
98 %% FEATURES %%
99
100 %MSA (Mean Spike Amplitude)
101 MSA = mean(SA);
102
103 %MSF (Mean Spike Frequency)
104 MSF = (spike_no+2)/time_dur;
105
106 %MSS (Mean Spike Slope)
107 MSS = mean(SS)/5.1923e-04;
108
```

```
109      %MNPPS (Mean Number of Peaks per Spike)
110      MNPPS = peak_no/spike_no;
111
112      %MSD (Mean Spike Duration)
113      MSD = mean(SD)*5.1923e-04;
114
115      temp = [MSA, MSF, MSS, MNPPS, MSD];
116      feat(i,(k-1)*5+1:k*5) = temp;
117      %-----%
118      st = st + wininc;
119      en = en + wininc;
120  end
121 end
```

B.3 Feature Generation Codes

The sEMG feature functions described in the previous section were implemented within the feature generation codes to extract feature vectors. In addition to the sEMG feature functions, a function, **emgprocess_trigno ()** was developed to filter the EMG signals with a 20–400 Hz bandpass filter and a 60 Hz notch filter as follows:

```

1  function f2 = emgprocess_trigno(rawsignal)
2  fs=1925.93; %Sample frequency
3
4  %Centre on x-axis
5  m = rawsignal - mean(rawsignal);
6
7  %Bandpass filter 20 - 400 Hz
8  [b,a]=butter(2,[20/(fs/2),400/(fs/2)]);
9  f1 = filtfilt(b,a,m);
10
11 %Notch filter 60 Hz
12 wo = 60/(fs/2);
13 bw = wo/10;
14 [b,a] = iirnotch(wo,bw);
15 f2 = filtfilt(b,a,f1);
16 end
```

Feature generation codes for extracting features were developed for both single and multiple windows. Features were extracted for each segment of data, and saved in separate files for each feature and motion type.

Single Window Feature Generation

The following code extracts features for one window segment of the data.

```

1  %Basic Feature Generation Code
2  number_of_channels = 7;
3  feature_list = {'mflfeat','myopfeat'};
4  health = {'Healthy','Injured'};
5  motion_sets = {'EF', 'EE', 'P', 'S', 'WF', 'WE', 'UD', 'RD', 'HC', 'HO'};
6  number_of_features = length(feature_list);
7
```

```
8 %GENERATE FEATURES
9 for h = 1:numel(health)
10    for k=1:numel(motion_sets)
11       if strcmp(health{h}, 'Injured') == 1
12          %Injured Subjects
13          subjects = {'S84','S85','S86',...
14             'S137'};
15       else
16          %Healthy Subjects
17          subjects = {'S84','S85','S86',...
18             'S137'};
19    end
20    for f = 1:numel(feature_list)
21       B = zeros(length(subjects),number_of_channels);
22       for s = 1:numel(subjects)
23          A = zeros(3,number_of_channels*(number_of_features));
24          for r = 1:3
25             %Import EMG data
26             input_data_file = strcat('C:\Users\Emma\Documents\Data\Repetition Data',...
27               ',motion_sets{k}, '\', health{h}, '\', subjects{s}, motion_sets{k}, '_R...
28               ', num2str(r), '.csv');
29             emg_data = xlsread(input_data_file);
30             %Filter EMG data
31             emg_data = emgprocess_trigno(emg_data);
32             %Extract features
33             st = 1;
34             for ch = 1:number_of_channels
35                feature_function = str2func(feature_list{f});
36                %Feature array for all repetitions for one subject
37                A(r,st) = feature_function(emg_data(:,ch));
38                st = st+1;
39             end
40           end
41           B((s-1)*3+1:s*3,:) = A; %Feature array for all subjects
42       end
43       %Save array
44       savefilename = strcat('C:\Users\Emma\Documents\Data\Feature Data\', health{h}, '\...
45         , motion_sets{k}, feature_list, '.xlsx');
46       xlswrite(savefilename,B);
47    end
48 end
```

 46 **end**

Multi-window Feature Generation

The following code is similar to the first feature generation code, but is developed for multiple windows. The subject number for each window is saved within the feature set to allow patients to be identifiable during the next step of leave-one-patient-out cross-validation.

```

1 %Generate Multi-window Features
2 number_of_channels = 7;
3 feature_list = {'mflfeat','myopfeat'};
4 health = {'Healthy','Injured'};
5 motion_sets = {'EF','EE','P','S','WF','WE','UD','RD','HC','HO'};
6
7 %Window Sizes
8 window_size = 500;
9 increment_size = 250;
10 number_of_features = numel(feature_list);
11
12 for f = 1:numel(feature_list)
13     %Develop list of subjects
14     for h = 1:numel(health)
15         for k=1:numel(motion_sets)
16             if strcmp(health{h}, 'Injured') == 1
17                 %Injured Subjects
18                 subjects = {'S84','S85','S86',...
19                             'S137'};
20             else
21                 %Healthy Subjects
22                 subjects = {'S84','S85','S86',...
23                             'S137'};
24             end
25             B = [];
26             for s = 1:numel(subjects)
27                 R = [];
28                 for r = 1:3
29                     A = [];
30                     %Import EMG data
31                     input_data_file = strcat('C:\Users\Emma\Documents\Data\Repetition Data',...
32                                         ',motion_sets{k}, '\', health{h}, '\', subjects{s}, motion_sets{k}, '_R

```

```
        ',num2str(r), '.csv');

32    emg_data = xlsread(input_data_file);
33
%Filter EMG data
34    emg_data = emgprocess_trigno(emg_data);
35
36    %Calculate number of windows
37    datasize = length(emg_data);
38    numwin = floor((datasize - window_size)/increment_size)+1;
39
%Develop feature array
40    st = 1;
41
for ch = 1:number_of_channels
    feature_function = str2func(feature_list{f});
    A = [A,feature_function(emg_data(:,ch),window_size,increment_size)
        ];
end
45    R = [R;A]; %Array of all repetitions for each subject
46
end
47    R = [R,ones(size(R,1),1)*s]; %Save subject numbers
48    B = [B;R]; %Feature array of all subjects
49
end
50
%Save array
51    savefilename = strcat('C:\Users\Emma\Documents\Data\Feature Data\',health{h}, '\
        ',motion_sets{k},feature_list{f}, '.xlsx');
52    xlswrite(savefilename,B);
53
end
54
end
55 end
```

B.4 Classification

Following feature extraction, classification models for individual features or for feature sets were developed and evaluated. The classification model code imports the feature data from the individual excel files for each feature. The classification model options are linear discriminant analysis (LDA), support vector machines (SVM), or random forest (RF). The accuracy of classification using leave-one-patient out is determined for each individual motion. Classification model codes were developed to categorize between two classes (healthy or injured) and between three classes (healthy, early stages of rehabilitation, late stages of rehabilitation).

Healthy or Injured classification

The following code categorizes between the healthy and injured limbs of the patients.

```

1 %Basic Classification
2 feature_list = {'mflfeat', 'myopfeat'};
3 model_type = 'LDA'; %LDA, SVM, or RF
4 motion_sets = {'EF', 'EE', 'P', 'S', 'WF', 'WE', 'UD', 'RD', 'HC', 'HO'};
5
6 A = zeros(1,numel(motion_sets));
7 for k = 1:numel(motion_sets)
8     healthy = [];
9     injured = [];
10    %Import feature sets
11    for f = 1:length(feature_list)
12        %Healthy features
13        healthy_name = strcat('C:\Users\Emma\Documents\Data\Feature Data\Healthy\',
14                               motion_sets{k},feature_list{f},'.xlsx');
15        healthytemp= xlsread(healthy_name);
16        healthy = [healthy,healthytemp];
17        %Injured features
18        injured_name = strcat('C:\Users\Emma\Documents\Data\Feature Data\Injured\',
19                               motion_sets{k},feature_list{f},'.xlsx');
20        injuredtemp = xlsread(injured_name);
21        injured = [injured,injuredtemp];
22    end
23
24    %Feature Set Arrays

```

```
23 full = [healthy;injured];
24 type = [ones(size(healthy,1),1);zeros(size(injured,1),1)];
25
26 match = 0; %Number of correct classifications
27 %Number of data sets
28 N = size(full,1);
29 nds = size(healthy,1);
30
31 for i = 1:3:nds
32     %Assign training data sets and test data sets
33     %Assign one subject to the test data set
34     train_data = full;
35     train_data([i:i+2,nds+i:nds+i+2],:) = [];
36     train_type = type;
37     train_type([i:i+2,nds+i:nds+i+2],:) = [];
38     test_data = full([i:i+2,nds+i:nds+i+2],:);
39     test_type = type([i:i+2,nds+i:nds+i+2],:);
40
41     %Train model
42     switch model_type
43         case 'LDA'
44             Mdl = fitcdiscr(train_data,train_type);
45         case 'SVM'
46             Mdl = fitcecoc(train_data,train_type);
47         case 'RF'
48             Mdl = TreeBagger(200,train_data,train_type);
49     end
50     label = predict(Mdl,test_data);
51     if strcmp(model_type,'RF') == 1
52         label = str2num(cell2mat(label));
53     end
54     test_result = sum(eq(label,test_type));
55     match = match + test_result;
56 end
57 accuracy = match/N*100 ;
58 A(k) = accuracy;
59 end
60 T = array2table(A,'VariableNames',{ 'EF' , 'EE' , 'P' , 'S' , 'WF' , 'WE' , 'UD' , 'RD' , 'HC' , 'HO' })
```

Three levels of health classification

The following code implements classifiers for three levels of health. The training data sets are developed using 12 data sets randomly from each group in order to balance the number of training sets representative of each of the three categories. The evaluation is repeated 10 times and the average of the classification accuracies is determined in order to obtain an estimate of the classification accuracy.

```
1 %Three Levels of Health Classification
2 feature_list = {'mflfeat', 'myopfeat'};
3 model_type = 'LDA'; %LDA, SVM, or RF
4 motion_sets = {'EF', 'EE', 'P', 'S', 'WF', 'WE', 'UD', 'RD', 'HC', 'HO'};
5
6 A = zeros(1,numel(data_sets));
7 for k = 1:numel(data_sets)
8     healthy = [];
9     injured = [];
10    %Import feature sets
11    for f = 1:length(feature_list)
12        %healthy features
13        healthy_name = strcat('C:\Users\Emma\Documents\Data\Feature Data\Healthy\' ,
14            motion_sets{k},feature_list{f}, '.xlsx');
15        healthytemp= xlsread(healthy_name);
16        healthy = [healthy,healthytemp];
17        %injured features
18        injured_name = strcat('C:\Users\Emma\Documents\Data\Feature Data\Injured\' ,
19            motion_sets{k},feature_list{f}, '.xlsx');
20        injuredtemp = xlsread(injured_name);
21        injured = [injured,injuredtemp];
22    end
23
24    %Hard Coded Groups of Early and Late Stage Patients
25    early = injured([1:3,7:9, 10:12, 13:15, 25:42,49:51,58:60, 73:75],:);
26    late = injured ([4:6,16:24,43:48, 52:57,61:72, 76:81],:);
27
28    match = 0;
29
30    %Repeat Classifications 10 times
31    for r = 1:10
32        %Assign training data sets and test data sets
```

```
31 %Assign 13 random patients from each health group
32 %to the training data set
33
34 %Healthy
35 dataset=randperm(27,13);
36 msize=numel(dataset);
37 test=dataset(randperm(msize,1));
38 testn = (1+(test-1)*3):(1+(test-1)*3+2);
39 train=dataset(find(dataset~=test));
40 for n = 1:length(train)
41     trainn(1+(n-1)*3:3+(n-1)*3) = (1+(train(n)-1)*3):(1+(train(n)-1)*3+2);
42 end
43 healthy_train = healthy(trainn,:);
44 healthy_test = healthy(testn,:);
45
46 %Early
47 dataset=randperm(13,13);
48 msize=numel(dataset);
49 test=dataset(randperm(msize,1));
50 testn = (1+(test-1)*3):(1+(test-1)*3+2);
51 train=dataset(find(dataset~=test));
52 for n = 1:length(train)
53     trainn(1+(n-1)*3:3+(n-1)*3) = (1+(train(n)-1)*3):(1+(train(n)-1)*3+2);
54 end
55 early_train = early(trainn,:);
56 early_test = early(testn,:);
57
58 %Late
59 dataset=randperm(14,13);
60 msize=numel(dataset);
61 test=dataset(randperm(msize,1));
62 testn = (1+(test-1)*3):(1+(test-1)*3+2);
63 train=dataset(find(dataset~=test));
64 for n = 1:length(train)
65     trainn(1+(n-1)*3:3+(n-1)*3) = (1+(train(n)-1)*3):(1+(train(n)-1)*3+2);
66 end
67 late_train = late(trainn,:);
68 late_test = late(testn,:);
69
70 %Training Data Set
71 train_data = [healthy_train; early_train; late_train];
```

```

72     train_type = [ones(12*3,1);(ones(12*3,1)+2); (ones(12*3,1)+1)];
73
74     %Test Data Set
75     test_data = [healthy_test; early_test; late_test];
76     test_type = [ones(3,1);ones(3,1)+2; ones(3,1)+1];
77
78     %Train models
79     switch model_type
80         case 'LDA'
81             Mdl = fitcdiscr(train_data,train_type);
82         case 'SVM'
83             Mdl = fitcecoc(train_data,train_type);
84         case 'RF'
85             Mdl = TreeBagger(200,train_data,train_type);
86     end
87     label = predict(Mdl,test_data);
88     if strcmp(model_type,'RF') == 1
89         label = str2num(cell2mat(label));
90     end
91     test_result = sum(eq(round(label),test_type));
92     match = match + test_result;
93 end
94 A(k)=match/(9*r)*100;
95 end
96 T = array2table(A,'VariableNames',{'EF', 'EE', 'P', 'S', 'WF', 'WE', 'UD', 'RD', 'HC', 'HO'})

```

B.5 Majority Vote

The majority vote code implements a separate classification for each of the motions in each data set. The final classification result is the mode of the outputs of the individual motion models. The weighted majority vote result is determined as the highest sum of the weights. A majority vote can also be implemented using only the top data sets.

```

1  %Majority Vote
2  feature_list = {'mflfeat','myopfeat'};
3  model_type = 'LDA'; %LDA, SVM, or RF
4  vote_type = 'TOP'; %ALL, WEIGHT, TOP
5  switch vote_type
6      case {'ALL','WEIGHT'}

```

```
7     motion_sets = {'EF','EE','P','S','WF','WE','UD','RD','HC','HO'};  
8     case 'TOP'  
9         motion_sets = {'EF','EE','P','S','WF','UD','HC'};  
10    end  
11    number_of_subjects = 27;  
12    nds = number_of_subjects*3; %Number of data sets  
13    N= nds*2;  
14    A = zeros(1,numel(motion_sets));  
15    match = 0; %Number of correct classifications  
16    for i = 1:3:nds  
17        final_label = zeros (6, numel(motion_sets));  
18        for k = 1:numel(motion_sets)  
19            healthy = [];  
20            injured = [];  
21            %Import feature sets  
22            for f = 1:length(feature_list)  
23                %Healthy features  
24                healthy_name = strcat('C:\Users\Emma\Documents\Data\Feature Data\Healthy\',  
25                    motion_sets{k},feature_list{f},'.xlsx');  
26                healthytemp= xlsread(healthy_name);  
27                healthy = [healthy,healthytemp];  
28                %Injured features  
29                injured_name = strcat('C:\Users\Emma\Documents\Data\Feature Data\Injured\',  
30                    motion_sets{k},feature_list{f},'.xlsx');  
31                injuredtemp = xlsread(injured_name);  
32                injured = [injured,injuredtemp];  
33            end  
34            %Feature Set Arrays  
35            full = [healthy;injured];  
36            type = [ones(nds,1);zeros(nds,1)];  
37            %Assign training data sets and test data sets  
38            %Assign one subject to the test data set  
39            train_data = full;  
40            train_data([i:i+2,ndsi:ndsi+i+2],:) = [];  
41            train_type = type;  
42            train_type([i:i+2,ndsi:ndsi+i+2],:) = [];  
43            test_data = full([i:i+2,ndsi:ndsi+i+2],:);  
44            test_type = type([i:i+2,ndsi:ndsi+i+2],:);  
45            %Train Model
```

```
46     switch model_type
47         case 'LDA'
48             Mdl = fitcdiscr(train_data,train_type);
49         case 'SVM'
50             Mdl = fitcecoc(train_data,train_type);
51         case 'RF'
52             Mdl = TreeBagger(200,train_data,train_type);
53     end
54
55     label = predict(Mdl,test_data);
56
57     if strcmp(model_type,'RF') == 1
58         label = str2num(cell2mat(label));
59     end
60
61     final_label(:,k) = label;
62
63 end
64
65 %Majority Vote
66
67 switch vote_type
68     case {'ALL','TOP'}
69         vote = mode(final_label)';
70     case 'WEIGHT'
71         %Assign weights based on previous results
72         weights = [71 72.8 67.9 67.9 69.1 63 64.8 67.3 67.3 60.5];
73         healthy_sum = sum(final_label.*weights,2);
74         injured_sum = sum(abs(final_label-1).*weights,2);
75         vote = healthy_sum>injured_sum;
76
77     end
78
79     test_result = sum(eq(round(vote),test_type));
80     match = match + test_result;
81
82 end
83
84 accuracy = match/N*100
```

VITA

Name: Emma Farago

Post-secondary Education and Degrees: University of Windsor
Windsor, Ontario, Canada
2012–2016 B.A.Sc.
Electrical Engineering

The University of Western Ontario
London, Ontario, Canada
2016–2018 M.E.Sc.
Electrical and Computer Engineering

The University of Western Ontario
London, Ontario, Canada
2009–2012 B.Sc.
Medical Sciences

Honours and Awards: NSERC Canadian Graduate Scholarship–Master’s Program
Transdisciplinary Bone and Joint Training Award

Related Work Experience: Teaching Assistant
ECE 4455 – Biomedical Systems Analysis
ECE 2277 – Digital Logic Design
ECE 2233 – Circuits and Systems
The University of Western Ontario
2016–2018

Research Assistant
The University of Western Ontario
2016–2018